

ทฤษฎีของการดูดซับทางเคมีของไฮดรอกไซด์และแอลกอฮอล์ที่มีจำนวนคาร์บอนหนึ่งถึงสามอะตอม

บนพอลิเมอร์คาร์บอนชนิดผนังเดี่ยว



นางสาวไรนา หวันระยอง

วิทยานิพนธ์นี้เป็นส่วนหนึ่งของการศึกษาตามหลักสูตรปริญญาวิทยาศาสตรมหาบัณฑิต

สาขาวิชาเคมี ภาควิชาเคมี

คณะวิทยาศาสตร์ จุฬาลงกรณ์มหาวิทยาลัย

ปีการศึกษา 2549

ลิขสิทธิ์ของจุฬาลงกรณ์มหาวิทยาลัย

THEORY OF CHEMISORPTIONS OF HYDROXIDE AND C1-C3 ALKOXIDES ON
SINGLE-WALLED CARBON NANOTUBES



Miss Raina Wanbayor

สถาบันวิทยบริการ
จุฬาลงกรณ์มหาวิทยาลัย

A Thesis Submitted in Partial Fulfillment of the Requirements
for the Degree of Master of Science Program in Chemistry
Faculty of Science
Chulalongkorn University
Academic Year 2006

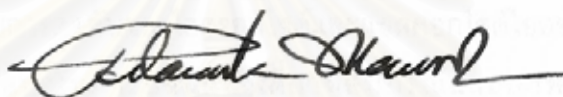
Thesis Title THEORY OF CHEMISORPTIONS OF HYDROXIDE AND
C1-C3 ALKOXIDES ON SINGLE-WALLED CARBON
NANOTUBES

By Miss Raina Wanbayor

Field of study Chemistry

Thesis Advisor Associate Professor Vithaya Ruangpornvisuti, Dr.rer.nat.

Accepted by the Faculty of Science, Chulalongkorn University in Partial
Fulfillment of the Requirements for the Master's Degree

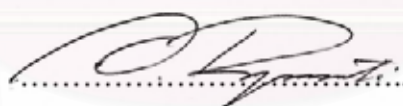


.....Dean of the Faculty of Science
(Professor Piamsak Menasveta, Ph.D.)

THESIS COMMITTEE



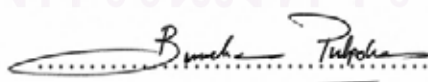
.....Chairman
(Professor Supot Hannongbua, Dr.rer.nat.)



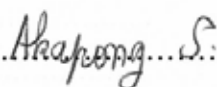
.....Thesis Advisor
(Associate Professor Vithaya Ruangpornvisuti, Dr.rer.nat.)



.....Member
(Associate Professor Chaihok Eab, Ph.D.)



.....Member
(Associate Professor Buncha Pulpoka, Ph.D.)



.....Member
(Akapong Suwattanamala, Ph.D.)

ไรนา หวันระยอง: ทฤษฎีของการดูดซับทางเคมีของไฮดรอกไซด์และแอลคอกไซด์ที่มีจำนวนคาร์บอนหนึ่งถึงสามอะตอมบนท่อนาโนคาร์บอนชนิดผนังเดี่ยว (THEORY OF CHEMISORPTIONS OF HYDROXIDE AND C1-C3 ALKOXIDES ON SINGLE-WALLED CARBON NANOTUBES)

อ.ที่ปรึกษา: รศ.ดร.วิทยา เรืองพรวิสุทธิ, 109 หน้า.

ศึกษาการดูดซับของโปรตอนและไฮดรอกไซด์บนท่อนาโนคาร์บอนผนังเดี่ยวที่สมบูรณ์และบกพร่องชนิดอาร์มแชร์ (5,5) แบบท่อปลายปิด C_{80} , C_{120} และแบบท่อปลายเปิด $C_{80}H_{20}$ และโครงสร้างที่ถูกโปรโตเนตกับโมเดลที่มีและไม่มีน้ำโดยวิธี HF, DFT และ ONIOM(MO:MO) พลังงานยึดเหนี่ยวและสมบัติทางเทอร์โมไดนามิกส์ของการดูดซับบนท่อนาโนคาร์บอนผนังเดี่ยวชนิดอาร์มแชร์ (5,5) แบบต่างๆ ได้จากวิธีคำนวณในระดับทฤษฎี ONIOM(B3LYP/6-31G(d):AM1) สำหรับการดูดซับของไฮดรอกไซด์และแอลคอกไซด์ไอออนที่มีจำนวนคาร์บอนหนึ่งถึงสามอะตอมบนท่อนาโนคาร์บอนผนังเดี่ยวที่สมบูรณ์และบกพร่องชนิดอาร์มแชร์ (5,5) แบบท่อปลายปิด C_{80} , C_{120} และแบบท่อปลายเปิด $C_{80}H_{20}$, $C_{120}H_{20}$ โดยวิธี ONIOM(B3LYP/6-31G(d):AM1) พบว่าการดูดซับไฮดรอกไซด์เกิดได้ดีกว่าแอลคอกไซด์บนท่อนาโนคาร์บอนผนังเดี่ยวทุกแบบ ในกรณีของแอลคอกไซด์ไอออนที่มีคาร์บอนหนึ่งถึงสามอะตอมพบว่าพลังงานยึดเหนี่ยวของการดูดซับบนท่อนาโนคาร์บอนผนังเดี่ยวทุกแบบเกิดขึ้นน้อยลงในขณะที่ขนาดของหมู่แอลคิลของแอลคอกไซด์เพิ่มขึ้นซึ่งประจุของออกซิเจนของแอลคอกไซด์เพิ่มขึ้นเช่นกัน

สถาบันวิทยบริการ จุฬาลงกรณ์มหาวิทยาลัย

ภาควิชา.....เคมี.....

สาขาวิชา.....เคมี.....

ปีการศึกษา.....2549.....

ลายมือชื่อผู้สมัคร.....*Yong Wanranyong*.....

ลายมือชื่ออาจารย์ที่ปรึกษา.....*[Signature]*.....

Advisor's signature.....*[Signature]*.....

Academic year.....2016.....

4872442423: CHEMISTRY

KEY WORD: CARBON NANOTUBE / ADSORPTION / PROTON / HYDROXIDE
/ ALKOXIDE / ONIOM

RAINA WANBAYOR: THEORY OF CHEMISORPTIONS OF
HYDROXIDE AND C1-C3 ALKOXIDES ON SINGLE-WALLED
CARBON NANOTUBES

THESIS ADVISOR: ASSOC. PROF. VITHAYA RUANGPORNVISUTI,
Dr.rer.nat., 109 pp.

The adsorptions of proton and hydroxide on the perfect and defect armchair (5,5) single-walled carbon nanotubes (SWCNTs) of cap-ended C_{80} , C_{120} and open-ended $C_{80}H_{20}$ and on their protonated structures with and without water models were studied using the HF, DFT and two-layered ONIOM(MO:MO) methods. The binding energies and thermodynamic properties of all the adsorptions on various types of armchair (5,5) SWCNTs were obtained at the ONIOM(B3LYP/6-31G(d):AM1) level of theory. For the adsorptions of hydroxide and C1 to C3 alkoxide ions on the perfect and defect armchair (5,5) SWCNTs of cap-ended C_{80} , C_{120} and open-ended $C_{80}H_{20}$, $C_{120}H_{20}$ were studied using ONIOM(B3LYP/6-31G(d):AM1) have been found that hydroxide was adsorbed better than alkoxide for all various types of SWCNTs. In the case of C1 to C3 alkoxide ions, as the binding energies of all adsorptions on various types of SWCNTs are decreased while the size of alkyl group of alkoxides are increased, the charged of alkoxide-oxygen are increased simultaneously.

สถาบันวิทยบริการ
จุฬาลงกรณ์มหาวิทยาลัย

Department.....Chemistry.....

Field of study...Chemistry.....

Academic year...2006.....

student's signature.....

Advisor's signature.....

Raina Wanbayor
Vithaya Ruangpornvisuti

ACKNOWLEDGEMENTS

I would like to express my appreciation to my advisor, Associate Professor Dr. Vithaya Ruangpornvisuti, for his continuous attention, kind suggestions and guidance throughout the course of this research. I deeply appreciate the support, encouragement and valuable advice of my committee members, Professor Dr. Supot Hannongbua, Associate Professor Dr. Chaihok Eab, Associate Professor Dr. Buncha Pulpoka and Dr. Akapong Suwattanamala for their suggestions and comments.

Special appreciation is extended to my colleagues at Supramolecular Chemistry Research Unit (SCRU), Department of chemistry, Faculty of Science, Chulalongkorn University, for their worthy, friendship throughout my study.

Finally, I would like to affectionately give all my gratitude to my parents and all the member of my family for their love care, kindness, encouragement and other assistance throughout my life. I hope my family is proud of my success.



สถาบันวิทยบริการ
จุฬาลงกรณ์มหาวิทยาลัย

CONTENTS

	Page
ABSTRACT IN THAI	iv
ABSTRACT IN ENGLISH	v
ACKNOWLEDGEMENTS	vi
CONTENTS.....	vii
LIST OF FIGURES	x
LIST OF TABLES	xvi
LIST OF ABBREVIATIONS	xviii
CHAPTER I INTRODUCTION.....	1
1.1 CarbonNanotube	1
1.2 Single-Walled Carbon Nanotubes	2
1.2.1 Vector Notation for SWCNTs	3
1.2.2 Structure of SWCNTs	5
1.2.3 Properties of SWCNTs	7
1.3 Defect Structures of SWCNTs	8
1.4 Adsorption	9
1.4.1 Physisorption	9
1.4.2 Chemisorption	11
1.5 Literature Reviews	15
1.6 Objectives	16
CHAPTER II EXPERIMENTAL.....	16
2.1 Ab Initio Method.....	16
2.1.1 The Hartree-Fock Method	16
2.1.2 Slater Determinants	17
2.1.3 Atomic and Molecular Energy.....	18
2.2 Basis set	21
2.2.1 Minimal Basis Sets.....	22

	Page
2.2.2 Split-Valence Basis Sets	22
2.2.3 Polarized Basis Sets.....	23
2.3 Semi-Empirical Methods.....	24
2.3.1 Austin Model 1 (AM1).....	24
2.3.2 Parametric Number 3 (PM3).....	25
2.4 Density Functional Theory.....	26
2.4.1 The Kohn-Sham Energy and the Kohn-Sham Equations.....	27
2.4.1.1 The Kohn-Sham Energy.....	27
2.4.1.2 The Kohn-Sham Equations.....	29
2.4.2 The Local Density Methods	31
2.4.3 Gradient Corrected Methods.....	32
2.4.4 Hybrid Methods	32
2.5 ONIOM Method.....	34
2.5.1 ONIOM Energy Definition.....	35
2.5.2 Treatment of Link Atoms.....	37
CHAPTER III DETAILS OF THE CALCULATIONS.....	39
3.1 The Adsorptions of Proton and Hydroxide on Various Types of SWCNTs.....	44
3.2 The Chemisorptions of Hydroxide and C1 to C3 alkoxides.....	48
CHAPTER IV RESULTS AND DISCUSSION.....	50
4.1 The Adsorptions of Proton and Hydroxide on Various Types of SWCNTs.....	50
4.1.1 Ab Initio (HF/3-21G) Calculation for Reaction Systems of Perfect and Defect Cap-Ended C ₈₀ SWCNTs.....	51
4.1.2 Preliminary Calculations for a Two-Layered ONIOM(MO:MO) Methods.....	55
4.1.2.1 Strain Energies and Geometrical Structures.....	58
4.1.2.2 Energies and Thermodynamic Quantities.....	62

	Page
4.1.2.3 Reaction Sequence on the Cap-Ended C ₁₂₀ SWCN...	63
4.2 The Chemisorptions of Hydroxide and C1 to C3 Alkoxides.....	64
4.2.1 Geometrical Structures.....	64
4.2.2 Energies and Thermodynamic Quantities.....	72
CHAPTER IV CONCLUSIONS.....	73
5.1 The Adsorptions of Proton and Hydroxide on Various Types of SWCNTs.....	73
5.2 The Chemisorptions of Hydroxide and C1 to C3 Alkoxides.....	73
5.3 Suggestions for Future Work.....	74
REFERENCES.....	75
APPENDICES.....	80
Appendix A.....	81
Appendix B.....	94
Appendix C.....	96
CURRICULUM VITAE.....	109

สถาบันวิทยบริการ
จุฬาลงกรณ์มหาวิทยาลัย

LIST OF FIGURES

Figure	Page
1.1 The structures of carbon nanotubes (a) MWNT and (b) SWCNT.....	2
1.2 A graphene sheet is rolled-up to SWCNT	3
1.3 The graphene honeycomb lattice with the lattice vectors a_1 and a_2 and the chiral vector $C_h = na_1 + ma_2$	4
1.4 The zigzag and armchair patterns along the chiral vector of the graphene lattice.....	6
1.5 The armchair (a) and zigzag (b) single-walled carbon nanotube	6
2.1 The ONIOM extrapolation scheme for a molecular system partitioned into two (left) and three (right) layers.....	35
2.2 Definition of different atom sets within the ONIOM scheme.....	37
3.1 Eight different characteristics of cap-ended and open-ended armchair (5,5) SWCNT structures have been investigated. (a) a perfect cap-ended C_{80} (b) a defect cap-ended C_{80} (c) a perfect open-ended $C_{80}H_{20}$ (d) a defect open-ended $C_{80}H_{20}$ (e) a perfect cap-ended C_{120} (f) a defect cap-ended C_{120} (g) a perfect open-ended $C_{120}H_{20}$ (g) a defect open-ended $C_{120}H_{20}$	41
3.2 Four models have been investigated for high-layered of ONIOM(MO:MO) method (a) a pyrene (C_{16}) as model 1 (b) a 5-6-6-pyrene-5-5-6 (C_{29}) as model 2 (c) a 5-7-7-5 (C_{16}) Stone-Wales defect as model 3 and (d) an ovalene (C_{32}) as model 4.....	42
3.3 The two-layered ONIOM models of cap-ended C_{80} (a) a perfect C_{80} model 1 (b) a perfect C_{80} model 2 and (c) a defect C_{80} model 3.....	42
3.4 The two-layered ONIOM models of cap-ended C_{120} (a) a perfect C_{120} model 1 (b) a perfect C_{120} model 3 and (c) a perfect C_{120} model 4.....	43
3.5 The two-layered ONIOM models of open-ended (a) a perfect $C_{80}H_{20}$ model 1 (b) a defect $C_{80}H_{20}$ model 3 (c) a perfect $C_{120}H_{20}$ model 1 (d) a defect $C_{120}H_{20}$ model 3.....	43

Figure	Page
3.6 The two-layered ONIOM model of SWCNTs for adsorptions proton with hydroxide ion (a) a perfect cap-ended C_{80} model 1 (b) a defect cap-ended C_{80} model 2 (c) a defect cap-ended C_{80} model 3 (d) a perfect cap-ended C_{120} model 4 (e) a defect cap-ended C_{120} model 3 (f) a perfect open-ended $C_{80}H_{20}$ model 1 and (g) a defect open-ended $C_{80}H_{20}$ model 3.....	45
3.7 The high-layered ONIOM method for adsorptions proton, hydroxide ion and water on cap-ended C_{80} model 1 (a) SWCNT- H^+ (b) SWCNT- OH^- (c) SWCNT- H^+-OH^- (d) SWCT- $H^+ H_2O$ (e) SWCT- $OH^- H_2O$ (f) SWCT- $H^+-OH^- H_2O$	46
3.8 The high-layered ONIOM method for adsorptions proton, hydroxide ion and water on cap-ended C_{80} model 2 (a) SWCNT- H^+ (b) SWCNT- OH^- (c) SWCNT- H^+-OH^- (d) SWCT- $H^+ H_2O$ (e) SWCT- $OH^- H_2O$ (f) SWCT- $H^+-OH^- H_2O$	46
3.9 The high-layered ONIOM method for adsorptions proton, hydroxide ion and water on cap-ended C_{80} and C_{120} model 3 (a) SWCNT- H^+ (b) SWCNT- OH^- (c) SWCNT- H^+-OH^- (d) SWCT- $H^+ H_2O$ (e) SWCT- $OH^- H_2O$ (f) SWCT- $H^+-OH^- H_2O$	47
3.10 The high-layered ONIOM method for adsorptions proton, hydroxide ion and water molecule of cap-ended C_{120} model 4 (a) SWCNT- H^+ (b) SWCNT- OH^- (c) SWCNT- H^+-OH^- (d) SWCT- $H^+ H_2O$ (e) SWCT- $OH^- H_2O$ (f) SWCT- $H^+-OH^- H_2O$	47
3.11 The high-layered ONIOM method for the chemisorptions of C1 to C3 alkoxide ions (methoxide ion, ethoxide ion and n-propoxide ion) on cap-ended (C_{80} and C_{120}) and open-ended ($C_{80}H_{20}$ and $C_{120}H_{20}$) perfect as model 1 (a) SWCNT- OMe^- (b) SWCNT- OEt^- (c) SWCNT- OPr^- (d) SWCNT- H^+-OMe^- (e) SWCNT- H^+-OEt^- (f) SWCNT- H^+-OPr^-	48
3.12 The high-layered ONIOM method for the adsorptions C1 to C3 alkoxide ions (methoxide ion, ethoxide ion and n-propoxide ion) on cap-ended (C_{80} and C_{120}) and open-ended ($C_{80}H_{20}$ and $C_{120}H_{20}$) defect as model 3 (a) SWCNT- OMe^- (b) SWCNT- OEt^- (c) SWCNT- OPr^- (d) SWCNT- H^+-OMe^- (e) SWCNT- H^+-OEt^- (f) SWCNT- H^+-OPr^-	49

Figure	Page	
4.1	Optimized structures of various adsorbing species on the perfect capped C_{80} SWCNT computed at HF/3-21G level of theory (a) SWCNT- H^+ (b) SWCNT- OH^- (c) SWCNT- H^+-OH^- (d) SWCNT- $H^+ \cdots H_2O$ (e) SWCNT- $OH^- \cdots H_2O$ (f) SWCNT- $H^+-OH^- \cdots H_2O$ 51	51
4.2	Optimized structures of various adsorbing species on the defect capped C_{80} SWCNT computed at HF/3-21G level of theory (a) SWCNT- H^+ (b) SWCNT- OH^- (c) SWCNT- H^+-OH^- (d) SWCNT- $H^+ \cdots H_2O$ (e) SWCNT- $OH^- \cdots H_2O$ (f) SWCNT- $H^+-OH^- \cdots H_2O$ 51	51
4.3	Optimized structures of various adsorbing species on the perfect open-ended $C_{80}H_{20}$ SWCNTs computed at ONIOM(B3LYP/6-31G(d):AM1) level of theory (a) SWCNT- H^+ (b) SWCNT- OH^- (c) SWCNT- H^+-OH^- (d) SWCNT- $H^+ \cdots H_2O$ (e) SWCNT- $OH^- \cdots H_2O$ (f) SWCNT- $H^+-OH^- \cdots H_2O$... 59	59
4.4	Optimized structures of various adsorbing species on the defect open-ended $C_{80}H_{20}$ SWCNTs computed at ONIOM(B3LYP/6-31G(d): AM1) (a) SWCNT- H^+ (b) SWCNT- OH^- (c) SWCNT- H^+-OH^- (d) SWCNT- $H^+ \cdots H_2O$ (e) SWCNT- $OH^- \cdots H_2O$ (f) SWCNT- $H^+-OH^- \cdots H_2O$ 59	59
4.5	Optimized structures of various adsorbing species on the perfect capped C_{120} SWCNTs computed at ONIOM(B3LYP/6-31G(d) :AM1) level of theory (a) SWCNT- H^+ (b) SWCNT- OH^- (c) SWCNT- H^+-OH^- (d) SWCNT- $H^+ \cdots H_2O$ (e) SWCNT- $OH^- \cdots H_2O$ (f) SWCNT- $H^+-OH^- \cdots H_2O$ 60	60
4.6	Optimized structures of various adsorbing species on the perfect open-ended C_{120} SWCNTs computed at ONIOM(B3LYP/6-31 G(d):AM1) level of theory (a) SWCNT- H^+ (b) SWCNT- OH^- (c) SWCNT- H^+-OH^- (d) SWCNT- $H^+ \cdots H_2O$ (e) SWCNT- $OH^- \cdots H_2O$ (f) SWCNT- $H^+-OH^- \cdots H_2O$... 60	60
4.7	Optimized structures of various adsorbing species on the perfect capped C_{80} SWCNTs computed at ONIOM(B3LYP/6-31G(d) :AM1) level of theory (a) SWCNT- OH^- (b) SWCNT- OMe^- (c) SWCNT- OEt^- (d) SWCNT- OPr^- (e) SWCNT- H^+-OH^- (f) SWCNT- H^+-OMe^- (g) SWCNT- H^+-OEt^- (h) SWCNT- H^+-OPr^- 65	65

Figure	Page	
4.8	Optimized structures of various adsorbed species on the defect capped C_{80} SWCNT computed at ONIOM(B3LYP/6-31G(d):AM1) level of theory (a) SWCNT-OH ⁻ (b) SWCNT-OMe ⁻ (c) SWCNT-OEt ⁻ (d) SWCNT-OPr ⁻ (e) SWCNT-H ⁺ -OH ⁻ (f) SWCNT-H ⁺ -OMe ⁻ (g) SWCNT-H ⁺ -OEt ⁻ (h) SWCNT-H ⁺ -OPr ⁻	65
4.9	Optimized structures of various adsorbed species on the perfect capped $C_{80}H_{20}$ SWCNT computed at ONIOM(B3LYP/6-31G(d): AM1) level of theory (a) SWCNT-OH ⁻ (b) SWCNT-OMe ⁻ (c) SWCNT-OEt ⁻ (d) SWCNT-OPr ⁻ (e) SWCNT-H ⁺ -OH ⁻ (f) SWCNT-H ⁺ -OMe ⁻ (g) SWCNT-H ⁺ -OEt ⁻ (h) SWCNT-H ⁺ -OPr ⁻	66
4.10	Optimized structures of various adsorbing species on the perfect capped $C_{80}H_{20}$ SWCNT computed at ONIOM(B3LYP/6-31G(d): AM1) level of theory (a) SWCNT-OH ⁻ (b) SWCNT-OMe ⁻ (c) SWCNT-OEt ⁻ (d) SWCNT-OPr ⁻ (e) SWCNT-H ⁺ -OH ⁻ (f) SWCNT-H ⁺ -OMe ⁻ (g) SWCNT-H ⁺ -OEt ⁻ (h) SWCNT-H ⁺ -OPr ⁻	66
4.11	Optimized structures of various adsorbed species on the perfect capped C_{120} SWCNT computed at ONIOM(B3LYP/6-31G(d): AM1) level of theory (a) SWCNT-OH ⁻ (b) SWCNT-OMe ⁻ (c) SWCNT-OEt ⁻ (d) SWCNT-OPr ⁻ (e) SWCNT-H ⁺ -OH ⁻ (f) SWCNT-H ⁺ -OMe ⁻ (g) SWCNT-H ⁺ -OEt ⁻ (h) SWCNT-H ⁺ -OPr ⁻	67
4.12	Optimized structures of various adsorbed species on the perfect capped C_{120} SWCNT computed at ONIOM(B3LYP/6-31G(d): AM1) level of theory (a) SWCNT-OH ⁻ (b) SWCNT-OMe ⁻ (c) SWCNT-OEt ⁻ (d) SWCNT-OPr ⁻ (e) SWCNT-H ⁺ -OH ⁻ (f) SWCNT-H ⁺ -OMe ⁻ (g) SWCNT-H ⁺ -OEt ⁻ (h) SWCNT-H ⁺ -OPr ⁻	67
4.13	Optimized structures of various adsorbed species on the perfect capped $C_{120}H_{20}$ SWCNT computed at ONIOM(B3LYP/6-31G(d):AM1) level of theory (a) SWCNT-OH ⁻ (b) SWCNT-OMe ⁻ (c) SWCNT-OEt ⁻ (d) SWCNT-OPr ⁻ (e) SWCNT-H ⁺ -OH ⁻ (f) SWCNT-H ⁺ -OMe ⁻ (g) SWCNT-H ⁺ -OEt ⁻ (h) SWCNT-H ⁺ -OPr ⁻	68

Figure	Page	
4.14	Optimized structures of various adsorbed species on the perfect cap-ended $C_{120}H_{20}$ SWCNT computed at ONIOM(B3LYP/6-31G(d):AM1) level of theory (a) SWCNT-OH ⁻ (b) SWCNT-OMe ⁻ (c) SWCNT-OEt ⁻ (d) SWCNT-OPr ⁻ (e) SWCNT-H ⁺ -OH ⁻ (f) SWCNT-H ⁺ -OMe ⁻ (g) SWCNT-H ⁺ -OEt ⁻ (h) SWCNT-H ⁺ -OPr ⁻	68
A-1	The bond lengths (Å) of the adsorptions of proton, hydroxide ion and water molecule with perfect cap-ended C_{80} SWCNTs computed at the HF/3-21G level of theory.....	81
A-2	The bond lengths (Å) of the adsorptions of proton, hydroxide ion and mono-hydration with perfect cap-ended C_{80} SWCNTs computed at the HF/3-21G level of theory.....	82
A-3	The bond lengths (Å) of the adsorptions of proton, hydroxide ion and mono-hydration with perfect cap-ended C_{80} SWCNTs model 1(high layer) computed at ONIOM(B3LYP/6-31G(d):AM1) level of theory.....	83
A-4	The bond lengths (Å) of the adsorptions of proton, hydroxide ion and mono-hydration with perfect cap-ended C_{80} SWCNTs model 2(high layer) computed at the ONIOM(B3LYP/6-31G(d):AM1) level of theory.....	83
A-5	The bond lengths (Å) of the adsorptions of proton, hydroxide ion and mono-hydration with defect cap-ended C_{80} SWCNTs model 3 (high layer) computed at the ONIOM(B3LYP/6-31G(d) :AM1) level of theory.....	84
A-6	The bond lengths (Å) at a high-layered ONIOM method of the adsorptions of proton, hydroxide ion and mono-hydration with perfect cap-ended $C_{80}H_{20}$ SWCNTs model 1 (high layer) computed at the ONIOM(B3LYP/6-31G(d):AM1) level of theory.....	84
A-7	The bond lengths (Å) of adsorptions of proton, hydroxide ion and mono-hydration with defect cap-ended $C_{80}H_{20}$ SWCNTs model 3 (high layer) computed at the ONIOM(B3LYP/6-31G(d) :AM1) level of theory.....	85
A-8	The bond lengths (Å) of adsorptions of proton, hydroxide ion and mono-hydration with perfect cap-ended C_{120} SWCNTs model 4 (high layer) computed at the ONIOM(B3LYP/6-31G(d) :AM1) level of theory.....	85

Figure	Page
A-9 The bond lengths (Å) of adsorptions of proton and C1 to C3 alkoxide ions with perfect cap-ended C ₈₀ SWCNTs model 1 (high layer) computed at the ONIOM(B3LYP/6-31G(d):AM1) level of theory.....	86
A-10 The bond lengths (Å) of adsorptions of proton and C1 to C3 alkoxide ions with perfect cap-ended C ₈₀ SWCNTs model 3 (high layer) computed at the ONIOM(B3LYP/6-31G(d):AM1) level of theory.....	87
A-11 The bond lengths (Å) of adsorptions of proton and C1 to C3 alkoxide ions with perfect cap-ended C ₈₀ H ₂₀ SWCNTs model 1 (high layer) computed at the ONIOM(B3LYP/6-31G(d):AM1) level of theory.....	88
A-12 The bond lengths (Å) of adsorptions of proton and C1 to C3 alkoxide ions with perfect cap-ended C ₈₀ H ₂₀ SWCNTs model 3 (high layer) computed at the ONIOM(B3LYP/6-31G(d):AM1) level of theory.....	89
A-13 The bond lengths (Å) of adsorptions of proton and C1 to C3 alkoxide ions with perfect cap-ended C ₁₂₀ SWCNTs model 1 (high layer) computed at the ONIOM(B3LYP/6-31G(d):AM1) level of theory.....	90
A-14 The bond lengths (Å) of adsorptions of proton and C1 to C3 alkoxide ions with defect cap-ended C ₁₂₀ SWCNTs model 3 (high layer) computed at at the ONIOM(B3LYP/6-31G(d):AM1) level of theory.....	91
A-15 The bond lengths (Å) of adsorptions of proton and C1 to C3 alkoxide ions with perfect open-ended C ₁₂₀ H ₂₀ SWCNTs model 1 (high layer) computed at the ONIOM(B3LYP/6-31G(d):AM1) level of theory.....	92
A-16 The bond lengths (Å) of adsorptions of proton and C1 to C3 alkoxide ions with defect open-ended C ₁₂₀ H ₂₀ SWCNTs model 3 (high layer) computed at at the ONIOM(B3LYP/6-31G(d):AM1) level of theory.....	93

LIST OF TABLES

Table	Page
4.1	Energies and thermodynamic quantities (in kcal/mol) of adsorption reaction on perfect and defect cap-ended C ₈₀ SWCNTs computed at HF/3-21G level of theory 52
4.2	Strain energies (ΔE_{st}) (in kcal/mol) and binding energies ($\Delta E_{binding}$) for perfect and defect cap-ended C ₈₀ SWCNTs of the various complexes computed at HF/3-21G level of theory 53
4.3	Reaction energies on the perfect cap-ended C ₈₀ SWCNT computed at the various methods..... 56
4.4	Geometrical parameters for the geometries of perfect cap-ended C ₈₀ SWCNT complexes with proton, hydroxide ion and water molecule at various levels of theory..... 57
4.5	Strain energies (in kcal/mol) for C ₈₀ , C ₈₀ H ₂₀ and the cap-ended perfect and defect C ₁₂₀ SWCNTs of the various complexes computed at various levels of theory 61
4.6	Energetic and thermodynamic quantities (in kcal/mol) of adsorption on reactions various types of perfect and defect SWCNTs at different computation models..... 61
4.7	Binding energies (in kcal/mol) for SWCNTs of the various complexes computed at two-layered ONIOM(B3LYP/6-31G(d):AM1) level of Theory..... 69
4.8	Energies and thermodynamic quantities (in kcal/mol) of adsorption reaction on various types of perfect and defect SWCNTs at different computation models..... 70
4.9	Charge on oxygen atom of adsorbing species and adsorption energies (in kcal/mol) in reaction systems on various types of SWCNTs at different computation models..... 71

Table	Page
B-1 The bond lengths (\AA) for the geometries of defect cap-ended C_{80} and defect open-ended SWCNTs (model 3) complexes with proton, hydroxide and water molecule computed at HF/3-21G and ONIOM(B3LYP/6-31G(d) levels of theory.....	94
B-2 Energy gap (in eV) of various types of SWCNTs with adsorbing species computed at ONIOM(B3LYP6-31G(d):AM1).....	36



สถาบันวิทยบริการ
จุฬาลงกรณ์มหาวิทยาลัย

LIST OF ABBREVIATIONS

au	=	Atomic units
AM1	=	Austin model 1
B3LYP	=	Becke's three parameter hybrid functional using the LYP correlation function
DFT	=	Density functional theory
GGA	=	Generalized gradient approximation
HF	=	Hartree-Fock
IMOMO	=	Integrated molecular orbital-molecular orbital
kcal/mol	=	Kilocalorie per mole
KS	=	Kohn-Sham
LCAO	=	Linear combination of atomic orbitals
LDA	=	Local density approximation
LSD	=	Local spin density approximation
LYP	=	Lee-Yang-Parr functional
MM	=	Molecular mechanics
MNDO	=	Modified neglect of differential overlap
MO	=	Molecular orbital
MP2	=	The second-order Møller-Plesset perturbation theory
ONIOM	=	Our own N-layered integrated molecular orbital and molecular mechanics
QM	=	Quantum mechanics
QM/MM	=	Quantum mechanical/molecular mechanical
SCF	=	Self-consistent field
STO	=	Slater type orbital
STO-3G	=	Slater type orbital approximated by 3 gaussian type orbitals
VWN	=	Vosko-Wilk-Nusair functional
ZPE	=	Zero-point energy

CHAPTER I

INTRODUCTION

Carbon nanotubes, a new structure form of carbon discovered in 1991, have attracted scientists' attention due to several interesting properties. The mechanical, chemical, and electrical properties of these new materials were considerably studied.

1.1 Carbon Nanotubes

A carbon nanotube is a member of the fullerene (C_{60}) structural family, whereas fullerene is a spherical shape, a carbon nanotube is a cylindrical one, at least one end typically capped with a hemisphere of the fullerene structure. Produced by arc discharge from carbon electrodes, carbon nanotubes were discovered by Sumio Iijima in 1991. Molecular carbon fiber consists of tiny cylinders of graphite sheets and can be grown by several techniques in the laboratory [1-3]. They can be considered as single molecules, concerning their small size about nanometer in diameter and micrometer long. There are infinitely many ways to turn over a sheet into a cylinder, consequential in different diameters and microscopic structure of the tube. Two main types of nanotubes as called multi-walled nanotubes (MWCNTs) and single-walled nanotubes (SWCNTs) are shown in Figure 1.1. Its MWCNT consists of multiple layers of graphite rolled in to form a tube shape. Their inner and outer diameters are around 5 and 100 nm, respectively. The structure of a SWCNT can be conceptualized by wrapping a one-atom-thick layer of graphite called graphene into a seamless cylinder. MWCNTs are similar to SWCNTs, but much larger diameters. Confinement effects expected to be less dominant than in SWCNTs because of the large circumference.

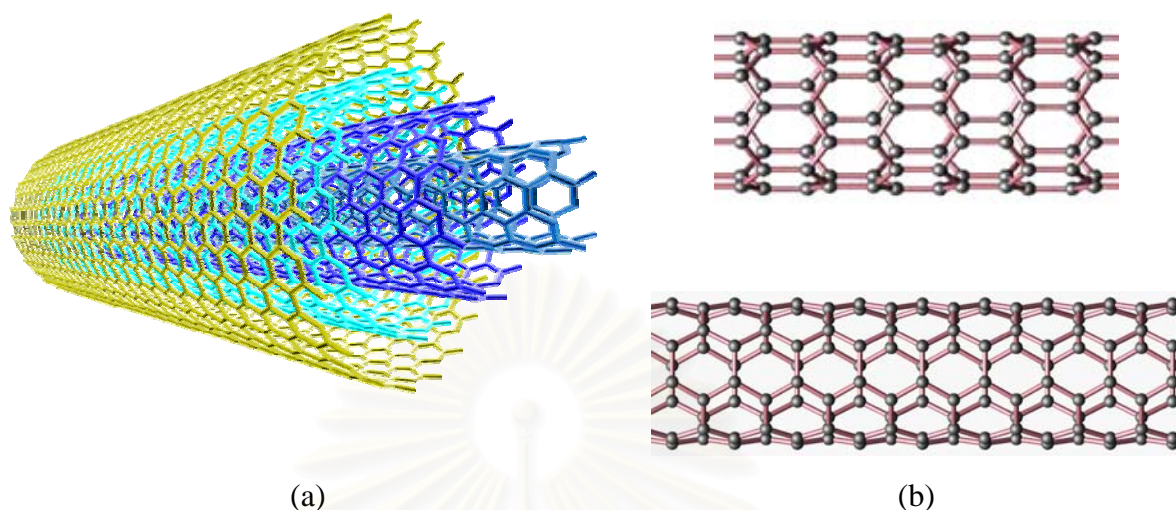


Figure 1.1 The structures of carbon nanotubes (a) MWNT and (b) SWCNT

Studied theoretically and experimentally in different field such as mechanics [4-5], optics [6], electronics and others [7-9], many properties of the MWNTs are already quit close to graphite. Some properties of carbon nanotube can be explained within a macroscopic model of a homogeneous cylinder, whereas others depend crucially on the microscopic structure of the tubes. The fairly complex microscopic structure with tens to hundreds of atoms in the unit cell can be described in a very general way with the help of the nanotube symmetry. Single-walled carbon nanotubes are a very important variety of carbon nanotube because they exhibit important electric properties that are not shared by the multi-walled carbon nanotube (MWNT) variants and SWNTs can be excellent conductors.

1.2 Single-Walled Carbon Nanotube

Single-walled carbon nanotube (SWCNT) can be imagined as rolled-up rectangular strips of hexagonal graphite monolayers. Working with SWCNTs grown by conventional laser ablation methods [10], the atomic structure of carbon nanotubes can be investigated either by direct imaging techniques, such as transmission electron microscopy [11] or scanning probe microscopy [12]. The short side of the rectangle becomes the tube diameter and therefore is quantized by the requirement that the rolled-up tube must have a continuous lattice structure. Similarly, the rectangle must be properly oriented with respect to the flat hexagonal lattice, which allows only a finite number of roll-up choices.

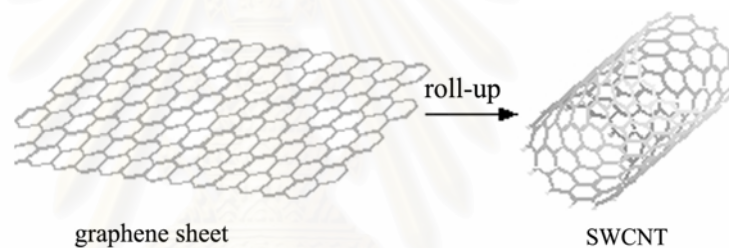


Figure 1.2 A graphene sheet is rolled-up to SWCNT.

1.2.1 Vector Notation for SWCNTs

Because of their microscopic structure are closely related to graphene, the SWCNTs tubes are usually labeled in term of the graphene lattice vector, which label C_h . Figure 1.3 shows the graphene honeycomb lattice. The unit cell is spanned by the two vectors a_1 and a_2 contains two carbon atoms. In carbon nanotube, the graphene sheet is rolled up in such a way that a graphene lattice vector becomes the circumferential of the tube. Thus the vector C_h can be expressed as

$$C_h = na_1 + ma_2 \quad (1.1)$$

This circumferential vector C_h , which is usually denoted by the pair of integers (n,m) , is called the chiral vector and uniquely defines a particular tube.

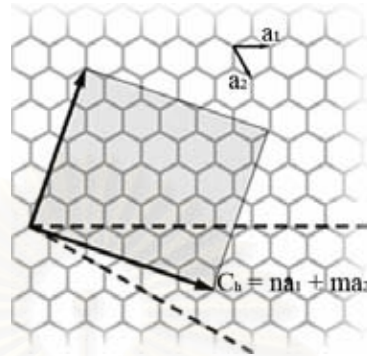


Figure 1.3 The graphene honeycomb lattice with the lattice vectors a_1 and a_2 and the chiral vector $C_h = na_1 + ma_2$.

The direction of the chiral vector measured by the chiral angle θ , which is defined as the angle between a_1 and C_h . The chiral angle can be calculated from

$$\cos \theta = \frac{a_1 \cdot C_h}{|a_1| |C_h|} = \frac{n_1 + m/2}{\sqrt{n^2 + nm + m^2}} \quad (1.2)$$

For each tube with θ between 0° and 30° an equivalent tube with θ between 30° and 60° is found, but the helix of graphene lattice points around the tube changes from right-hand to left-hand.

The geometry of the graphene lattice and chiral vector of tube determine its structural parameters like diameter, unit cell, and its number of carbon atoms. Then diameter of the tube is given by the length of the chiral vector

$$d = \frac{|C_h|}{\pi} = \frac{a_0}{\pi} \sqrt{n^2 + nm + m^2} = \frac{a_0}{\pi} \sqrt{N} \quad (1.3)$$

where $N = n^2 + nm + m^2$. The smallest graphene lattice vector a perpendicular to C_h defines the translational period a along the tube axis. Thus, the nanotubes unit cell is formed by a cylindrical surface with height a and diameter d . the number of carbon atoms

in the unit cell, n_c , can be calculated from the area $S_t = aC_h$ of the cylinder surface and area S_g of the hexagonal graphene unit cell. The ratio of these two gives the number q of graphene hexagons in the nanotubes unit cell.

$$q = \frac{S_t}{S_g} = \frac{2(n^2 + nm + m^2)}{n\mathfrak{R}} \quad (1.4)$$

Where $\mathfrak{R} = 3$ if $(n-m)/3n$ is integer and $\mathfrak{R} = 1$ otherwise. Since the graphene unit cell contains two carbon atoms, there are carbon atoms in the unit cell of the nanotube.

$$n_c = 2q = \frac{4(n^2 + nm + m^2)}{n\mathfrak{R}} \quad (1.5)$$

In achiral tubes, $q = 2n$.

1.2.2 Structure of SWCNTs

There are two possible high symmetry structures for SWCNTs, known as zigzag and armchair. The simplest way of specifying the structure of an individual tube is in term of a chiral vector, which label C_h , jointing two equivalent points on the original graphene lattice. The cylinder is produced by rolling up the sheet such that the two end-point of the vector are superimposed. The chiral vector thus forms the circumference of the nanotubes circular cross-section, and different values of n and m lead to different nanotube structures. Because of the symmetry of the honeycomb lattice, many of the cylinders produced in this way will be equivalent. Figure 1.4 shows a small part of this point on the lattice labeled. Each pair of integers (n,m) represents a possible tube structure. It can be seen that $m = 0$ ($n,0$) are called zigzag tubes and their chiral angle is 0° . Because they exhibit a zigzag pattern along the circumference, while $n = m$ (n,m) are called armchair tubes and their chiral angle is 30° . Both, zigzag and armchair tubes are called achiral tubes.

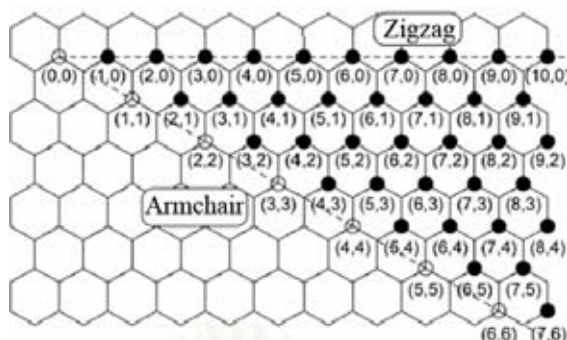


Figure 1.4 The zigzag and armchair patterns along the chiral vector of the graphene lattice.

The most basic properties of SWCNTs, such as diameter, chirality, and the lattice vector along the tube axis are described above. To obtain geometrically the atomic positions of a given (n,m) nanotube, we could construct the corresponding graphene rectangle and roll it up into a cylinder. The atomic positions are, on the other hand, determined by the chiral indices (n,m) as well. SWCNTs are still very expensive to produce, and the development of more affordable synthesis techniques is vital to the future of carbon nanotechnology.

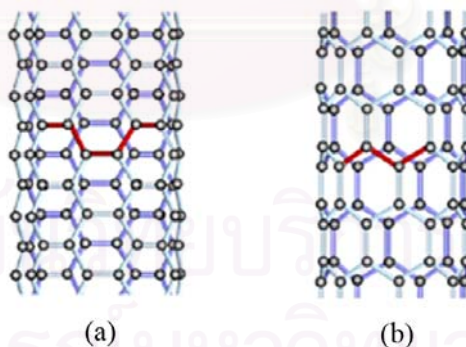


Figure 1.5 The armchair (a) and zigzag (b) single-walled carbon nanotube.

1.2.3 Properties of SWCNTs

The properties of carbon nanotubes are different from those of graphite because of their strain and nonplanar morphology [13]. The curvature leads to a loss of spatial overlap of the atomic p orbitals and a shift in hybridization of the carbon atoms from the sp^2 of graphite. Carbon nanotubes have two types of bonds. Along the cylinder wall the σ bonds form the hexagonal network, which is found in graphite in its pure form. The π bonds point perpendicular to the nanotubes surface. This bonding structure, which is stronger than the sp^3 bonds found in diamond, provides the molecules with their unique strength.

1.2.3.1 Physical Properties

Mechanical Properties

The strength of the sp^2 carbon-carbon bonds gives carbon nanotubes amazing mechanical properties. The stiffness of a material is measured in terms of its Young's modulus [14], the much smaller Van der Waals for defining Young's modulus and tensile strength, the rate of change of stress with applied strain. The Young's modulus of the best nanotubes can be as high as 1000 GPa which is higher than steel. The tensile strength, or breaking strain of nanotubes can be up to 63 GPa which is higher than steel. These properties, coupled with the lightness of carbon nanotubes, gives them great potential in applications such as aerospace.

Electrical Properties

The in-plane σ bonds are most important for the electronic properties of carbon nanotubes. Especially notable is the fact that nanotubes can be metallic or semiconductor character depending on diameter and chirality of the tubes. There are two basic approaches to calculate the electronic energy bands of a material. The idea of the free-electron approximation is that the electrons in a crystal move essentially as free particle.

Due to symmetry and unique electronic structure of graphene, the structure of a nanotube strongly affects its electronic properties. For a given (n,m) nanotube, if $2n + m = 3q$ (where q is an integer), then the semiconductor is metallic, otherwise the nanotube is a semiconductor. Thus all armchair ($n=m$) nanotubes are metallic. Some nanotubes have conductivities higher than that of copper, while others behave more like silicon. This is great interest in the possibility of constructing nanoscale electronic devices from nanotubes, and some progress is being made in this area.

1.2.3.2 Chemical Properties

Carbon nanotubes are insoluble in all organic solvents and aqueous solutions. They can be dispersed in some solvents by sonication, but precipitation immediately occurred when this process is interrupted [15]. In contrast, it has been indicated that carbon nanotubes can interact with different types of compounds. The development of efficient methodologies for the chemical modification of carbon nanotube has simulated the preparation of soluble carbon nanotube that can be employed in several biological applications [16]. The functionalization approaches are widely employed for modification of carbon nanotube, can be oxidized using strong acid and generating carboxylic groups. Chemical modification of carbon nanotubes has attracted great attention to modify their chemical and physical properties. There are mainly two types of functionalization approaches for modification, side wall and terminal functionalizations [17]. Firstly, required functional groups are directly attached to the surface of carbon nanotubes by forming covalent bond, such hydrogenation, and noncovalent functionalization can be achieved from noncovalent interaction, such as hydrophobic π -stacking and adsorption. Secondly, commonly refer to the use of nanotube-bound carboxylic acids to improve their solubility.

SWCNTs have a large specific surface area exhibited very good adsorption properties lead to given their capacity for adsorption, such as adsorbing the gaseous molecule on the surface. The adsorption properties provide the opportunities for applications, such as gases storage [18]. These SWCNT structures contain a number of different adsorption sites with different adsorption potential. Both experimental and

theoretical chemistry were studied the physisorption and chemisorption of hydrogen [19], carbon tetrafluoride [20], nonane [21], nitrogen [22], protein [23], oxygen and water [24], methane and krypton [25] with carbon nanotubes. Recently, carbon nanotubes have been reported as supports for catalyst [26].

1.3 Defect Structures of SWCNTs

Perfect graphene sheets and carbon nanotubes are known to have high chemical stability and unique physical properties resulting from the strong π -interaction of their hexagonal network. However, defects are believed to have a role in physical and chemical properties of graphenes and carbon nanotubes. As with any material, the existence of defect affects the material properties. Defects can occur in the form of atomic vacancies, dopants, pentagon and heptagon. Recently, experimental and theoretical investigations revealed that these defective sites are chemically more reactive than the perfect sites in carbon nanotubes [27]. Defects inevitably arise during the growth of SWCNTs and may also be introduced after some post synthesis. It is also known that defects have a substantial influence on the observed chemical behavior of carbon nanotubes. Another well-known form of defect that occurs in carbon nanotubes is known as the “Stone Wales” defect or pyracylene, transformation, which is the 90° rotation of two carbon atoms with respect to the midpoint of the bond, which creates a pentagon and heptagon pair (5-7-7-5) by rearrangement of the bonds, as shown in Figure 1.6.

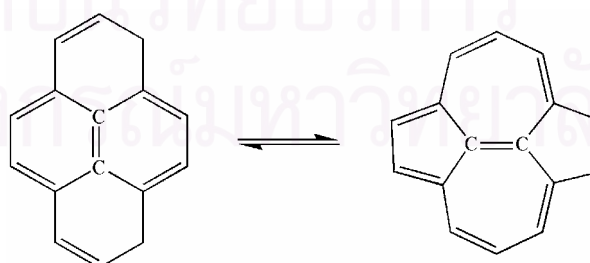


Figure 1.6 The “Stone-Wales defect” of SWCNT.

The Stone-Wales transformation is also used to describe the structural changes of sp^2 -bonded carbon nanosystems, is thought to have important implications for nanotubes mechanical properties. By theoretical studies, Lu *et al.* [27] investigation revealed the higher chemical reactivity of Stone-Wales defect sites than that of perfect in the side walls of zigzag SWCNTs. Yang *et al.* [28] indicated that the electronic properties of the metallic carbon nanotubes with a Stone-Wales defect share some common characters on electronic conductance of the tubes.

1.4 Adsorption

Adsorption occurred on solid surface is a very important due to its wide potential application involved in the reaction with the surface of solid catalyst in the catalysis district. Generally, the investigations about the adsorption on solid surface can approximately be classified into two categories. One is the adsorption on the perfect surface, the other happens on the defective surface. It is normally agreed that the perfect surface, under most conditions, is chemically inert towards the adsorption and dissociation of small molecules and, in discrete contrast, the surface with various defect is able to display relatively high surface reactivity and thus contributes to the catalytic reaction. Molecules and atoms can attach to surface of solid to two ways, physisorption (or physical adsorption) and chemisorption (or chemical adsorption).

1.4.1 Physisorption

Physisorption is mainly the result of Van der Waals interactions between the molecules of the adsorbing surface (the adsorbent) and the adsorbate molecules. Van der Waals interactions have a long range but are weak, and the energy released when a particle is physisorbed and often results in the formation of multilayers of adsorbate molecules. Physisorption usually in the dominated at very low temperatures and occurs very rapidly.

1.4.2 Chemisorption

In chemisorption a bond is usually formed that is stronger than a Van der Waals bond. It need not be a covalent bond and tends to find sites that maximize their coordination number with adsorbate molecules. The enthalpy of chemisorption is greater than that for physisorption. A chemisorbed molecule may be torn apart at the demand of the surface atoms.

The enthalpy of adsorption depends on the extent of surface coverage, mainly because the adsorbate molecules interact. If the adsorbate molecules repel each other the enthalpy of adsorption becomes less exothermic as coverage increase. If the adsorbate molecules attract each other, then they tend to cluster together in island, and growth occurs at the borders.

1.5 Literature Reviews

Extensive theoretical and experimental research investigated properties and chemical reactivity of single-walled carbon nanotubes, especially, functionalization [15], adsorption properties. SWCNTs exhibit excellent adsorption properties, both physisorption and chemisorption because of their high specific surface. Both experimental and computational chemistry explored very good adsorption properties to lead to many applications, such as gas sensor [18], biosensor [16], hydrogen storage [14], electronic device [7-9,29]. In 2001, Chang *et al.* [30] studied the adsorption of ammonia and nitrogen dioxide molecules on the zigzag (10,0) SWCNT using density functional theory. The calculations result indicated that both ammonia and nitrogen dioxide molecules are bound to SWCNT via physisorption. The electron charge transfer is found to be from SWCNT to nitrogen dioxide molecule from ammonia to SWCNT. Ellison *et al.* [31] are also investigated the adsorption of ammonia and nitrogen dioxide on heterogeneous bundle of SWCNTs using FTIR spectroscopy and temperature-programmed desorption (TPD). Both ammonia and nitrogen dioxide adsorbed at room temperature. The FTIR data suggest that ammonia interact with the SWCNTs via both the

lone pair, electrons and of hydrogen atom. TPD data confirm that ammonia and nitrogen dioxide are adsorbed on SWCNTs and that nitrogen dioxide is slightly more strongly bound than ammonia.

In 2002, Ricca and Drocco [32] studied the physisorption and chemisorption of oxygen molecule on the inner and outer walls of the closed-ended zigzag (9,0) SWCNT using the ONIOM(B3LYP/6-31G+(d,p):UFF) method and MP2 correlation. Oxygen molecule occurring physisorbed both inner and outer walls of SWCNTs but the binding energies is weak by about 2.46, 2.28 kcal/mol, respectively, and occurred above a six-membered ring and a lot of charge transfer happens. Chemisorption being above a double bond on the outer walls is favorable by about 20 kcal/mol but has a very high barrier of 64.56 kcal/mol. Sorescu and Jordan [33] studied the adsorption of oxygen atoms and oxygen molecules on graphite and zigzag (8,0) SWCNT using spin-polarized density functional theory employing the PW91 plane-wave basis set. An oxygen atom is bound to graphite and to the outside and inside surface of SWCNT to give stable epoxide-like structures. Adsorption energy of these is 44 kcal/mol. It was found that the oxygen molecule showed very weakly physisorb to graphite and SWCNT surface and reaction of oxygen molecule with the SWCNT surface to give two epoxide groups.

In 2003, Chakrapani *et al.* [34] studied the chemisorption of acetone on the open-ended zigzag (9,0) and (10,0) perfect and Stone-Wales defect SWCNTs using temperature-programmed desorption (TPD), X-ray photoelectron spectroscopy, Raman spectroscopy and ONIOM(PW91/3-21G:PM3) method. All experiments confirm that acetone chemisorbs on perfect and Stone-Wales defect SWCNTs. The theoretical calculations are good agreement with the experimental TDP data and found that high the binding energies for chemisorption are 23.1 and 16.1 kcal/mol for Stone-Wales defect SWCNTs. The binding energy also depends on the diameter of the carbon nanotube.

In this year, Luo *et al.* [35] performed density functional theory calculations with Dmol 3 code, found that oxygen and water are adsorbed on the tip of closed and open-ended zigzag (9,0) SWCNT. Oxygen molecules can be adsorbed on the end of closed SWCNT but they decompose and chemisorbed on the end of open-ended SWCNT. Water molecules can be adsorbed on the end of both closed and open-ended SWCNTs and extra negative charge strengthens the adsorption. As, Ellison *et al.* (2005) [36] investigated the

interaction of water with SWCNT using FTIR spectroscopy and density functional theory (B3LYP/STO-3G) calculations. FTIR data confirm that the water molecules adsorbed on SWCNT at room temperature, forming C-O bond. The calculated results for zigzag (7,0) SWCNT model with defect site on the tube wall indicate that cleavage of an O-H bond upon adsorption to form adsorbed -H and -OH groups is energetically favorable at defect sites.

In 2004, Han and Lee [37] using density functional theory investigated physisorption and chemisorption properties of hydrogen on the zigzag (10,0) SWCNT walls. The most stable state of physisorption of hydrogen outside the SWCNT with a vertical orientation to the tube axis above the center of a hexagon surface SWCNT and the binding energy is very weak is about -0.792 kcal/mol. Two atoms of hydrogen can be chemisorption above two adjacent carbon atoms of a hexagon surface of SWCNT with a C-H bond length of 1.10 Å and one C-H bond energy of -45.761 kcal/mol. The reaction pathway and transition state are also investigated. It is found that Gibbs free energy changes from physisorption to chemisorption.

In 2005, Bettinger [38] studied the reactivity at the sidewalls of perfect and Stone-Wales defect armchair (5,5) and zigzag (10,0) SWCNTs with methylene group using density functional theory (PBE/6-31G(d)//PBE/3-21) imposing periodic boundary conditions (PBCs). In the calculation results of infinite tube models (PBCs) are indicated that the reaction energy for methylene addition to various models confirm that Stone-Wales defects are more highly reactive than perfects SWCNTs wall both armchair and zigzag. The methylene additions are exothermic. While some of the bonds show higher reactivity than those in the perfect tubes, others are less reactive.

In 2005, Xu and Li [39] studied the adsorption of nitrogen molecule with active sites of open-ended armchair (5,5) and zigzag (8,0) SWCNTs using ONIOM(B3LYP/6-31G(d):PM3) method. The nitrogen molecule can be chemisorbed at the edge site of zigzag SWCNT surface and the N-N bond is activated but physisorbed on the sidewall is very weak and no charge transfer between the nitrogen molecule and SWCNT. The adsorption of nitrogen molecule at the edge of armchair SWCNT surface is quit weak. The zigzag edge sites of a SWCNT with open tips are much more active centers for the adsorption and activation of nitrogen molecule.

In 2005, Gómez and Martínez-Magadán [40] using density functional theory within a generalized gradient approximation (GGA//B3LYP/DZVP) studied the adsorption both physisorption and chemisorption processes of dibenzothiophene on open-ended zigzag (7,7) and chiral (10,5) carbon nanotubes. The energy for the physisorption process of the zigzag (7,7) and chiral (10,5) carbon nanotubes was 30.59 and 79.44 kcal/mol, respectively, while for the chemisorption process was 130.15 and 152.26 kcal/mol, respectively. The calculated results suggested that the physisorption process is more likely to occur for the zigzag (7,7) than for the chiral (10,5) carbon nanotubes.

In 2006, Mavrandonakis [41] studied the interaction of various glycine radicals on the side walls both armchair (4,4) and zigzag (8,0) SWCNTs using density functional theory employing the B3LYP functional. The calculated results found that the interaction potentials of the N-centered glycine radical with the SWCNT having a smallest amount was 16.9 kcal/mol and 20.2 kcal/mol for an armchair and a zigzag, respectively. On the other hand, the C-centered radical can be bound to the SWCNT walls with endothermic reaction

In 2006, Crespo and Yang [42] investigated the adsorption of benzene, thiophene and cyclohexane on SWCNTs using standard gravimetric techniques. The experiments data confirm the adsorption depended on diameter, thus stronger adsorption occurs for the smaller SWCNTs. Isothermic heats of adsorption were calculated from the adsorption isotherms and followed the order thiophene, benzene and cyclohexane, respectively.

To the best of our knowledge there is no experimental and theoretical report about the adsorption of hydroxide and alkoxide on carbon nanotube. The main propose of the research is to calculate the adsorption of hydroxide and C1 to C3 alkoxides on various SWCNTs by *ab initio* and two-layered ONIOM(MO:MO) methods. Theoretical adsorption studies both on perfect and defect tubes offer an useful information. Besides that, the study also gives the elementary information to bring the single-walled carbon nanotube with hydroxide and alkoxide to become used as catalysts, because hydroxide and alkoxide groups are strong bases.

1.6 Objectives

The objective of this study is to investigate the chemisorption of hydroxide and C1 to C3 alkoxide ions on the perfect and defect armchair (5,5) SWCNTs of the capped C_{80} , C_{120} and open-ended $C_{80}H_{20}$, $C_{120}H_{20}$ using *ab initio* Hartree–Fock (HF) with 3-21G basis set and two-layered ONIOM(MO:MO) methods. The geometry optimization were obtained at HF/3-21G level of theory and two-layered ONIOM(MO:MO) methods at the ONIOM(HF/3-21G:AM1), ONIOM(HF/3-21G:PM3), and ONIOM(B3LYP/6-31G(d):AM1) levels of theory. The binding energies and thermodynamic properties of the adsorptions of proton, hydroxide ion and water on various types of armchair (5,5) SWCNTs were obtained at the HF/3-21G and ONIOM(B3LYP/6-31G(d):AM1) calculations. The geometry, energetic and thermodynamic quantities of the chemisorptions of hydroxide ion and C1 to C3 alkoxide ions on various types of armchair (5,5) SWCNTs were obtained at ONIOM(B3LYP/6-31G(d):AM1) level of theory.

CHAPTER II

THEORETICAL BACKGROUND

Quantum chemistry applied quantum mechanics to problems in chemistry. The influence of quantum chemistry is evident in all branches of chemistry. Physical chemists use quantum mechanics to calculate thermodynamic properties of gases; to interpret molecular spectra, thereby allowing experimental determination of molecular properties; to calculate molecular properties theoretically; to calculate properties of transition states in chemical reactions [43].

2.1 Ab Initio Method

A quantum mechanic was first applied to molecules of real chemical systems, that dose not rely on calibration against measured chemical parameters and it therefore called *ab initio*. The term *ab initio* is a Latin meaning “from the first”. The simplest kind of *ab initio* is Hartree-Fock (HF) approximation.

2.1.1 The Hartree-Fock Method

The Hartree-Fock method is the basis of molecular theory, may be solved by mapping the orbitals on a set of grid point. The starting point for the Hartree-Fock method is a set of approximate one-electron wavefunctions known as orbitals. For a molecular or crystalline calculation, the initial approximate one-electron wavefunctions are typically a linear combination of atomic orbitals (LCAO). The simplest possible way of making Ψ as a combination of these molecular orbitals is by forming their Hartree product [44].

$$\Psi_0 = \psi_0(1)\psi_0(2)\psi_0(3)\dots\dots\dots\psi_0(n) \quad (2.1)$$

Here ψ_0 is a function of the coordinates of all electrons in the atom, $\psi_0(1)$ is a function of the coordinates of electron 1, $\psi_0(2)$ is a function of the coordinates of electron 2, etc., the one- electron $\psi_0(1)$, $\psi_0(2)$, etc. are called atomic orbitals. To apply the Hartree process, to solved one-electron Schrödinger equation in which the electron- electron repulsion comes from electron one and an average, smeared-out electrostatic field calculated from $\psi_0(2)\psi_0(3)\dots\dots\dots\psi_0(n)$, due to all other electrons. Solving this equation gives $\psi_1(1)$, an improved version of $\psi_0(1)$, next solved for electron 2 a one-electron Schrödinger equation with electron two moving in an average field due to the electrons of $\psi_1(1)\psi_0(3)\dots\dots\dots\psi_0(n)$, continuing to electron n moving in an a field due to $\psi_1(1)\psi_1(2)\dots\dots\dots\psi_1(n-1)$. These completes the first cycle calculations and gives

$$\Psi_1 = \psi_1(1)\psi_1(2)\psi_1(3)\dots\dots\dots\psi_1(n) \quad (2.2)$$

Repetition of the cycle gives

$$\Psi_2 = \psi_2(1)\psi_2(2)\psi_2(3)\dots\dots\dots\psi_2(n) \quad (2.3)$$

The process is continued for k cycles till we have a wavefunction ψ_k and energy calculated from ψ_k that are essentially the same as the wavefunction and energy from the previous cycle.

2.1.2 Slater Determinants

The Hartree wavefunction is product of one-electron functions called orbitals, these are functions of the usual space coordinates x , y , z . It is convenient to write it as a sum of permutations over the diagonal of the determinant. The Slater wavefunction is composed, not just of spatial orbitals, but of spin orbitals. A spin orbital ψ (spin) is the

product of a spatial orbital and a spin function, α or β . To construct a Slater wavefunction (Slater determinants) for a closed-shell species, we used each of the occupied spatial orbitals to make two spin orbitals, by multiplying the spatial orbital by α and, separately, by β . The spin orbitals are then filled with the available electrons. Slater determinants enforce the Pauli exclusions principle, which forbids any two electrons in a system to have all quantum number the same, two rows (or columns, in the alternative formulation) would be identical and the determinant, hence the wavefunction would vanish. For $2n$ electrons the general form of a Slater determinant is clearly the $2n \times 2n$ determinant

$$\Psi_{2n} = \frac{1}{\sqrt{(2n)!}} \times \begin{vmatrix} \psi_1(1)\alpha(1) & \psi_1(1)\beta(1) & \psi_2\alpha(2)\psi_2\beta(2) & \psi_2(1)\beta(1) & \dots & \psi_n(1)\beta(1) \\ \psi_1(2)\alpha(2) & \psi_1(2)\beta(2) & \psi_2\alpha(2)\psi_2\beta(2) & \psi_2(2)\beta(2) & \dots & \psi_n(2)\beta(2) \\ \vdots & \vdots & \vdots & \vdots & & \\ \psi_1(2n)\alpha(2n) & \psi_1(2n)\beta(2n) & \psi_2\alpha(2n)\psi_2\beta(2n) & \psi_2(2n)\beta(2n) & \dots & \psi_n(2n)\beta(2n) \end{vmatrix} \quad (2.4)$$

The Slater determinant for the total wavefunction Ψ of a $2n$ -electron atom or molecule is a $2n \times 2n$ determinant with $2n$ rows due to the $2n$ electron and $2n$ columns due to the $2n$ spin orbitals Ψ , since these are closed-shell species, the number of spatial orbitals ψ is half the number of electrons.

2.1.3 Atomic and Molecular Energy

The HF equations is to express the energy of the molecule or atom in terms of the total wavefunction Ψ , the energy will then be minimized with respect to each of the component molecular spin orbitals $\psi\alpha$ and $\psi\beta$. The derivation of these equations involves considerable algebraic manipulation, which is at times hard to follow without actually writing out the intermediate expression. It followed from the Schrödinger equation that the energy of a system is given by

$$E = \frac{\int \Psi^* \hat{H} \Psi d\tau}{\int \Psi^* \Psi d\tau} \quad (2.5)$$

The total wavefunction Ψ has been specified and allowance has been made for the possibility of Ψ being a complex function by utilizing its complex conjugate Ψ^* , this ensures that E , the energy of the atom or molecule, will be real. If Ψ is complex then $\Psi^2 d\tau$ will not be a real number, while $\Psi^* \Psi d\tau = |\Psi|^2 d\tau$ will, as must be the case for a probability. Integration is with respect to three spatial coordinates and spin coordinate, for each electron. This is symbolized by $d\tau$, which means $dx dy dz$, so for a $2n$ -electron system these integrals are actually $4 \times 2n$ -fold, each electron having its set of four coordinates. Working with the usual normalized wavefunctions makes the denominator unity can then be written as

$$E = \int \Psi^* \hat{H} \Psi d\tau \quad (2.6)$$

The Slater determinant and the molecular Hamiltonian gives, after much algebraic manipulation

$$E = 2 \sum_{i=1}^{electron} H_{ii} + \sum_{i=1}^{electron} \sum_{j=1}^{electron} (2J_{ij} - K_{ij}) \quad (2.7)$$

for the electronics energy of a $2n$ -electron molecule, the term in (2.19) have these meaning

$$H_{ii} = \int \psi_i^*(1) \hat{H}^{core}(1) \psi_i(1) dv \quad (2.8)$$

where

$$\hat{H}^{core}(1) = -\frac{1}{2} \nabla_1^2 - \sum_{all \mu} \frac{Z_\mu}{r_{\mu 1}} \quad (2.9)$$

The operator \hat{H}^{core} is so called because it leads to H_{ii} , the electronic energy of a single electron moving simply under the attraction of a nuclear “core”, with all the other electrons stripped away, H_{ii} is the electronic energy of species. The $\hat{H}^{core}(1)$ represented

the kinetic energy of electrons 1 plus the potential energy of attraction of that electron to each of the nuclei μ . In summation, over the discrete spin variable, these give 0 or 1. We are left three integration variable (x, y, z) and so the integral is threefold.

$$J_{ij} = \int \psi_i^*(1)\psi_i(1)\frac{1}{r_{12}}\psi_j^*(2)\psi_j(2)dv_1dv_2 \quad (2.10)$$

J is called a coulomb integral, it represents the electrostatic repulsion between an electron in ψ_i and one in ψ_j . The integrals J and K allow each electron to experience the average electrostatic repulsion of a charge could due to all the other electrons. J represents potential energy corresponding to a destabilizing electrostatic repulsion, it is positive. As for H_{ii} , the integration is with respect to spatial coordinates because the spin coordinates have been integrated out. The ab initio coulomb integral J is not the same as what we called a coulomb integral, the ab initio coulomb integral can also be written

$$J_{ij} = \int \psi_i^*(1)\psi_j^*(2)\left(\frac{1}{r_{12}}\right)\psi_j^*(1)\psi_j(2)dv_1dv_2 \quad (2.11)$$

the repulsion between electron 1 and 2 can be written

$$K_{ij} = \int \psi_i^*(1)\psi_j^*(2)\left(\frac{1}{r_{12}}\right)\psi_j^*(1)\psi_j(2)dv_1dv_2 \quad (2.12)$$

K is called exchange integral, mathematically it arises from Slater determinant expansion terms that differ only in exchange of electrons [44].

2.2 Basis set

A basis set used in chemistry is a set of mathematical functions (basis functions) used to create the molecular orbitals, which are expanded as a linear combination of such functions with the weights or coefficients to be determined, which yield molecular orbitals. When molecular calculations are performed, it is common to use a basis composed of a finite number of atomic orbitals, centered at each atomic nucleus within the molecule. These basis functions are usually centered on the atomic nuclei and so bear some resemblance to atomic orbitals. Approximating molecular orbitals as linear combinations of basis functions is usually called LCAO or linear combinations of atomic orbitals approach, although the functions not necessarily conventional atomic orbitals, they can be any set of mathematical functions that are convenient to manipulate and which in linear combinations give useful representations of molecular orbitals. The basis functions describe the electron distribution around an atom combining atomic basis functions yields the electron distribution in the molecule as a whole.

Slater functions are good approximations to atomic wavefunctions and would be the natural choice for ab initio basis functions, were it not for the fact that the evaluation of certain two-electron integrals requires excessive computer time if Slater functions are used. Actually, things are a little more complicated. A single Gaussian is a poor approximation to the nearly ideal description of an atomic wavefunction that a Slater function provides. The solution to the problem of this poor function behaviour is to use several Gaussians to approximate a Slater function. In the simplest version of this basis, n Gaussian functions are superimposed with fixed coefficients to form one Slater type orbital (STO) [45].

An individual molecular orbital is defined as

$$\phi_i = \sum_{\mu=1}^N c_{\mu i} \chi_{\mu} \quad (2.13)$$

where the coefficients $c_{\mu i}$ are known as the *molecular orbital expansion coefficients*. The basis functions $\chi_1 \dots \chi_N$ are also chosen to be normalized.

2.2.1 Minimal Basis Sets

A minimal basis set consists of one Slater functions for each inner-shell and valence-shell atomic orbitals of each atom. The essential idea of the minimal basis set is that we select one basis function for every atomic orbital that is required to describe the free atom. Several minimal basis sets are in common use, but by far the most common are the STO-nG basis sets, $n = 3, 4, 5,$ and 6 . The individual GTOs are called primitive orbitals, while the combined functions are called contracted functions. The STO-nG basis sets are available for almost all elements in the periodic table.

The STO-3G basis set introduces us to the concept of contracted shell in constructing contracted Gaussian from primitive Gaussian. The Gaussian of a contraction shell share common exponents. Example carbon has one s shell and sp shell. This means that the $2s$ and $2p$ Gaussians share common α exponents (which differ from those of the $1s$ functions). Consider the contracted Gaussians.

$$\begin{aligned}\phi(2s) &= d_{1s}e^{-\alpha_{1s}r} + d_{2s}e^{-\alpha_{2s}r} + d_{3s}e^{-\alpha_{3s}r} \\ \phi(2p_x) &= d_{1p_x}e^{-\alpha_{1p}r} + d_{2p_x}e^{-\alpha_{2p}r} + d_{3p_x}e^{-\alpha_{3p}r} \\ \phi(2p_y) &= d_{1p_y}e^{-\alpha_{1p}r} + d_{2p_y}e^{-\alpha_{2p}r} + d_{3p_y}e^{-\alpha_{3p}r} \\ \phi(2p_z) &= d_{1p_z}e^{-\alpha_{1p}r} + d_{2p_z}e^{-\alpha_{2p}r} + d_{3p_z}e^{-\alpha_{3p}r}\end{aligned}$$

2.2.2 Split-Valence Basis Sets

A split-valence basis set uses two (or more) GTOs for each valence atomic orbital but only one GTO for each inner-shell (core) atomic orbital. A split-valence basis set is minimal for inner-shell atomic orbitals and double zeta for the valence atomic orbitals. Split-valence basis sets are called valence double zeta (VDZ), valence triple zeta (VTZ), according to the number of GTOs used for each valence atomic orbitals.

$3-21G$ (pronounced “three two one jee”) The valence functions are split into one basis function with two GTOs, split each valence orbitals into two part, an inner shell and an outer shell, and one with only one GTO. The core orbitals are each represented by one basis functions, each composed of three Gaussian.

6-31G (pronounced “six three one jee”) The core consists of six primitives in inner-shell GTOs which are not split, while the valence orbitals are described by one orbital constructed valence-shell atomic orbitals from three primitive GTOs and one that is a primitive GTO.

2.2.3 Polarized Basis Sets

To each of these basis sets can be add polarization functions (*). Polarization functions are indicated after the G, with a separate designation for heavy atom those beyond helium. Sometime it is helpful to have polarization functions on the hydrogens as well, a *6-31G** basis with three 2p functions on each H and He atom is called the *6-31G*** (or *6-31G(d,p)*). Thus, H and He atom have a 1s orbital represented by an inner $1s'$ and outer $1s'$ basis function, making two basis function. To *6-31G** basis is identical *6-31G(d)* is valence zeta polarized basis set that adds to the *6-31G* set six *d*-type Cartesian-Gaussian polarization functions, each composed of three Gaussian of inner and one Gaussian of outer, no each of Li through Ca and ten *f*-orbitals Cartesian-Gaussian polarization functions on each of the atoms Sc through Zn.

6-31G(d) basis set for carbon atom, has a $1s$ function represented by six Gaussian, and inner $2s$, $2p_x$, $2p_y$ and $2p_z$ ($2s'$, $2p'_x$, $2p'_y$, $2p'_z$) function, each composed of three Gaussian, and an outer $2s$, $2p_x$, $2p_y$ and $2p_z$ ($2s''$, $2p''_x$, $2p''_y$, $2p''_z$) function, each composed of one Gaussian, and six 3d functions, making a lot of 15 functions. That can be summarized is ($1s$, $2s'$, $2p'$, $2p'$, $2p'$, $2s''$, $2p''$, $2p''$, $2p''$, $3d$, $3d$, $3d$, $3d$, $3d$, $3d$).

สถาบันวิทยบริการ
จุฬาลงกรณ์มหาวิทยาลัย

2.3 Semi-Empirical Methods

Semi-Empirical methods are simplified versions of Hartree-Fock theory using empirical (identical to derived from experimental data) corrections in order to improve performance. These methods are usually referred to through acronyms encoding some of the underlying theoretical assumptions. The most frequently used methods the Neglect of Differential Diatomic Overlap (NDDO) integral approximation, *Intermediate Neglect of Differential Diatomic Overlap* (INDO) and *Complete Neglect of Differential Diatomic Overlap* (CNDO). A number of additional approximations are made to speed up calculations and a number of parameterized corrections are made in order to correct for the approximate quantum mechanical model. How the parameterization is performed characterizes the particular Semi-Empirical method, as *Modified Neglect of Differential Overlap* (MNDO), *Austin Model 1* (AM1), *Parametric Number 3* (PM3). The parameterization is performed such that the calculated energies are expressed as heats of formations instead of total energies.

2.3.1 AM1 Method

AM1 (Austin Model 1) is a semi-empirical method for the quantum calculation of molecular electronic structure. AM1 is an attempt to improve the MNDO model by reducing the repulsion of atoms at close separation distances. The core-core repulsion was modified by introducing attractive and repulsive Gaussian functions centered at internuclear points. That the core-core repulsions was modified to overcome the tendency of MNDO to overestimate repulsions between atoms separated by about their van der Waals distances. The core-core repulsion of AM1 has the form

$$V_{nn}(A, B) = V_{nn}^{MNDO}(A, B) + \frac{Z_A Z_B}{R_{AB}} \times \left(\sum_k a_{kA} e^{-b_{kA}(R_{AB} - c_{kA})^2} + \sum_k a_{kB} e^{-b_{kB}(R_{AB} - c_{kB})^2} \right) \quad (2.14)$$

where the core-core repulsion of MNDO model has the form

$$V_{mn}^{MNDO}(A, B) = Z_A Z_B \langle s_A s_B | s_A s_B \rangle \left(1 + e^{-\alpha_A R_{AB}} + e^{-\alpha_B R_{AB}} \right) \quad (2.18)$$

Where, α exponent is taking as fitting parameters. The core repulsion energy is here a function of both the electron-electron repulsion integral $\langle s_A s_A, s_B s_B \rangle$. Here, k is between 2 and 4 depending on the atom, R_{AB} being the internuclear separation and Z_A being the effective core charge including the nuclear charge and all core electrons. It should be noted that the Gaussian functions more or less were added as patches onto the underlying parameters, which explains why different number of Gaussians are used for each atom.

2.3.2 PM3 Method

PM3 (Parametric Number 3) is a variation of AM1, differing mainly in how the parameterization is done, two parameterization of MNDO-type methods, MNDO and AM1, had been carried out, and PM3 was at first called MNDO-PM3, meaning MNDO parameteric method 3. All parameters could then be optimized simultaneously, including the two-electron terms, and a significantly larger training set with several hundred data could be employed. In this parameterization, the AM1 expression for the core-core repulsions was kept, except only 2 Gaussian were assigned to each atom. These Gaussian parameters were included as an integral part of model, and allowed to vary freely. In a sense it has the best set of parameter for the given set of experimental data. The optimization process, however, still required some human intervention, in selecting experimental data and assigning appropriate weight factors to each of data. PM3 has been parameterized for the elements, H, Li, C, N, O, F, Mg, Al, Si, P, S, Cl, Zn, Ga, Ge, etc, parameter for many of the transition metals are also being developed under the name PM3, which includes d-orbitals. The PM3 set of parameters are determined exclusively from geometrical data, since there are very few reliable energetic data available for transition metal compound [45].

2.4 DFT Method

DFT (Density functional theory) is based not on the wavefunction, but rather on the electron probability density function or electron density function, commonly called simply the electron density or charge density, designated by $\rho(x, y, z)$. The most common implementation of density functional theory is through the Kohn-Sham method. Within the framework of Kohn-Sham DFT, the intractable many-body problem of interacting electrons in a static external potential is reduced to a tractable problem of non-interacting electrons moving in an effective potential. DFT is among the most popular and versatile methods available in computational chemistry. Comparing with the wave mechanics approach, it seems clear that the energy functional may be divided into three parts, kinetic energy, $T[\rho]$, attraction between the nuclei and electrons, $V_{ne}[\rho]$, and electron-electron repulsion, $V_{ee}[\rho]$ (the nuclear-nuclear repulsion is a constant in the Born-Oppenheimer approximation). Furthermore, with reference to Hartree-Fock theory, the $V_{ee}[\rho]$ term may be divided into a Coulomb and Exchange part, $J[\rho]$ and $K[\rho]$, implicitly including correlation energy in all terms the $V_{ne}[\rho]$ and $J[\rho]$ functionals are given by their classical expression, where the factor of $\frac{1}{2}$ in $J[\rho]$ allows the integration to run over all space for both variables [44].

$$\begin{aligned}
 V_{ne}[\rho] &= \sum_a \int \frac{Z_a \rho(r)}{|R_a - r|} dr \\
 J[\rho] &= \frac{1}{2} \iint \frac{\rho(r)\rho(r')}{|r - r'|} dr dr'
 \end{aligned}
 \tag{2.15}$$

Early attempts at deducing functionals for the kinetic and exchange energies considered a non-interacting uniform electron gas.

The foundation for the use of the DFT methods in computational chemistry was the introduction of orbitals by Kohn and Sham. The basic idea in the Kohn and Sham formalism is splitting the kinetic energy functional into two parts, one of which can be calculated exactly, and a small correlation term.

2.4.1 The Kohn-Sham Energy and the Kohn-Sham Equations

The first Kohn-Sham theorem tells us that it is worth looking for a way to calculate molecular properties from the electron density. The second theorem suggests that a variation approach might yield a way to calculate the energy and electron density (the electron density, in turn, could be used to calculate other properties). The two basic ideas behind the Kohn-Sham approach to DFT are, (1) to express the molecular energy as a sum of terms, only one of which, a relatively small term, involves the unknown functional. Thus even moderately large errors in this term will not introduce large errors into the total energy (2) to use an initial guess of the electron density ρ in the Kohn-Sham equations to calculate an initial guess of the Kohn-Sham orbitals. The final Kohn-Sham orbitals are used to calculate an electron density that in turn is used to calculate the energy.

2.4.1.1 The Kohn-Sham Energy

The ideal energy is that of an ideal system, a fictitious non-interacting reference system, defined as one in which the electrons do not interact and in which the ground state electron density ρ_r is exactly the same as in our real ground state system, $\rho_r = \rho_0$. The electronic energy of the molecule is the total internal “frozen-nuclei” energy can be found by adding the internuclear repulsions, and the 0 K total internal energy by further adding the zero-point energy.

The ground state electronic energy of our real molecule is the sum of the electron kinetic energy, the nucleus-electron attraction potential energies, and the electron-electron repulsion potential energies and each is a functional of the ground-state electron density

$$E_0 = \langle T[\rho_0] \rangle + \langle V_{ne}[\rho_0] \rangle + \langle V_{ee}[\rho_0] \rangle \quad (2.16)$$

Focusing on the middle term, the nucleus-electron potential energy is the sum over all $2n$ electrons of the potential corresponding to attraction of an electron for all the nuclei A

$$\langle V_{ne} \rangle = \sum_{i=1}^{2n} \sum_{\text{nuclei } A} -\frac{Z_A}{r_{iA}} = \sum_{i=1}^{2n} v(r_i) \quad (2.17)$$

where $v(r_i)$ is the external potential for the attraction of electron i to the nuclei. The density function ρ can be introduced into $\langle V_{ne} \rangle$ by using that

$$\int \Psi \sum_{i=1}^{2n} f(r_i) \Psi dt = \int \rho(r) f(r) dr \quad (2.18)$$

Where $f(r_i)$ is a function of the coordinates of the $2n$ electrons of a system and Ψ is the total wavefunction from equations (2.17 and (2.18), invoking the concept of expectation value $\langle V_{ne} \rangle = \langle \Psi | \hat{V}_{ne} | \Psi \rangle$, and since $\hat{V} = V_x$, and get,

$$E_0 = \int \rho_0(r) v(r) dr + \langle T[\rho_0] \rangle + \langle V_{ee}[\rho_0] \rangle \quad (2.19)$$

that can not know the function in $\langle T[\rho_0] \rangle$ and $\langle V_{ee}[\rho_0] \rangle$. The Kohn and Sham to introduced the idea of a reference system of non-interacting electrons. Let us to define the quantity $\Delta \langle T[\rho_0] \rangle$ as the deviation of the real kinetic energy from that of the reference system.

$$\Delta \langle T[\rho_0] \rangle \equiv \langle T[\rho_0] \rangle - \langle T_r[\rho_0] \rangle \quad (2.20)$$

Let us next define $\Delta \langle V_{ee} \rangle$ as the deviation of the real electron-electron repulsion energy from classical charged-cloud coulomb repulsion energy. This classical electrostatic repulsion energy is the summation of the repulsion energies for pairs of infinitesimal volume elements $\rho(r_1) dr_1$ and $\rho(r_2) dr_2$ separated by distance r_{12} , multiplied by one-half. The sum infinitesimals is and integral and so

$$\Delta\langle V_{ee}[\rho_0]\rangle = \langle V_{ee}[\rho_0]\rangle - \frac{1}{2} \iint \frac{\rho_0(r_1)\rho_0(r_2)}{r_{12}} dr_1 dr_2 \quad (2.21)$$

Actually, the classical charged-cloud repulsion is somewhat inappropriate for electrons in that smearing an electron out into a cloud forces it to repel itself, as any two regions of the cloud interact repulsively. This physically incorrect electro self-interacting will be compensated for by a good exchange-correlation functional can be written as

$$E_0 = \int \rho_0(r)v(r)dr + \langle T_r[\rho_0]\rangle + \frac{1}{2} \iint \frac{\rho_0(r_1)\rho_0(r_2)}{r_{12}} + \Delta\langle T[\rho_0]\rangle + \Delta\langle V_{ee}[\rho_0]\rangle \quad (2.22)$$

The sum of the kinetic energy deviation from the reference system and the electron-electron repulsion energy deviation from the classical system is called the exchange-correlation energy, E_{xc}

$$E_{xc}[\rho_0] \equiv \Delta\langle T[\rho_0]\rangle + \Delta\langle V_{ee}[\rho_0]\rangle \quad (2.23)$$

The $\Delta\langle T \rangle$ term represents the kinetic correlation energy of the electrons and the $\langle \Delta V_{ee} \rangle$ term the potential correlation energy and the exchange energy, although exchange and correlation energy in DFT do have exactly.

2.4.1.2 The Kohn-Sham Equations

The Kohn-Sham equations are theorem obtained by utilizing the variation principle, which the second Hohenberg-Kohn theorem assures applies to DFT. We use the fact that the electron density of the reference system, which is the same as that of our real system, is given by

$$\rho_0 = \rho_r = \sum_{i=1}^{2n} |\psi_i^{KS}(1)|^2 \quad (2.24)$$

where the ψ_i^{KS} are the Kohn-Sham spatial orbital. Substituting the above expression for the orbitals into the energy and varying E_0 with respect to the ψ_i^{KS} subject to the constraint that these remain orthonormal lead to the Kohn-Sham equations, procedure is similar to that used in deriving the Hartree-Fock equations,

$$\left[-\frac{1}{2}\nabla_i^2 - \sum_{\text{nuclei } A} \frac{Z_A}{r_{iA}} + \int \frac{\rho(r_2)}{r_{12}} dr_2 + v_{xc}(1) \right] \psi_i^{KS}(1) = \varepsilon_i^{KS} \psi_i^{KS}(1) \quad (2.25)$$

where ε_i^{KS} are the Kohn-Sham energy levels and $v_{xc}(1)$ is the *exchange correlation potential*, arbitrarily designated here for electron number 1, since the Kohn-Sham equations are a set of one-electron equations with the subscript i running from 1 to n , over all the $2n$ electron in the system. The exchange correlation potential is defined as the functional derivative of $E_{xc}[\rho_0(r)]$ with respect to $\rho(r)$

$$v_{xc}(r) = \frac{\delta E_{xc}[\rho(r)]}{\delta \rho(r)} \quad (2.26)$$

We need the derivative v_{xc} for the Kohn-Sham equations, and the exchange-correlation function itself for the energy equation. The Kohn-Sham equations can be written as

$$\hat{h}^{KS}(1) \psi_i^{KS}(1) = \varepsilon_i^{KS} \psi_i^{KS}(1) \quad (2.31)$$

The Kohn-Sham operator \hat{h}^{KS} is defined by equation (2.25). The difference between DFT method is the choice of the functional from of the exchange-correlation energy. Functional forms are often designed to have a certain limiting behavior, and fitting parameters to known accurate data. Which functional is the better will have to be settled by comparing the performance with experiments or high-level wave mechanics calculations.

2.4.2 LDA Methods

The LDA (Local Density Approximation) it is assumed that the density locally can be treated as a uniform electron gas, or equivalently that the density is a slowly varying function. The term local was perhaps used because for any point only the conditions (the electron density) at that point are considered, in contrast to so-called non-local methods in which for each point a gradient. For the LDA the exchange-correlation energy function E_{xc}^{LDA} and its derivative v_{xc}^{LDA} can be accurately calculated. The exchange energy for a uniform electron gas is given

$$\begin{aligned} E_x^{LDA}[\rho] &= -C_x \int \rho^{4/3}(r) dr \\ E_x^{LDA}[\rho] &= -C_x \rho^{1/3} \end{aligned} \quad (2.27)$$

In the more general case, where the α and β densities are not equal, LDA has been virtually abandoned and replaced by *Local Spin Density Approximation* (LSDA) can be written as

$$\begin{aligned} E_x^{LSDA}[\rho] &= -2^{1/3} C_x \int [\rho_\alpha^{4/3} + \rho_\beta^{4/3}] dr \\ E_x^{LSDA}[\rho] &= -2^{1/3} C_x [\rho_\alpha^{1/3} + \rho_\beta^{1/3}] \end{aligned} \quad (2.28)$$

LSDA may be also be written in terms of the total density and spin polarization and has the advantages that it can handle systems with one or more unpaired electrons, like radicals, and systems in which electrons are becoming unpaired, such as molecules far from their equilibrium.

2.4.3 GGA Methods

The electron density in an atom or molecule varies greatly from place to place. A step in this direction is to make the exchange and correlation energies dependent not only on the electron density, but also on derivatives of the density. Such methods are known as *Gradient Corrected* or *Generalized Gradient Approximation* (GGA). They are also called non-local functional, in contrast to the older, local (LDA) and LSDA functional. The exchange-correlation energy functional can be written as the sum of an exchange energy functional and correlation energy functional, both negative, i.e. $E_{xc} = E_x + E_c$; $|E_x|$ is much bigger than $|E_c|$. One popular functional is due to Lee, Yang and Parr (LYP) and has the form

$$E_c^{LYP} = -a \frac{\gamma}{(1+d\rho^{-1/3})} - ab \frac{\gamma e^{c\rho^{-1/3}}}{9(1+d\rho^{-1/3})\rho^{8/3}} \times \left[\frac{18(2^{2/3})C_F(\rho_\alpha^{8/3}) - 18\rho t_w + \rho_\alpha(2t_w^\alpha + \nabla^2\rho_\alpha)}{\rho_\beta(2t_w^\beta + \nabla^2\rho_\beta)} + \right] \quad (2.29)$$

$$\text{where } \gamma = 2 \left[1 - \frac{\rho_\alpha^2 + \rho_\beta^2}{\rho^2} \right] \quad \text{and} \quad t_w^\sigma = \frac{1}{8} \left(\frac{|\nabla\rho_\sigma|^2}{\rho_\sigma} - \nabla^2\rho_\sigma \right)$$

The parameters a , b , c and d are determined by fitting to data for the helium atom the t_w functional known as the local Weizsacker kinetic energy density.

2.4.4 Hybrid Methods

Hybrid functional augment the DFT exchange-correlation energy with a term calculated from Hartree-Fock theory. The Kohn-Sham orbitals are quite similar to the HF orbitals, give an expression, based on Kohn-Sham orbitals, for the HF exchange energy

$$E_x^{HF} = - \sum_{i=1}^n \sum_{j=1}^n \left\langle \psi_i^{KS}(1) \psi_i^{KS}(2) \left| \frac{1}{r_{ij}} \right| \psi_i^{KS}(2) \psi_j^{KS}(1) \right\rangle \quad (2.30)$$

Since the Kohn-Sham Slater determinant is an exact representation of the wavefunction of the noninteracting electron reference system, E_x^{HF} is the exact exchange energy for a system of noninteracting electron with electron density equal to real system. Including in a LSDA gradient-corrected DFT expression for E_{xc} ($E_{xc} = E_x + E_c$) a weighted contribution of the expression for E_x^{HF} give a FH/DFT exchange-correlation functional, commonly called a Hybrid DFT functional. The most popular Hybrid functional at present is based on an exchange-energy functional developed by Becke, and modified Steven *et al.* by introduction of the LYP correlation-energy functional. This exchange-correlation functional, called the Becke3 LYP or B3LYP functional is

$$E_{xc}^{B3LYP} = (1 - a_0 - a_x)E_x^{LSDA} + a_0E_x^{HF} + a_xE_x^{B88} + (1 - a_c)E_x^{VWN} + a_cE_c^{LYP} \quad (2.31)$$

Here E_x^{LSDA} is the kind accurate pure DFT LSDA non-gradient-corrected exchange functional, E_x^{HF} is the Kohn-Sham orbitals based HF exchange energy functional, E_x^{B88} is the Becke 88 exchange functional

$$E_x^{B88} = E_x^{LDA} + \Delta E_x^{B88}$$

$$\Delta E_x^{B88} = -\beta\rho^{1/3} \frac{x^2}{1 + 6\beta x \sinh^{-1} x}$$

The β parameter is is determined by fitting to known atomic data and x is a dimension gradient variable. The E_x^{VWN} is the Vosko, Wilk, Nusair function (VWN) can be written

$$E_x^{VWN} = E_x^{LDA} (1 + ax^2 + bx^4 + cx^6)^{1/5}$$

$$x = \frac{|\nabla\rho|}{\rho^{4/3}}$$

which forms part of the accurate functional for the homogeneous electron gas of the LDA and LSDA, and E_c^{LYP} is the LYP correlation functional. The parameters a_0 , a_x and a_c are those that give the best fit of the calculated energy to molecular atomization energies. This is thus gradient-corrected hybrid functional [44].

2.5 ONIOM Method

ONIOM (Our N-layer Integrated molecular Orbital + molecular Mechanics) method was developed in Morokuma group [46], allows the user to partition a chemical system into layers, which can then each be treated at a different level of theory are applied to different parts of a molecule. A molecule system can be divided into up to three layers and the three layers do not have to be inclusive, provides a possibility to achieve such high accuracy calculation on a large molecular system. The active part of the reaction is considered in the “model” system and is treated with both at “high” and “low” levels of molecular Orbital calculation, whereas the entire “real” system is treated only at the “low” level of molecular Orbital calculation, and then they are integrated to define the ONIOM total energy of the “real” system. ONIOM is a computationally efficient tool for the study of chemical reactions involving large molecular systems.

An obvious solution to problem is the partitioning of the system into two or more parts or layers, where the interesting or difficult part of the system (the inner layer) is treated at a high level of theory and the rest of the system (the outer layer) is treated at a low level of theory. These hybrid methods differ mainly in two aspects.

First, there are different ways to treat the boundary region of the different parts of the molecule. If there is no covalent bond between the layers, there is no special boundary region. However, if one is interested in the accurate description of a particular region of a large organic molecule or a macromolecule, covalent bonds have to be cut in order to generate the inner model system. This process leaves dangling bonds at the border of inner layer, which have to be saturated in order to avoid a chemically unrealistic model. Therefore, so-called link atom usually hydrogen atom are use.

The second crucial aspect in all the hybrid schemes is the interaction between the inner and outer part of the system. If the total energy $E(X-Y)$ of the entire system $X-Y$ (inner region X , outer region Y) is defined as

$$E(X-Y) = E_{high}(X) + E_{low}(Y) + E_{inner\ layer}(X,Y) \quad (2.32)$$

with $E_{inner\ layer}(X,Y)$ being a separate interaction energy between the two layers, this may be referred to as a connection scheme. On the other hand, if the total $E(X-Y)$ is calculated according to

$$E(X-Y) = E_{low}(X-Y) - E_{low}(X) + E_{high}(X) \quad (2.33)$$

In the latter case there is no necessity for a special interaction Hamiltonian, since the interaction between the two layers is consistently treated at the low level of theory. Obviously, both approaches are equivalent, if

$$E_{low}(Y) + E_{inner\ layer}(X,Y) = E_{low}(X-Y) - E_{low}(X) \quad (2.34)$$

i.e. if $E_{inner\ layer}(X,Y)$ corresponds to the exact interaction energy at the respectively low level.

2.5.1 ONIOM Energy Definition

The basic of ONIOM can be explained easily when it is considered as an extrapolation scheme in a two-dimensional space, spanned by the size of the system on one axis and the level of theory on the other axis.

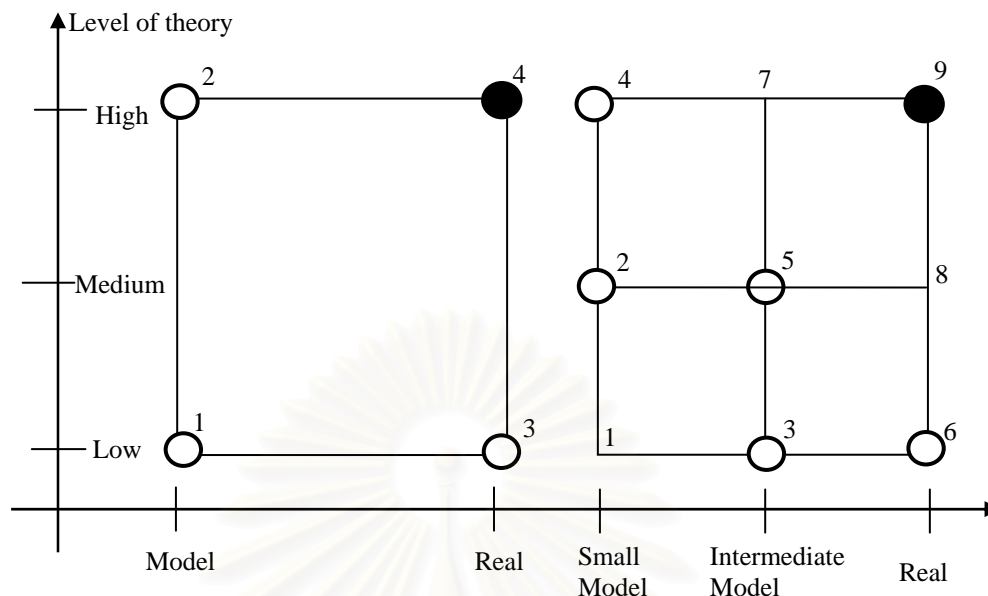


Figure 2.1 The ONIOM extrapolation scheme for a molecular system partitioned into two (left) and three (right) layers.

Figure 2.1 shows the extrapolation procedure schematically to describe the real system at the highest level of theory, the approximation of the target E_4 (point 4) in a system partitioned into the two-layer ONIOM or E_9 (point 9) in a system consisting of three layers. In the case of two layers, in extrapolated energy E_{ONIOM2} is then defined as

$$E_{ONIOM2} = E_3 - E_1 + E_2 \quad (2.35)$$

where E_3 is the energy of the entire (real) system calculated at low level method and E_1 and E_2 are the energies of the model system determined at the low and high level of theory, respectively. E_{ONIOM2} is an approximation to the true energy of the real system E_4

$$E_4 = E_{ONIOM2} + D \quad (2.36)$$

Thus, if the error D of the extrapolation procedure is the constant for two different structures, their relative energy ΔE_4 will be evaluated corrected by using the ONIOM energy ΔE_{ONIOM2} .

For a system partitioned into three different layers, the expression for the total energy ΔE_{ONIOM3} as an approximation for E_9 reads

$$E_{ONIOM3} = E_6 - E_3 + E_5 - E_2 + E_4 \quad (2.37)$$

Since the evaluation of E_1 does not require much computational effort, its value can be used to determine the effect of the three-layer approach as compared to a two-layer partitioning with points 1, 4, and 6. If the energy difference between the two-layer and three-layer extrapolation is constant, a two layer partitioning with the intermediate layer omitted would give comparably accurate result.

2.5.2 Treatment of Link Atoms

As mentioned before, an important and critical feature of all combination schemes is the treatment of the link atoms, as illustrated in Figure 2.2. The methodology in the case of three-layer ONIOM is exactly the same and will not be discussed explicitly.

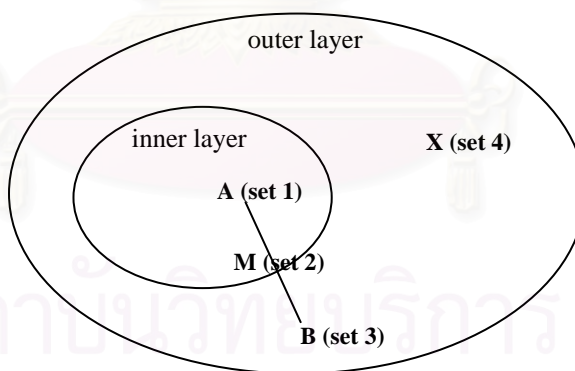


Figure 2.2 Definition of different atom sets within the ONIOM scheme.

Figure 2.2 shows the model system equal to inner layer + link atoms and real system equal to inner layer + outer layer. The atoms present both in the model system and real system are called set 1 atom and their coordinates are denoted by R_1 . The set 2 atoms

are the artificially introduced link atoms. They only occur in the model system and their coordinates are described by R_2 . In the real system there are replaced by the atoms described by R_3 . Atoms that belong to the outer layer and are not substituted by atoms are called set 4 atoms with the coordinates R_4 . The geometry of the real system is thus described by R_1 , R_3 and R_4 and they are the independent coordinates for the ONIOM energy

$$E_{ONIOM} = E_{ONIOM}(R_1, R_3, R_4) \quad (2.38)$$

In order to generate the model system, described by R_1 and the link atoms R_2 , defined R_2 as function of R_1 and R_3

$$R_2 = f(R_1, R_3) \quad (2.39)$$

The explicit functional form of the R_2 dependency can be chosen arbitrarily. However, considering the fact that the link atoms are introduced to mimic the corresponding covalent bonds of the real system, they should follow the movement of the atoms they replace. If atom A belong to set 1 and atom B belong to set 3, the set 2 link atom is placed onto the bond axis A-B in terms of internal coordinates choose the same bond angle for set 2 atom as for set 3. Therefore, in the model calculations the link atoms are always aligned along the bond vectors of the real system. For the exact position r_2 of a single H atom along an A-B bond ($r_2 - r_1$), introduced a fixed scale factor (or distance parameter) g . Hence,

$$r_2 = r_1 + g(r_3 - r_1) \quad (2.40)$$

If the A-B bond distance $|r_3 - r_1|$ changes during a geometry optimization, the A-H bond distance $|r_2 - r_1|$ also changes.

CHAPTER III

DETAILS OF THE CALCULATIONS

Geometry optimizations of the armchair (5,5) SWCNTs and their complexes with adsorbing species were performed using the *ab initio* Hartree–Fock (HF) with 3-21G basis set and the two-layered ONIOM(MO:MO) approaches with two different models. A relatively small section (model), essential for studying the property of interest, is treated at a higher theoretical level. The availability of methods such as DFT allows reasonable accuracy for sufficiently large model system. For the two-layered ONIOM approach, the DFT calculations have been performed with the Beck’s three-parameter hybrid method with the exchange functional of Lee, Yang, and Parr (B3LYP) level with 6-31G(d) basis set was used for the high layer and the semi-empirical PM3 and AM1 methods were employed for the low layer.

Our calculations have been done using different initial structures of SWCNTs. Each type of SWCNTs in this study is chosen perfect and defect armchair (5,5) SWCNTs, “cap-ended” with a half fullerene (C_{60}) [47] contains 80 and 120 carbon atoms only and “open-ended”, contains 80 and 120 carbon atoms, 20 hydrogen atoms that are used to saturate the edges of SWCNTs .

Eight different characteristics of (5,5) SWCNTs structures with their diameters in the parentheses, namely, (1) a perfect cap-ended C_{80} (6.9 Å) (2) a defect cap-ended C_{80} (6.8 Å) (3) a perfect open-ended $C_{80}H_{20}$ (6.8 Å) (4) a defect open-ended $C_{80}H_{20}$ (6.7 Å) (5) a perfect cap-ended C_{120} (6.8 Å) (6) a defect cap-ended C_{120} (6.7 Å) (7) a perfect open-ended $C_{120}H_{20}$ (6.8 Å) and (8) a defect open-ended $C_{120}H_{20}$ (6.7 Å) are shown in Figure 3.1.

Four models defined using the clusters of (1) a pyrene (C_{16}) as model 1, (2) a 5-6-6-pyrene-5-5-6 (C_{29}) as model 2, (3) a 5–7–7–5 (C_{16}) Stone-Wales defect structure as model 3 and (4) an ovalene (C_{32}) as model 4 were employed as the high layer of the two-layered ONIOM(B3LYP/6-31G(d):AM1) approach. These models are shown in Figure

3.2. Definitions of the low and high layers for the two-layered ONIOM approach are given from Figure 3.3 to Figure 3.5 for various types of armchair (5,5) SWCNTs.

The strain energy [48], which is the C-C bond distortion energy of the adsorption-state structures of SWCNTs based on various reactions were evaluated at the HF/3-21G and B3LYP/6-31G(d) levels of theory. Thermodynamic properties for all reactions were obtained from the frequencies calculations at the two-layered ONIOM(B3LYP/6-31G(d):AM1) level. All calculations were performed with the GAUSSIAN 03 program. The MOLDEN 4.2 program was used to display the molecular structure and observe the molecular geometry convergence *via* the Gaussian output files. The molecular graphics of all related species were generated with the MOLEKEL 4.3 program.

The binding energies ($\Delta E_{binding}$) of adsorbates on the SWCNTs were determined according to the expression

$$\Delta E_{binding} = E_{SWCNT-adsorbate} - E_{adsorbate} - E_{SWCNT} \quad (3.1)$$

Where E_{SWCNT} is the energy at its optimized geometry in the absence adsorbed species, $E_{adsorbate}$ is the energy of an isolated adsorbate, and $E_{SWCNT-adsorbate}$ corresponds to the energy at its optimized geometry upon adsorbate adsorption on the SWCNT surface.

The strain energies (ΔE_{st}) of adsorption-state structures of the SWCNTs are defined as Eqs. (3.2)

$$\Delta E_{st} = E_{SWCNT(\text{complex form})} - E_{SWCNT(\text{isolated form})} \quad (3.2)$$

and those obtained from the ONIOM calculations are evaluated using Equation. 3.3 and 3.4, respectively.

$$\begin{aligned} \Delta E_{binding} &= E[ONIOM(B3LYP/6-31G(d):AM1)]_{SWCNT-adsorbate} \\ &\quad - E[ONIOM(B3LYP/6-31G(d):AM1)]_{adsorbate} \\ &\quad - E[ONIOM(B3LYP/6-31G(d):AM1)]_{SWCNT} \end{aligned} \quad (3.3)$$

$$\Delta E_{\text{st}} = E[\text{ONIOM}(\text{B3LYP}/6\text{-}31\text{G}(\text{d}) : \text{AM1})]_{\text{SWCNT}(\text{complex form})} - E[\text{ONIOM}(\text{B3LYP}/6\text{-}31\text{G}(\text{d}) : \text{AM1})]_{\text{SWCNT}(\text{isolated form})} \quad (3.4)$$

The standard enthalpy ΔH_{298}° and Gibbs free ΔG_{298}° energy changes of adsorption reactions have been derived from the frequency calculations at the *ab initio* HF/3-21G and ONIOM(B3LYP/6-31G(d)) approaches.

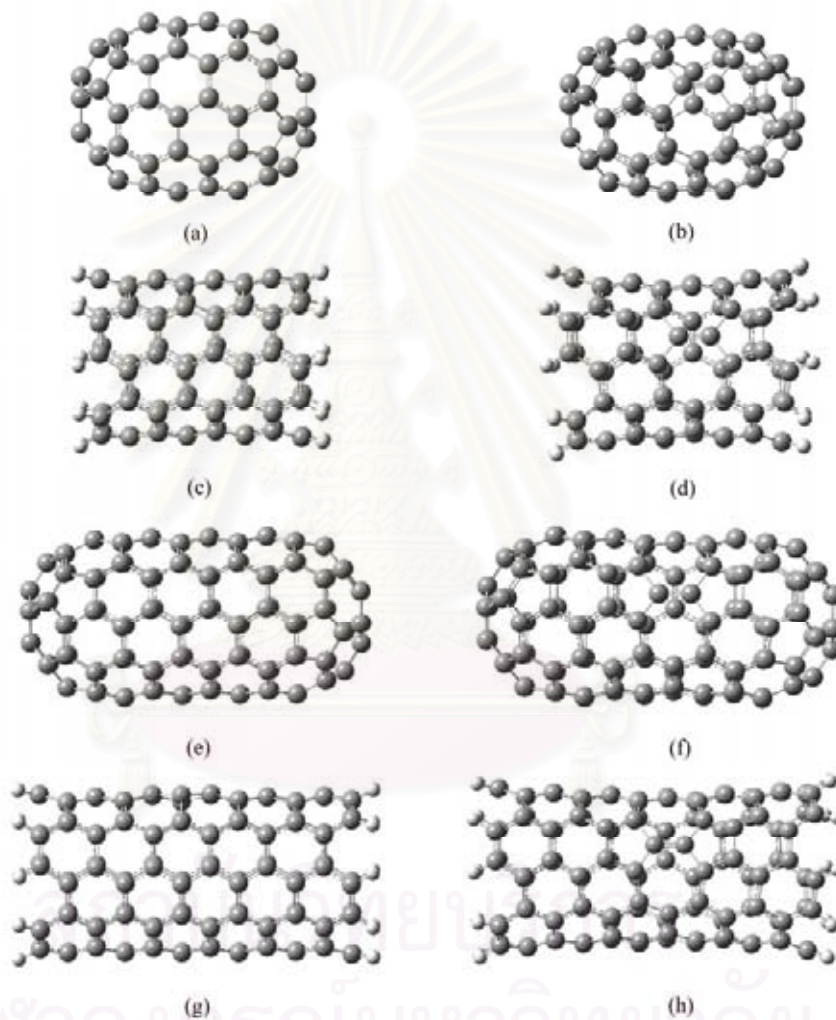


Figure 3.1 Eight different characteristics of cap-ended and open-ended armchair (5,5) SWCNT structures have been investigated. (a) a perfect cap-ended C_{80} (b) a defect cap-ended C_{80} (c) a perfect open-ended $\text{C}_{80}\text{H}_{20}$ (d) a defect open-ended $\text{C}_{80}\text{H}_{20}$ (e) a perfect cap-ended C_{120} (f) a defect cap-ended C_{120} (g) a perfect open-ended $\text{C}_{120}\text{H}_{20}$ (g) a defect open-ended $\text{C}_{120}\text{H}_{20}$

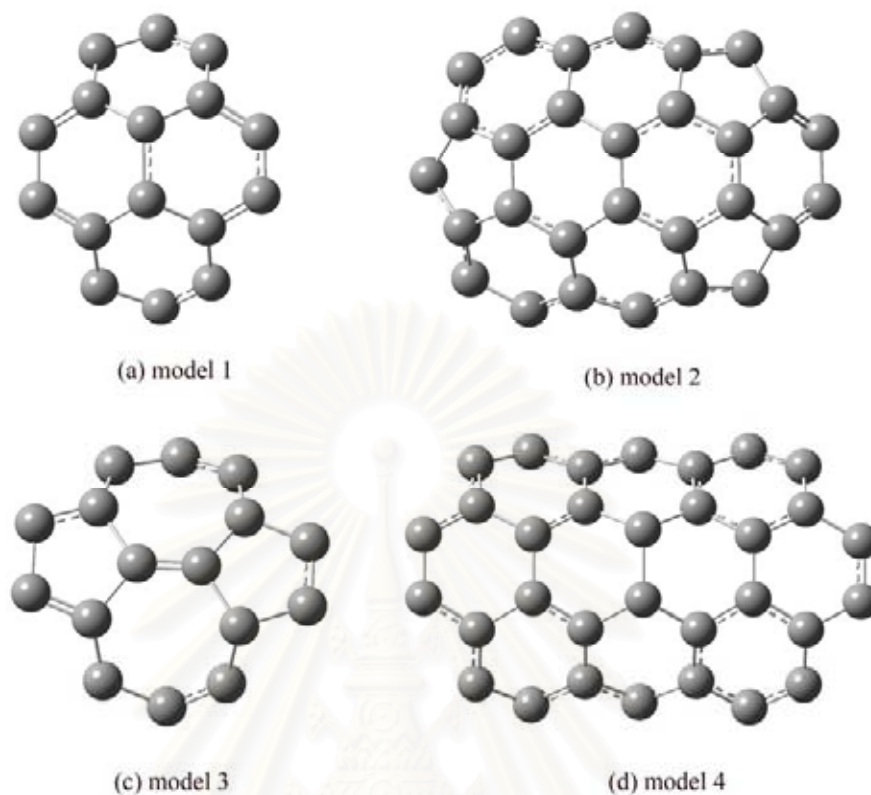


Figure 3.2 Four models have been investigated for high-layered of ONIOM(MO:MO) method (a) a pyrene (C_{16}) as model 1 (b) a 5-6-6-pyrene-5-5-6 (C_{29}) as model 2 (c) a 5-7-7-5 (C_{16}) Stone-Wales defect as model 3 and (d) an ovalene (C_{32}) as model 4

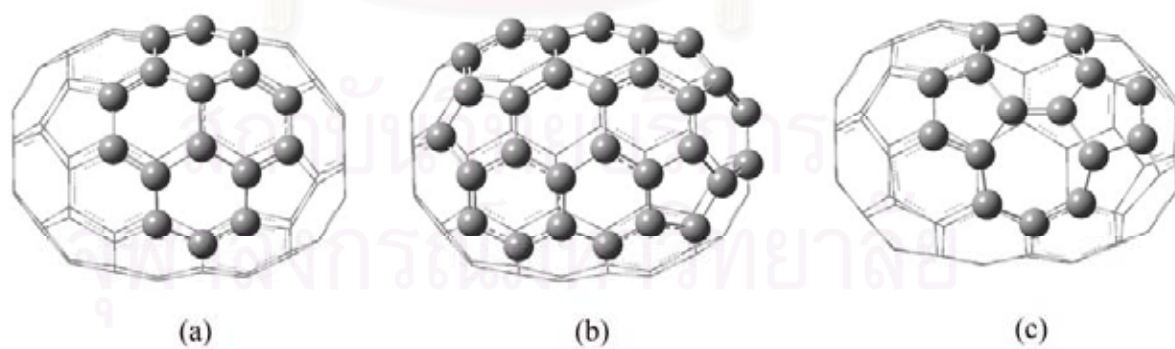


Figure 3.3 The two-layered ONIOM models of cap-ended C_{80} (a) a perfect C_{80} model 1 (b) a perfect C_{80} model 2 and (c) a defect C_{80} model 3

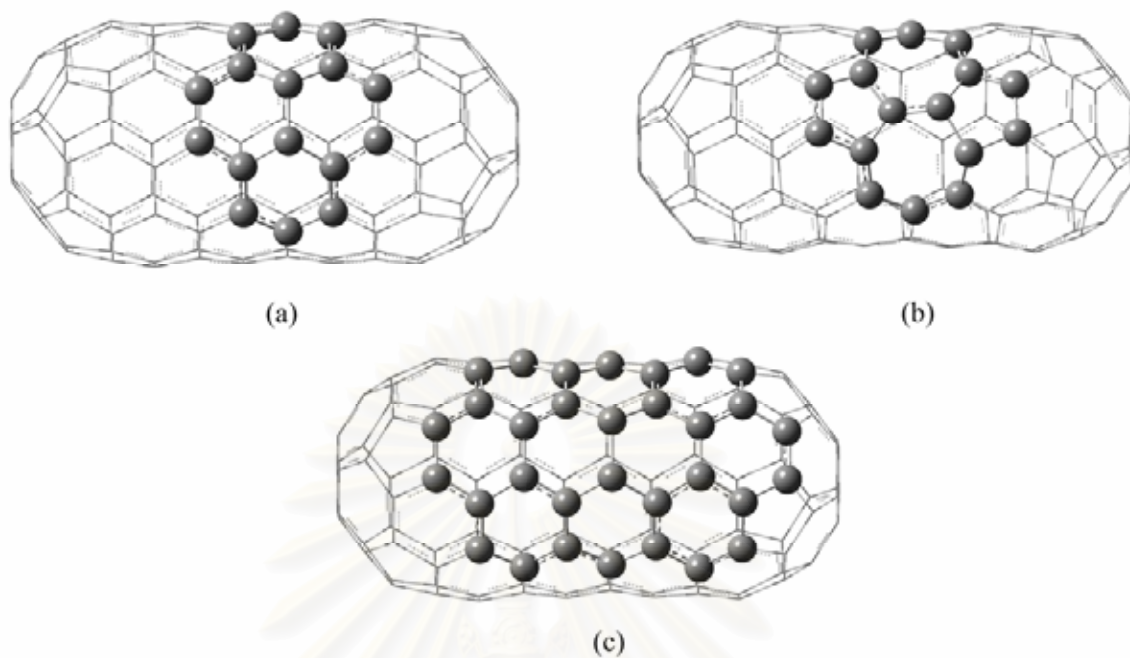


Figure 3.4 The two-layered ONIOM models of cap-ended C_{120} (a) a perfect C_{120} model 1 (b) a perfect C_{120} model 3 and (c) a perfect C_{120} model 4

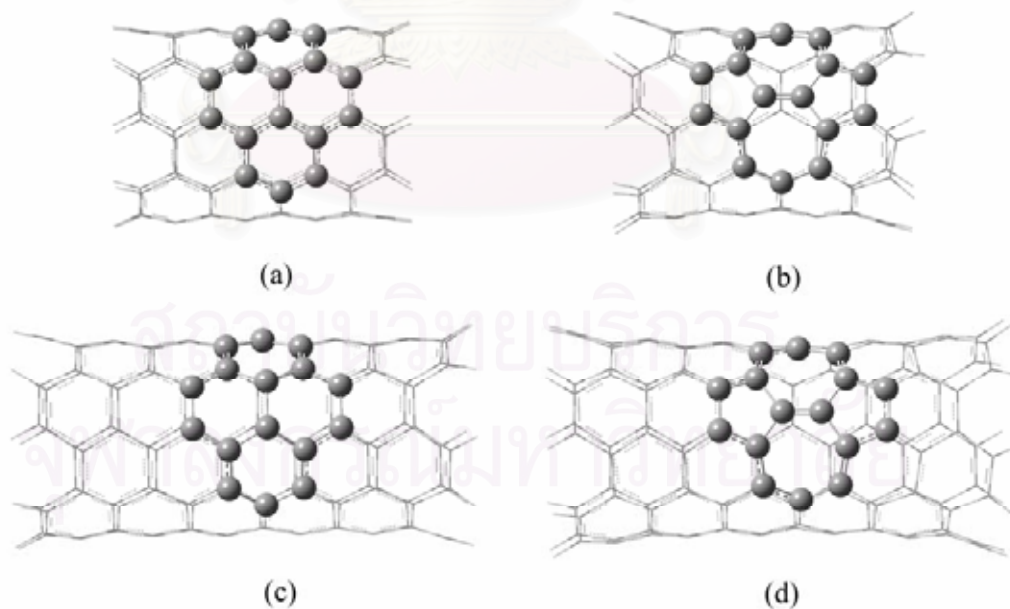


Figure 3.5 The two-layered ONIOM models of open-ended (a) a perfect $C_{80}H_{20}$ model 1 (b) a defect $C_{80}H_{20}$ model 3. (c) a perfect $C_{120}H_{20}$ model 1 (d) a defect $C_{120}H_{20}$ model 3

3.1 The Adsorptions of Proton and Hydroxide on Various Types of SWCNTs

The adsorption of proton, hydroxide on various types of SWCNTs were studied with the SWCNT models similar to those described in our previous studies of the water adsorption on hydroxylated graphite surfaces using a two-layered ONIOM approach [49]. On the SWCNT surface, proton is placed on one of the two carbons located at the central of the various models (model 1 to model 4) as shown in Figure 3.2, as well as the hydroxide ion is placed on the SWCNT surface. An also, proton and hydroxide ions are thus added on the SWCNT surface between two carbon atoms at the central of the various models are shown in Figure 3.6

All structures have been first full optimized using HF level of theory with 3-21G basis set for perfect and defect cap-ended C_{80} to form complex with adsorbing species. In the second step, the ONIOM method has been used to implement a proton, hydroxide ion and mono-hydration on the surface of SWCNTs. The central part of the system containing the proton, hydroxide ion and water molecule, is treated with a high level of theory by using HF with 3-21 G basis set and DFT performed B3LYP with 6-31G(d) basis set, whereas the rest of the system is taken into account with the semi empirical AM1 and PM3 method. For the high layers in our ONIOM calculations are shown in Figure 3.7 to Figure 3.10 of various types of armchair (5,5) SWCT models.

In the ONIOM calculations for cap-ended C_{80} are used for three models, model 1, model 2 for perfect cap-ended and model 3 for defect cap-ended (Figure 3.3) and cap-ended C_{120} are used for two models, model 3 for defect cap-ended and model 4 for perfect cap-ended shown in Figures 3.3 (b) and (c), respectively. Also, open-ended $C_{80}H_{20}$ are used to two models, model 1 for perfect open-ended and model 3 for defect open-ended (Figure 3.5).

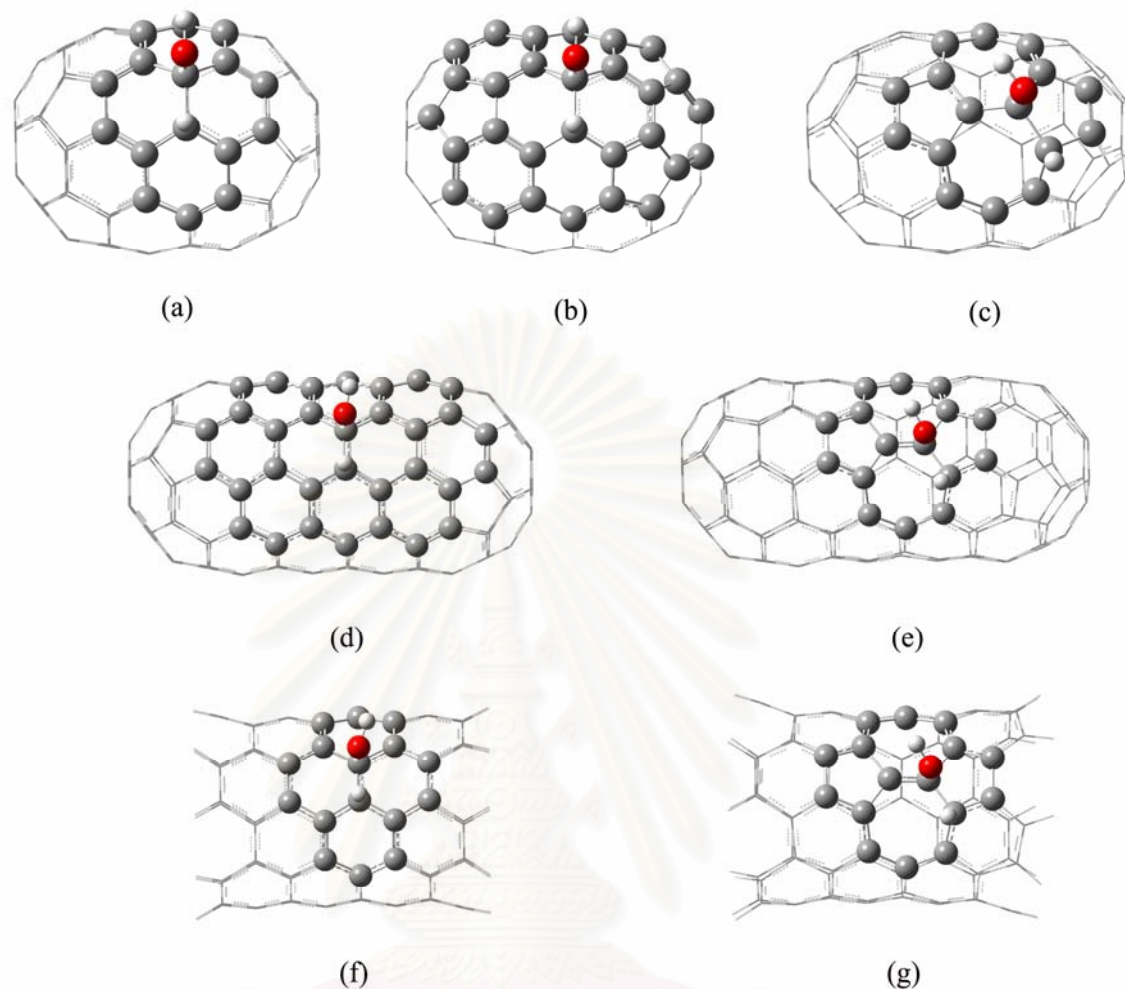


Figure 3.6 The two-layered ONIOM model of SWCNTs for adsorption of proton with hydroxide ion (a) a perfect cap-ended C_{80} model 1 (b) a defect cap-ended C_{80} model 2 (c) a defect cap-ended C_{80} model 3 (d) a perfect cap-ended C_{120} model 4 (e) a defect cap-ended C_{120} model 3 (f) a perfect open-ended $C_{80}H_{20}$ model 1 and (g) a defect open-ended $C_{80}H_{20}$ model 3

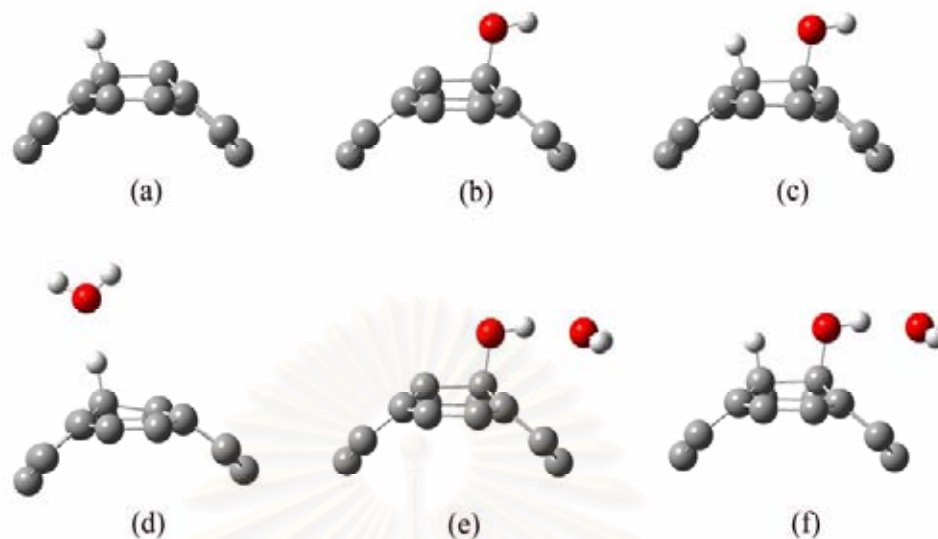


Figure 3.7 The high-layered ONIOM method for adsorptions proton, hydroxide ion and water on cap-ended C₈₀ model 1 (a) SWCNT-H⁺ (b) SWCNT-OH⁻ (c) SWCNT-H⁺-OH⁻ (d) SWCT-H⁺...H₂O (e) SWCT-OH⁻...H₂O (f) SWCT H⁺-OH⁻...H₂O

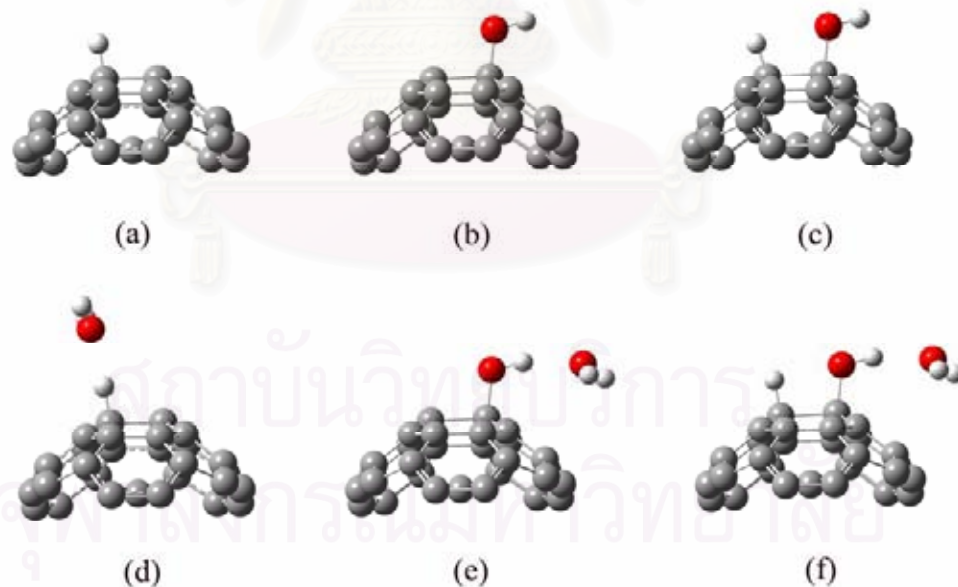


Figure 3.8 The high-layered ONIOM method for adsorptions proton, hydroxide ion and water on cap-ended C₈₀ model 2 (a) SWCNT-H⁺ (b) SWCNT-OH⁻ (c) SWCNT-H⁺-OH⁻ (d) SWCT-H⁺...H₂O (e) SWCT-OH⁻...H₂O (f) SWCT-H⁺-OH⁻...H₂O

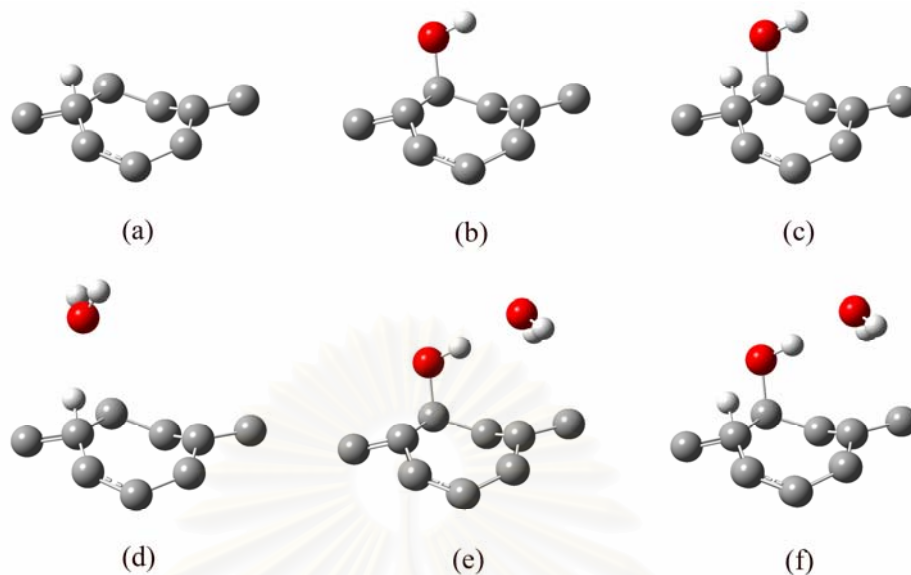


Figure 3.9 The high-layered ONIOM method for adsorptions proton, hydroxide ion and water on cap-ended C_{80} and C_{120} model 3 (a) SWCNT- H^+ (b) SWCNT- OH^- (c) SWCNT- H^+ - OH^- (d) SWCNT- H^+ ... H_2O (e) SWCNT- OH^- ... H_2O (f) SWCNT- H^+ - OH^- ... H_2O

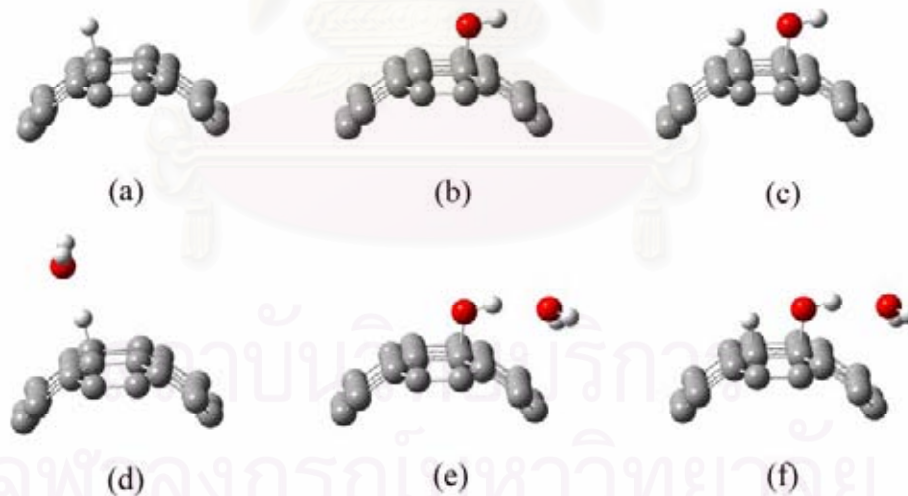


Figure 3.10 The high-layered ONIOM method for adsorptions proton, hydroxide ion and water molecule of cap-ended C_{120} model 4 (a) SWCNT- H^+ (b) SWCNT- OH^- (c) SWCNT- H^+ - OH^- (d) SWCNT- H^+ ... H_2O (e) SWCNT- OH^- ... H_2O (f) SWCNT- H^+ - OH^- ... H_2O

3.2 The Chemisorptions of Hydroxide and C1 to C3 alkoxides

The study was done for the chemisorption, the process whereby the adsorbate is on the any type of SWCNT surfaces and taking place on the carbon atom of central part of the system. Similar SWCNT models were also used to investigate in section 2.1 using ONIOM(B3LYP/6-31G(d):AM1) method [50]. All geometry optimizations have used model 1 for perfect tube and model 3 for defect tube, both cap-ended (C_{80} and C_{120}) and open-ended ($C_{80}H_{20}$ and $C_{120}H_{20}$) are shown in Figure 3.11 and Figure 3.10, respectively.

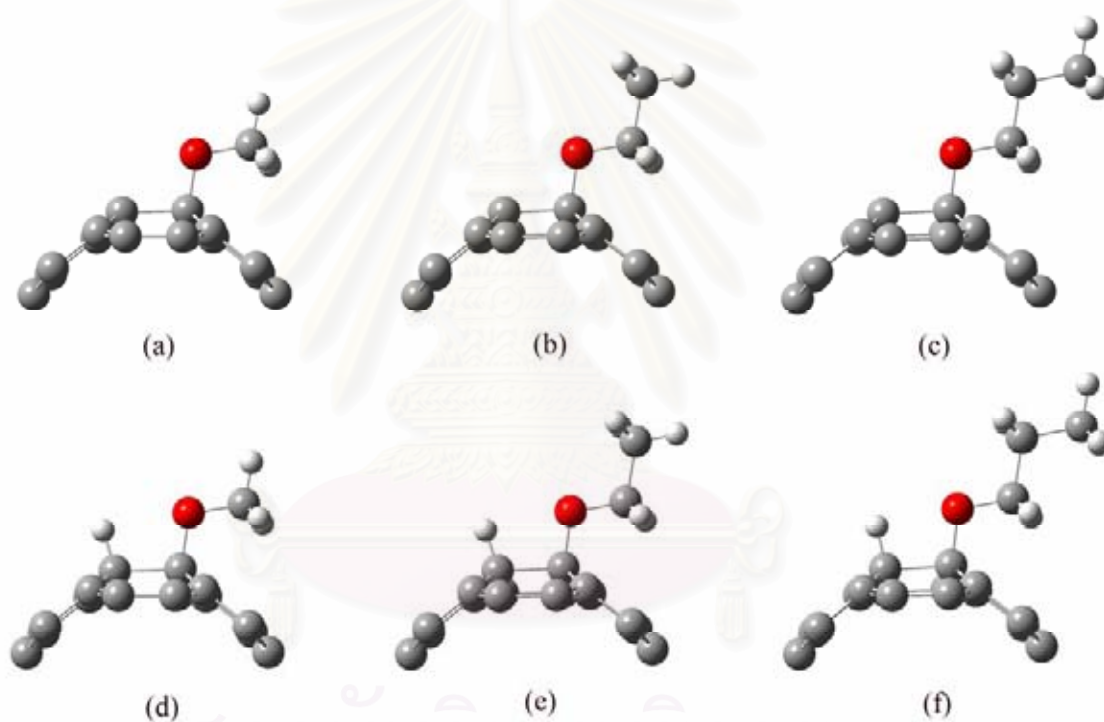


Figure 3.11 The high-layered ONIOM method for the chemisorptions of C1 to C3 alkoxide ions (methoxide ion, ethoxide ion and n-propoxide ion) on cap-ended (C_{80} and C_{120}) and open-ended ($C_{80}H_{20}$ and $C_{120}H_{20}$) perfect as model 1 (a) SWCNT-OMe⁻ (b) SWCNT-OEt⁻ (c) SWCNT-OPr⁻ (d) SWCNT-H⁺-OMe⁻ (e) SWCNT-H⁺-OEt⁻ (f) SWCNT-H⁺-OPr⁻.

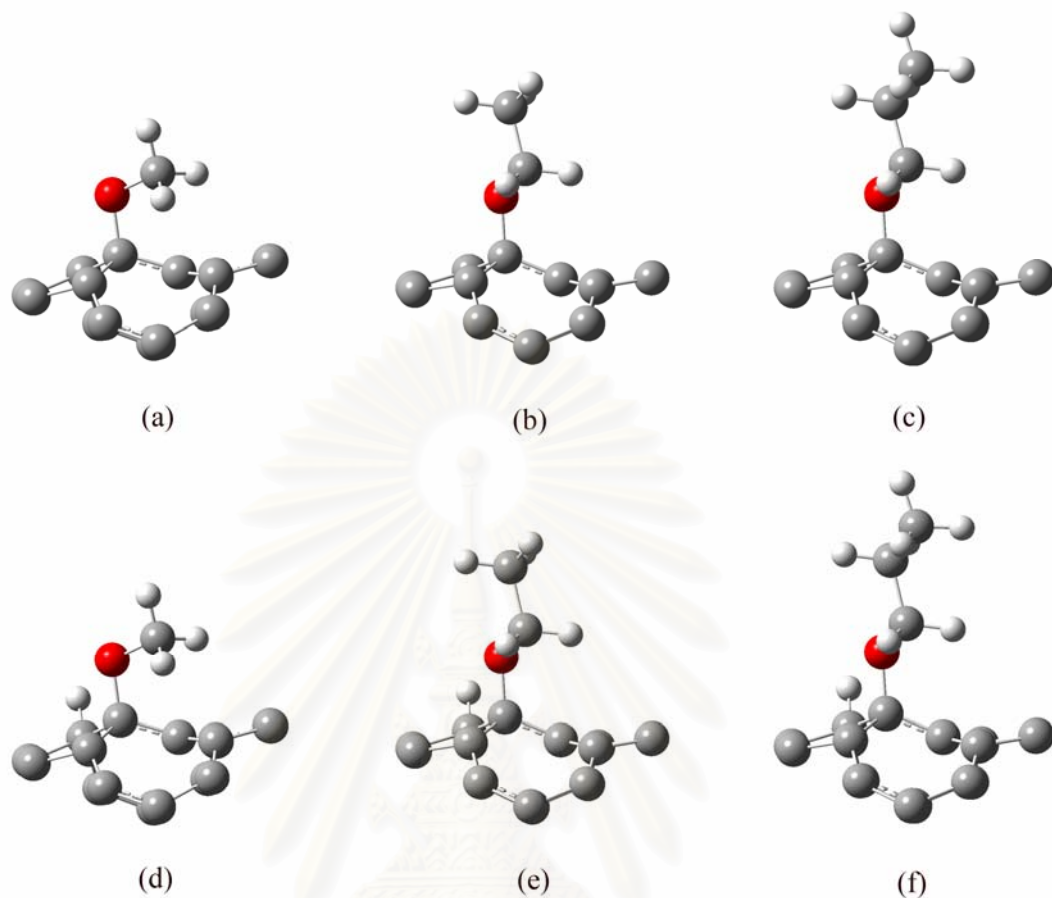


Figure 3.12 The high-layered ONIOM method for the adsorptions C1 to C3 alkoxide ions (methoxide ion, ethoxide ion and n-propoxide ion) on cap-ended (C_{80} and C_{120}) and open-ended ($C_{80}H_{20}$ and $C_{120}H_{20}$) defect as model 3 (a) SWCNT-OMe⁻ (b) SWCNT-OEt⁻ (c) SWCNT-OPr⁻ (d) SWCNT-H⁺-OMe⁻ (e) SWCNT-H⁺-OEt⁻ (f) SWCNT-H⁺-OPr⁻.

สถาบันวิทยบริการ
จุฬาลงกรณ์มหาวิทยาลัย

CHATER IV

RESULTS AND DISCUSSION

This chapter is divided into two parts, firstly, the adsorptions of proton, hydroxide and water molecule, secondly, the chemisorptions of hydroxide and C1 to C3 alkoxide ions. The details of results and discussion are shown below.

4.1 The Adsorptions of Proton and Hydroxide on Various Types of SWCNTs

4.1.1 Ab Initio (HF/3-21G) Calculation for Reaction Systems of Perfect and Defect Cap-Ended C₈₀ SWCNTs

As a first step of our investigation, it is important to find the most stable geometry of the reaction systems. The involved adsorbing species such as proton, hydroxide ion and water molecule adsorbed on perfect and defect cap-ended C₈₀ SWCNTs are performed using the *ab initio* Hartree–Fock (HF) with 3-21G basis set. Their optimized structures are shown in Figures 4.1 and 4.2, respectively for perfect and defect models. The diameter of the perfect model is 6.95 while another one is 6.81 Å. The SWCNT-H⁺ and SWCNT-OH⁻ systems, proton and hydroxide ion are formed σ bond with carbon atom of the SWCNT surface. The optimized structures of perfect SWCNT-H⁺, SWCNT-OH⁻ and defect SWCNT-H⁺, SWCNT-OH⁻ have been shown in Figures 4.1(a), 4.2(a), 4.1(b), and 4.2(b), respectively. For SWCNT-H⁺-OH⁻ system, a C-C π bond has been broken then proton and hydroxide ions are bonded with such two carbon atoms afterward. The distances between those broken carbon atom are extended to be 1.657 Å for perfect and 1.575 Å for defect cap-ended C₈₀, respectively. Figures 4.1(c) and 4.2(c) have been shown for perfect and defect models. The optimized geometries of the mono-hydration systems for protonated (SWCNT-H⁺...H₂O), hydroxylated (SWCNT-OH⁻...H₂O) and

protonated-hydroxylated (SWCNT-H⁺-OH⁻...H₂O) are shown in Figure 4.1 (d), (e), and (f) for perfect and Figure 4.2 (d), (e) and (f) for defect cap-ended C₈₀ SWCNT, respectively.

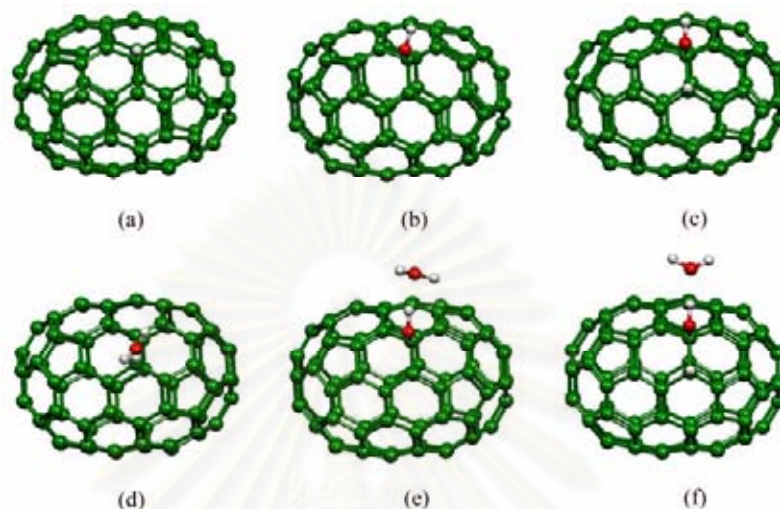


Figure 4.1 Optimized structures of various adsorbing species on the perfect cap-ended C₈₀ SWCNT computed at HF/3-21G level of theory (a) SWCNT-H⁺ (b) SWCNT-OH⁻ (c) SWCNT-H⁺-OH⁻ (d) SWCNT-H⁺...H₂O (e) SWCNT-OH⁻...H₂O (f) SWCNT-H⁺-OH⁻...H₂O.

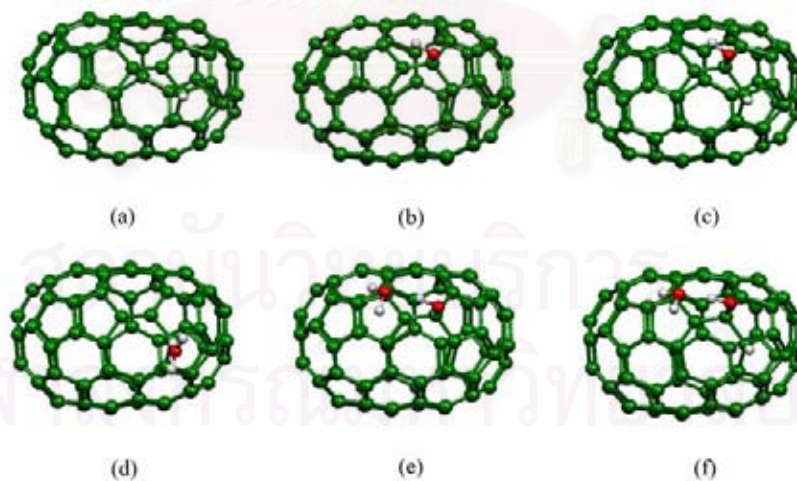


Figure 4.2 Optimized structures of various adsorbing species on the defect cap-ended C₈₀ SWCNT computed at HF/3-21G level of theory (a) SWCNT-H⁺ (b) SWCNT-OH⁻ (c) SWCNT-H⁺-OH⁻ (d) SWCNT-H⁺...H₂O (e) SWCNT-OH⁻...H₂O (f) SWCNT-H⁺-OH⁻...H₂O.

Their energies and thermodynamic quantities are presented in Table 4.1, and binding and strain energies perfect and defect cap-ended C₈₀ SWCNTs are presented in Table 4.2.

Table 4.1 Energies and thermodynamic quantities (in kcal/mol) of adsorption reaction on perfect and defect cap-ended C₈₀ SWCNTs computed at HF/3-21G level of theory.

Reaction	ΔE_{ZPE}	ΔH_{298}°	ΔG_{298}°
<i>Perfect SWNTs</i>			
SWCNT + H ⁺ → SWCNT-H ⁺	-215.65	-215.63	-215.78
SWCNT + OH ⁻ → SWCNT-OH ⁻	-139.31	-140.45	129.78
SWCNT-H ⁺ + OH ⁻ → SCWNT-H ⁺ -OH ⁻	-215.58	-216.63	-206.00
SWCNT-H ⁺ + H ₂ O → SWCNT-H ⁺ ...H ₂ O	-12.81	-12.66	-5.60
SWCNT-OH ⁻ + H ₂ O → SWCNT-OH ⁻ ...H ₂ O	-10.63	-11.23	-1.75
SWCNT-H ⁺ -OH ⁻ + H ₂ O → SWCNT-H ⁺ -OH ⁻ ...H ₂ O	-12.77	-12.92	-4.67
<i>Defect SWNTs</i>			
SWCNT + H ⁺ → SWCNT-H ⁺	-251.29	-251.59	-251.47
SWCNT + OH ⁻ → SWCNT-OH ⁻	-114.74	-115.62	-105.45
SWCNT-H ⁺ + OH ⁻ → SWCNT-H ⁺ -OH ⁻	-188.09	-189.10	-178.66
SWCNT-H ⁺ + H ₂ O → SWCNT-H ⁺ ...H ₂ O	-11.06	-10.82	-4.22
SWCNT-OH ⁻ + H ₂ O → SWCNT-OH ⁻ ...H ₂ O	-13.05	-13.73	-4.04
SWCNT-H ⁺ -OH ⁻ + H ₂ O → SWCNT-H ⁺ -OH ⁻ ...H ₂ O	-13.86	-14.47	-5.14

สถาบันวิทยบริการ
จุฬาลงกรณ์มหาวิทยาลัย

Table 4.2 Strain energies (ΔE_{st}) (in kcal/mol) and binding energies ($\Delta E_{binding}$) for perfect and defect cap-ended C_{80} SWCNTs of the various complexes computed at HF/3-21G level of theory

Tubes based on the complexes with	Perfect cap-ended C_{80}		Defect cap-ended C_{80}	
	ΔE_{st}	$\Delta E_{binding}$	ΔE_{st}	$\Delta E_{binding}$
H^+	16.51	-224.71	28.07	-259.96
OH^-	16.17	-114.77	36.89	-118.87
H^+OH^-	33.02	-221.13	66.79	-192.76
H^+ with H_2O	6.30	-14.05	24.09	-12.41
OH^- with H_2O	20.75	-13.65	42.61	-15.99
H^+OH^- with H_2O	33.87	-14.97	56.53	-16.64

Table 4.1 shows that the computed energies and thermodynamic quantities were derived from the frequency calculations at 298.15 K of reaction systems. It is found that the negative values of the energies denoted exothermic adsorption processes. The protonation (SWCNT- H^+) is more preferred than the hydroxylation (SWCNT- OH^-) for both perfect and defect cap-ended C_{80} SWCNTs. The binding energies of protonation and hydroxylation of the perfect are -224.71 and -114.77, and are -259.96 and -118.87 kcal/mol for defect models as shown in Table 4.2. Because of electron delocalization, so protonation reaction is occurred easier than hydroxylation.

Table 4.2 shows the binding energy of all reaction systems of perfect and defect models. -244.71, -144.77, -221.13, -14.05, -13.65 and -14.97 kcal/mol, respectively are binding energies of SWCNT- H^+ , SWCNT- OH^- , SWCNT- H^+OH^- , SWCNT- $H^+ \cdots H_2O$, SWCNT- $OH^- \cdots H_2O$ and SWCNT- $H^+OH^- \cdots H_2O$ for the perfect model and are -259.96, -118.87, 192.76, -12.41, -16.07 and -16.64 kcal/mol for defect model. Based on binding energies, mono-hydration is preferred in SWNT- H^+OH^- both perfect and defect tubes. The binding energy of mono-hydration of graphite is ~ 3.99 kcal/mol [49]. The previous work concluded that adsorption of SWCNT depended on curvature of the structure [50]. So, mono-hydration of graphite is lower than those of SWCNT because of its planar structure.

For the mono-hydration systems, the distances between oxygen atom of water molecule and adsorbing atom on SWCNT are 1.830, 1.821, 1.705 Å for perfect model; SWCNT-H⁺...H₂O, SWCNT-OH⁻...H₂O and SWCNT-H⁺-OH⁻...H₂O and 1.944, 1.769, 1.705 Å for defect models, respectively. The Mulliken charges on oxygen atom of water molecules are 0.082, 0.054, 0.072 and 0.067, 0.061, 0.076 for perfect and defect SWCNT-H⁺...H₂O, SWCNT-OH⁻...H₂O and SWCNT-H⁺-OH⁻...H₂O models, respectively. Thus, charge transferring from SWCNT-H⁺, SWCNT-OH⁻ and SWCNT-H⁺-OH⁻ to water molecule might be occurred.

The relative binding energies of SWCNT and adsorbing molecules are in decreasing order: SWCNT-H⁺ > SWCNT-H⁺-OH⁻ > SWCNT-OH⁻ for both perfect and defect cap-ended C₈₀ SWCNTs. For mono-hydration systems, their binding energies are in decreasing order: SWCNT-H⁺-OH⁻...H₂O > SWCNT-H⁺...H₂O > SWCNT-OH⁻...H₂O both perfect and defect cap-ended C₈₀ SWCNTs.

From the data in Table 4.2, the stepwise-adsorption feature as protonation, hydroxylation and hydration can therefore be proposed, as shown in equation. (4.1).



However, when proton and hydroxide ions are bound with carbon atoms of SWCNT, the C-C bond can be exothermally broken. Thus, stronger mono-hydration occurred in SWCNT-H⁺-OH⁻...H₂O than SWCNT-H⁺...H₂O and SWCNT-OH⁻...H₂O for both perfect and defect cap-ended C₈₀ SWCNTs. It was found that the mono-hydration of defect SWCNT-H⁺-OH⁻...H₂O is stronger than those of perfect model in which the calculated binding energies are -16.64 and -14.97 kcal/mol, respectively.

The strain energy [48], which is the C-C bond distortion energy of the adsorption-state structures of SWCNTs based on various reaction systems were evaluated at the HF/3-21G level of theory. Table 4.2 shows that the strain energies of the involved adsorbing species in the systems are within the ranges 6.30-33.87 and 24.09-56.53 kcal/mol for perfect and defect cap-ended C₈₀ SWCNT. Because of more extension of all

C-C bonds and also dropping of the 5-7-7-5 ring in the structure, so strain energy of defect tube is more than those of perfect tube.

4.1.2 Preliminary Calculations for a Two-Layered ONIOM(MO:MO) Methods

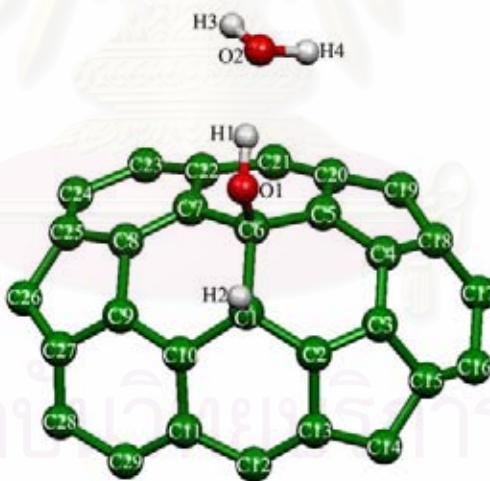
The two-layered ONIOM calculations were performed at the ONIOM(HF/3-21G:PM3), ONIOM(HF/3-21G:AM1) and ONIOM(B3LYP/6-31G(d):AM1) levels of theory and compared to the HF/3-21G energy for the adsorption on the perfect cap-ended armchair (5,5) C₈₀ SWCNT. Their binding energies were obtained and presented in Table 4.3. Based on the ONIOM(B3LYP/6-31G(d):AM1) result, either with model 1 or model 2 for the protonation and hydroxylation on the perfect cap-ended C₈₀ SWCNT are underestimated compared to HF/3-21G level. On the other hand, the hydroxylation reactions on the protonated cap-ended SWCNT are over estimated compared to the HF/3-21G computation. For the hydration reaction, the ONIOM(HF/3-21G:PM3) and ONIOM(HF/3-21G:AM1) calculations are not significantly different to HF/3-21G result. The ONIOM(B3LYP/6-31G(d):AM1) level was therefore selected as more reliable method to be employed for all the calculations of adsorptions on either cap-ended and open-ended (5,5) SWCNTs. Geometrical data for the structures of perfect cap-ended C₈₀ SWCNT model 2 complexes with proton and hydroxide in the systems with water computed at various methods are listed in Table 4.4.

Table 4.3 Reaction energies on the perfect cap-ended C₈₀ SWCNT computed at the various methods.

Reactions	$\Delta_r E^a$						
	HF/3-21G	ONIOM					
		(HF/3-21G:PM3)		(HF/3-21G:AM1)		(B3LYP/6-31G(d):AM1)	
		model 1	model 2	model 1	model 2	model 1	model 2
SWCNT + H ⁺ → SWCNT-H ⁺	-224.71	-197.96	-190.30	-193.09	-183.94	-194.45	-188.62
SWCNT + OH ⁻ → SWCNT-OH ⁻	-144.77	-119.11	-122.49	-123.81	-128.29	-112.65	- ^b
SWCNT-H ⁺ + OH ⁻ → SWCNT-H ⁺ -OH ⁻	-221.13	-228.92	-235.57	-233.71	-241.73	-222.96	-213.69
SWCNT-H ⁺ + H ₂ O → SWCNT-H ⁺ ...H ₂ O	-14.05	-15.52	-15.19	-15.89	-15.87	-11.27	-10.65
SWCNT-OH ⁻ + H ₂ O → SWCNT-OH ⁻ ...H ₂ O	-13.65	-13.88	-13.79	-13.78	-13.76	-11.45	- ^b
SWCNT-H ⁺ -OH ⁻ + H ₂ O → SWCNT-H ⁺ -OH ⁻ ...H ₂ O	-14.97	-14.99	-15.28	-15.18	-15.64	-11.14	-10.26

^a In kcal/mol.

^b No convergence was found.



The optimized structure of mono-hydration for protonated-hydroxylated system of perfect cap-ended C₈₀ SWCNT model 2 at the high level of theory and some selected geometrical parameters (bond and bond angle) are listed in Table 4.4

Table 4.4 Geometrical parameters for the geometries of perfect cap-ended C₈₀ SWCNT complexes with proton, hydroxide ion and water molecule at various levels of theory.

Parameters	HF/3-21G	ONIOM (HF/3- 21G:PM3), model 1	ONIOM (HF/3- 21G:PM3), model 2	ONIOM (HF/3- 21G:AM), model 1	ONIOM (HF/3- 21G:AM), model 2	ONIOM (B3LYP/ 6- 31G(d): AM1), model 1	ONIOM (B3LYP/ 6- 31G(d): AM1), model 2
SWCNT							
C1-C2	1.489	1.496	1.494	1.494	1.494	1.502	1.495
C2-C3	1.349	1.377	1.347	1.382	1.347	1.390	1.379
C3-C4	1.447	1.430	1.442	1.427	1.441	1.449	1.444
C4-C5	1.348	1.376	1.349	1.381	1.349	1.389	1.382
C5-C6	1.496	1.504	1.531	1.502	1.499	1.513	1.501
C1-C6	1.661	1.687	1.664	1.685	1.664	1.682	1.678
C6-C7	1.531	1.538	1.537	1.537	1.535	1.548	1.532
C7-C8	1.365	1.365	1.361	1.367	1.362	1.374	1.392
C8-C9	1.497	1.508	1.495	1.513	1.494	1.543	1.490
C9-C10	1.365	1.366	1.367	1.368	1.368	1.375	1.378
C1-C10	1.523	1.530	1.525	1.529	1.525	1.535	1.521
C10-C11	1.445	1.459	1.452	1.463	1.450	1.485	1.479
C11-C12	1.470	1.461	1.464	1.459	1.468	1.475	1.443
C12-C13	1.370	1.394	1.409	1.395	1.383	1.414	1.436
C2-C13	1.479	1.462	1.477	1.461	1.477	1.479	1.471
C13-C14	1.417	1.417	1.416	1.421	1.421	1.425	1.398
C14-C15	1.443	1.460	1.451	1.461	1.451	1.456	1.495
C3-C15	1.483	1.461	1.511	1.462	1.495	1.466	1.495
C15-C16	1.351	1.372	1.357	1.374	1.359	1.373	1.348
C16-C17	1.478	1.470	1.491	1.474	1.489	1.474	1.557
C17-C18	1.351	1.371	1.368	1.373	1.373	1.373	1.349
C4-C18	1.485	1.463	1.514	1.464	1.494	1.468	1.490
C18-C19	1.440	1.458	1.435	1.459	1.433	1.454	1.496
C19-C20	1.419	1.417	1.425	1.421	1.431	1.425	1.401
C5-C20	1.478	1.462	1.482	1.462	1.482	1.481	1.463
C20-C21	1.371	1.396	1.380	1.397	1.379	1.416	1.448
C21-C22	1.470	1.464	1.465	1.461	1.470	1.479	1.442
C7-C22	1.444	1.462	1.460	1.466	1.459	1.489	1.459
C22-C23	1.374	1.381	1.381	1.380	1.383	1.382	1.425
C23-C24	1.421	1.439	1.436	1.446	1.438	1.447	1.428
C24-C25	1.369	1.381	1.372	1.382	1.375	1.382	1.385
C8-C25	1.425	1.434	1.438	1.437	1.436	1.442	1.431
C25-C26	1.446	1.454	1.451	1.460	1.453	1.457	1.494
C26-C27	1.446	1.455	1.446	1.460	1.450	1.458	1.432
C27-C28	1.369	1.382	1.378	1.383	1.380	1.382	1.399
C28-C29	1.422	1.439	1.433	1.446	1.434	1.447	1.451
C11-C29	1.373	1.381	1.384	1.380	1.385	1.382	1.406
Absorbent							
C1-H2	1.084	1.084	1.084	1.085	1.085	1.099	1.100
C6-O1	1.436	1.436	1.436	1.434	1.435	1.425	1.432
O1-H1	0.982	0.983	0.983	0.984	0.983	0.988	0.985
H1...O2	1.705	1.719	1.704	1.710	1.695	1.824	1.838
angle							
O1-H1-O2	164.8	162.9	164.6	163.3	164.9	166.1	168.6
C6-O1-H1	108.8	108.9	108.9	109.0	108.9	107.3	107.0

The geometrical parameters of the SWCNT-H⁺-OH⁻...H₂O model 2 optimized with a variety of ONIOM methods are listed in Table 4.4. The structures optimized with all ONIOM methods are not significantly different compared to full HF/3-21 calculation. So, the ONIOM method is reliable for calculation. For saving calculation's time, the ONIOM method with high level B3LYP/6-31G(d) and low level AM1 is chosen for calculation.

4.1.2.1 Strain Energies and Geometrical Structures

Strain energies of various C₈₀ and C₈₀H₂₀ SWCNTs models are computed at B3LYP/6-31G(d)//ONIOM(B3LYP/6-31G(d):AM1) level for and at the level with models 3 and 4 for the perfect cap-ended and defect C₁₂₀ SWCNTs are listed in Table 4.5. The ONIOM(B3LYP/6-31G(d):AM1)-optimized structures for the perfect and defect cap-ended SWCNTs as C₈₀, their complexes C₈₀-H⁺, C₈₀-OH⁻, C₈₀-H⁺-OH⁻ are shown in Figures A-3 and A-5, respectively. The ONIOM(B3LYP/6-31G(d):AM1)-optimized structures for the perfect and defect cap-ended C₁₂₀ SWCNTs and its complexes C₁₂₀-H⁺, C₁₂₀-OH⁻ and C₁₂₀-H⁺-OH⁻ are shown in Figures A-8 and A-9, respectively. The ONIOM(B3LYP/6-31G(d):AM1)-optimized structures for the perfect and defect open-ended C₈₀H₂₀ SWCNTs, their complexes C₈₀H₂₀-H⁺, C₈₀H₂₀-OH⁻, C₈₀H₂₀-H⁺-OH⁻ are shown in Figures A-6 and A-7, respectively.

The most stable geometry for the various perfect and defect SWCNT models; perfect open-ended C₈₀H₂₀, defect open-ended C₈₀H₂₀, perfect cap-ended C₁₂₀ and defect cap-ended C₁₂₀ are shown in Figures 4.3, 4.4, 4.5, and 4.6, respectively.

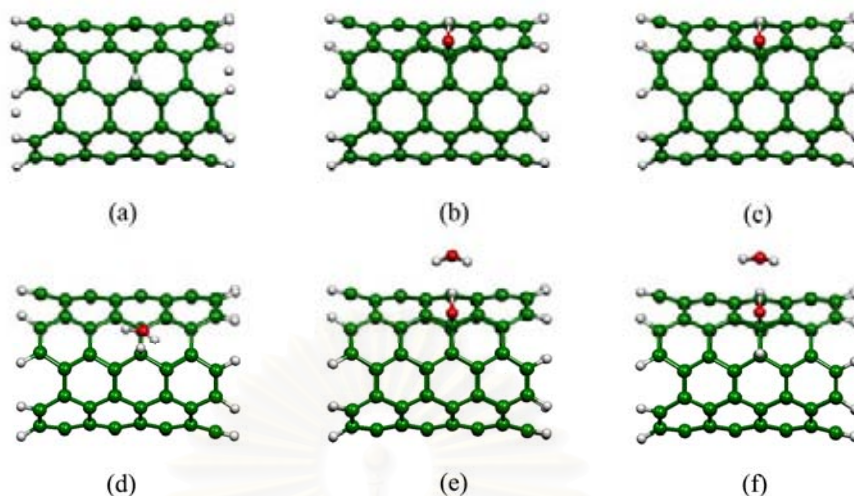


Figure 4.3 Optimized structures of various adsorbing species on the perfect open-ended $C_{80}H_{20}$ SWCNTs computed at ONIOM(B3LYP/6-31G(d):AM1) level of theory (a) SWCNT- H^+ (b) SWCNT- OH^- (c) SWCNT- H^+ - OH^- (d) SWCNT- H^+ \cdots H $_2$ O (e) SWCNT- OH^- \cdots H $_2$ O (f) SWCNT- H^+ - OH^- \cdots H $_2$ O.

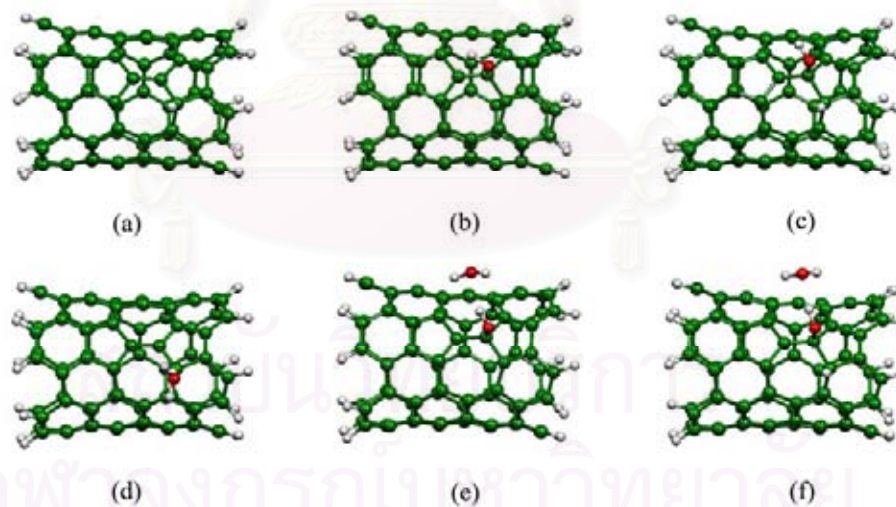


Figure 4.4 Optimized structures of various adsorbing species on the defect open-ended $C_{80}H_{20}$ SWCNTs computed at ONIOM(B3LYP/6-31G(d):AM1) (a) SWCNT- H^+ (b) SWCNT- OH^- (c) SWCNT- H^+ - OH^- (d) SWCNT- H^+ \cdots H $_2$ O (e) SWCNT- OH^- \cdots H $_2$ O (f) SWCNT- H^+ - OH^- \cdots H $_2$ O.

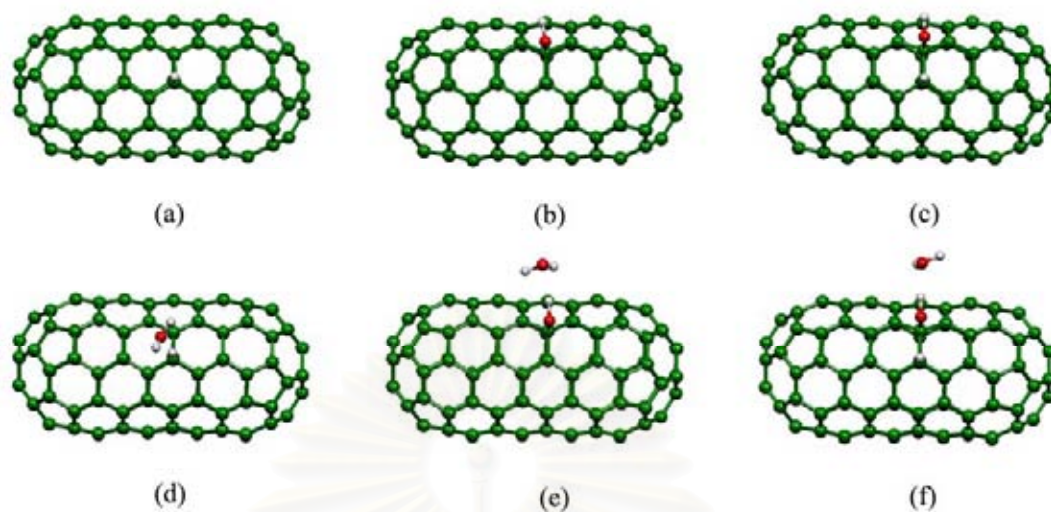


Figure 4.5 Optimized structures of various adsorbing species on the perfect cap-ended C_{120} SWCNTs computed at ONIOM(B3LYP/6-31G(d):AM1) level of theory (a) SWCNT- H^+ (b) SWCNT- OH^- (c) SWCNT- H^+-OH^- (d) SWCNT- $H^+\cdots H_2O$ (e) SWCNT- $OH^- \cdots H_2O$ (f) SWCNT- $H^+-OH^- \cdots H_2O$.

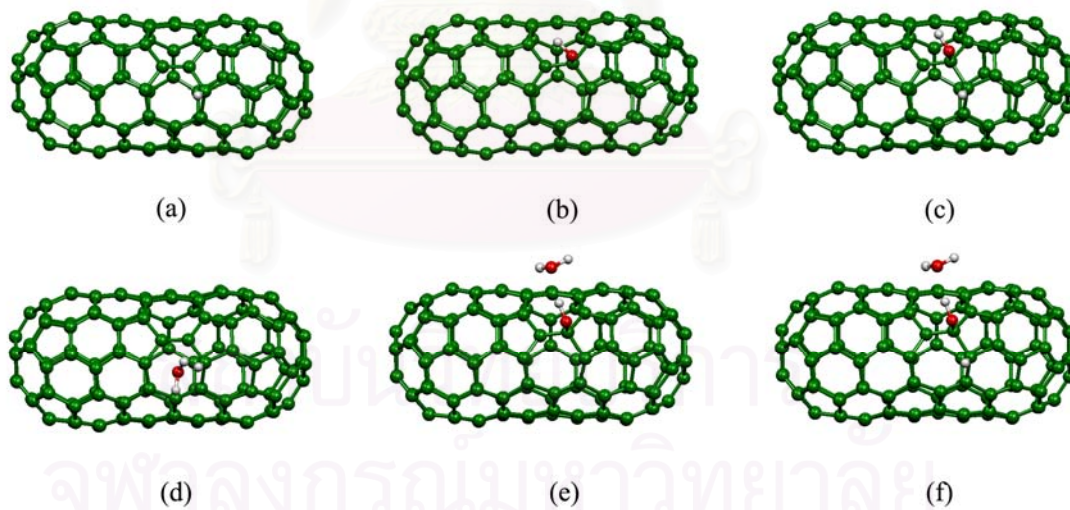


Figure 4.6 Optimized structures of various adsorbing species on the perfect open-ended C_{120} SWCNTs computed at ONIOM(B3LYP/6-31G(d):AM1) level of theory (a) SWCNT- H^+ (b) SWCNT- OH^- (c) SWCNT- H^+-OH^- (d) SWCNT- $H^+\cdots H_2O$ (e) SWCNT- $OH^- \cdots H_2O$ (f) SWCNT- $H^+-OH^- \cdots H_2O$.

Table 4.5 Strain energies (in kcal/mol) for C₈₀, C₈₀H₂₀ and the cap-ended perfect and defect C₁₂₀ SWCNTs of the various complexes computed at various levels of theory

Tubes based on the complexes with	ΔE_{st}							
	Perfect cap-ended C ₈₀ ^a	Perfect cap-ended C ₈₀ ^b	Perfect cap-ended C ₈₀ ^c	Perfect open-ended C ₈₀ H ₂₀ ^b	Defect cap-ended C ₈₀ ^d	Defect open-ended C ₈₀ H ₂₀ ^d	Perfect cap-ended C ₁₂₀ ^e	Defect cap-ended C ₁₂₀ ^d
H ⁺	16.51	16.21	20.42	37.06	8.83	25.30	6.18	43.87
OH ⁻	16.17	25.25	- ^f	25.72	31.88	25.64	10.60	41.94
H ⁺ -OH ⁻	33.02	42.87	46.32	39.20	34.36	61.66	32.33	62.96
H ⁺ with H ₂ O	6.30	13.56	16.33	19.35	4.52	22.61	3.55	29.33
OH ⁻ with H ₂ O	20.75	27.82	- ^f	26.98	33.11	34.66	16.23	74.81
H ⁺ -OH ⁻ with H ₂ O	33.87	44.67	47.67	41.52	35.34	67.68	40.76	65.10

^a Computed at the HF/3-21G level.

^b Computed at the B3LYP/6-31G(d)//ONIOM(B3LYP/6-31G(d):AM1) of model 1.

^c Computed at the B3LYP/6-31G(d)//ONIOM(B3LYP/6-31G(d):AM1) of model 2.

^d Computed at the B3LYP/6-31G(d)//ONIOM(B3LYP/6-31G(d):AM1) of model 3.

^e Computed at the B3LYP/6-31G(d)//ONIOM(B3LYP/6-31G(d):AM1) of model 4.

^f No convergence was found.

Table 4.6 Energetic and thermodynamic quantities (in kcal/mol) of adsorption reactions on various types of perfect and defect SWCNTs at different computation models.

Reaction	ΔE_{ZPE}	ΔH_{298}°	ΔG_{298}°	ΔE_{ZPE}	ΔH_{298}°	ΔG_{298}°	ΔE_{ZPE}	ΔH_{298}°	ΔG_{298}°
Perfect SWCNTs	Cap-ended C ₈₀ , model 1 ^a			Open-ended C ₈₀ H ₂₀ , model 1 ^a			Cap-ended C ₁₂₀ , model 4 ^b		
SWCNT + H ⁺ → SWCNT-H ⁺	-187.47	-187.54	-187.65	-218.97	-218.90	-219.03	-195.50	-195.36	-195.62
SWCNT + OH ⁻ → SWCNT-OH ⁻	-109.59	-110.57	-100.15	-80.71	-81.71	-71.27	-105.01	-105.93	-95.64
SWCNT-H ⁺ + OH ⁻ → SWCNT-H ⁺ -OH ⁻	-214.74	-233.25	-205.22	-188.34	-189.45	-178.84	-200.09	-201.45	-190.52
SWCNT-H ⁺ + H ₂ O → SWCNT-H ⁺ ...H ₂ O	-10.09	-9.99	-2.85	-6.91	-6.72	0.11	-8.12	-7.94	-1.05
SWCNT-OH ⁻ + H ₂ O → SWCNT-OH ⁻ ...H ₂ O	-8.95	-9.50	0.01	-8.57	-9.05	0.33	-6.94	-7.25	1.38
SWCNT-H ⁺ -OH ⁻ + H ₂ O → SWCNT-H ⁺ -OH ⁻ ...H ₂ O	-8.92	8.15	-0.41	-8.35	-8.73	0.28	-7.93	-8.09	0.03
Defect SWCNTs	Cap-ended C ₈₀ , model 3 ^c			Open-ended C ₈₀ H ₂₀ , model 3 ^c			Cap-ended C ₁₂₀ , model 3 ^a		
SWCNT + H ⁺ → SWCNT-H ⁺	-223.47	-223.41	-223.52	-223.10	-222.44	-223.94	-208.05	-207.95	-208.11
SWCNT + OH ⁻ → SWCNT-OH ⁻	-110.69	-111.88	-101.65	-72.10	-72.50	-63.48	-108.18	-109.14	-98.77
SWCNT-H ⁺ + OH ⁻ → SWCNT-H ⁺ -OH ⁻	-178.41	-179.30	-196.09	-141.40	-142.44	-131.98	-177.51	-178.57	-168.02
SWCNT-H ⁺ + H ₂ O → SWCNT-H ⁺ ...H ₂ O	-7.52	-7.26	-1.11	-6.02	-5.70	0.54	-6.97	-6.74	0.20
SWCNT-OH ⁻ + H ₂ O → SWCNT-OH ⁻ ...H ₂ O	-10.70	-11.23	-1.94	-8.49	-9.07	0.55	-8.64	-8.82	-0.72
SWCNT-H ⁺ -OH ⁻ + H ₂ O → SWCNT-H ⁺ -OH ⁻ ...H ₂ O	-9.91	-10.39	-1.35	-7.85	-8.19	0.70	-7.65	-7.91	0.67

^a ONIOM(B3LYP/6-31G(d):AM1) with a pyrene as a high layer model.

^b ONIOM(B3LYP/6-31G(d):AM1) with an ovalene as a high layer model.

^c ONIOM(B3LYP/6-31G(d):AM1) with a 5-7-7-5 cluster as a high layer model.

For the hydroxylation reactions on the protonated cap-ended SWCNT, all the ONIOM results related to the HF/3-21G computation are over estimated, except the computed at the ONIOM(B3LYP/6-31G(d):AM1) level (-213.69 kcal/mol) of which the energy is close to the HF/3-21G result (-221.13 kcal/mol). The mono-hydration for protonated and hydroxylated perfect cap-ended C₈₀ SWCNT are somewhat weak as shown at the last three lines in Table 4.3. For the hydration reaction, the HF/3-21G and all the ONIOM(HF/3-21G:MO) calculations seem to be over-estimated as compared to the ONIOM(B3LYP/6-31G(d):AM1) energies. The ONIOM(B3LYP/6-31G(d):AM1) level was therefore selected as more reliable method to be employed for all the calculations of adsorptions on either cap-ended and open-ended (5,5) SWCNTs.

Strain energies for perfect and defect cap-ended C₈₀, C₁₂₀ and open-ended C₈₀H₂₀ SWCNTs of the various complexes computed at the HF/3-21G and ONIOM(B3LYP/6-31G(d):AM1) levels of theory are listed in Table 4.5. Table 4.5 shows that all the protonated-hydroxylated (H⁺-OH⁻) SWCNTs highly affect to the SWCNTs structures of which strain energies in the systems without and with a water molecule are within the ranges of 33.02-61.60 and 33.87-47.67 kcal/mol, respectively. In the systems without and with a water molecule, strain of the SWCNTs caused by the hydroxylation being larger than that caused by the protonation were found.

4.1.2.2 Energies and Thermodynamic Quantities

The zero-point (ΔE_{ZPE}), enthalpy (ΔH_{298}^0) and Gibbs free (ΔG_{298}^0) energies of the adsorption and hydration reaction obtained from vibrational frequency correction at 298.15 K using ONIOM(B3LYP/6-31G(d):AM1) level are listed in Table 4.6. All the adsorption reaction at 298.15 K are exothermic reactions.

All the adsorptions at 298.15 K are exothermic reactions. In the systems without water, the protonation and hydroxylation of all types of SWCNTs and hydroxylation of their protonated structures are spontaneous reactions. Relative stabilities of adsorptions on the perfect SWCNTs are in decreasing order: open-ended $C_{80}H_{20} >$ cap-ended $C_{120} \sim$ cap-ended C_{80} for protonation and cap-ended $C_{80} >$ cap-ended $C_{120} >$ open-ended $C_{80}H_{20}$ for their protonated forms, and on the defect SWCNTs are cap-ended $C_{80} \sim$ open-ended $C_{80}H_{20} >$ cap-ended C_{120} for protonation and cap-ended $C_{80} \sim$ cap-ended $C_{120} >$ open-ended $C_{80}H_{20}$ for their protonated forms.

4.1.2.3 Reaction Sequence on the Cap-Ended C_{120} SWCNT

On the cap-ended C_{120} SWCNT, the most preferable adsorption mechanism can be proposed as a reaction sequence: protonation, hydroxylation and hydration, as shown in equation. (4.2).



For the perfect cap-ended C_{120} SWCNT, the reaction energies (kcal/mol) obtained at the ONIOM(B3LYP/6-31G(d):AM1) level are $\Delta E_{ads}^1 = -202.3$, $\Delta E_{ads}^2 = -204.9$ and $\Delta E_{ads}^3 = -9.8$. For the defect cap-ended C_{120} SWCNT, the preferable reaction energies obtained at the ONIOM(B3LYP/6-31G(d):AM1) level are $\Delta E_{ads}^1 = -213.9$, $\Delta E_{ads}^2 = -180.9$ and $\Delta E_{ads}^3 = -8.0$ kcal/mol. The hydroxylation of protonated perfect cap-ended C_{120} SWCNT is more preferable than that of its corresponding defect tube by 9.3 kcal/mol.

4.2 The Chemisorptions of Hydroxide and C1 to C3 Alkoxides

4.2.1 Geometrical Structures

The geometrical structures of the involved adsorbing species in the reaction systems hydroxylated SWCNT (SWCNT-OH⁻), methoxylated SWCNT (SWCNT-OMe⁻), ethoxylated SWCNT (SWCNT-OEt⁻), n-propoxylated SWCNT (SWCNT-OPr⁻), hydroxide ion with protonated SWCNT (SWCNT-H⁺-OH⁻), methoxide ion with protonated SWCNT (SWCNT-H⁺-OMe⁻), ethoxide ion with protonated SWCNT (SWCNT-H⁺-OEt⁻) and n-propoxide ion with protonated SWCNT (SWCNT-H⁺-OPr⁻) of model 1 for perfect SWCNTs (cap-ended C₈₀ and C₁₂₀, open-ended C₈₀H₂₀ and C₁₂₀H₂₀) and model 3 for defect SWCNTs (cap-ended C₈₀ and C₁₂₀, open-ended C₈₀H₂₀ and C₁₂₀H₂₀) were computed at ONIOM(B3LYP/6-31G(d):AM1) method. The optimized geometries of the involved adsorbing species in the reaction systems of various types SWCNTs, perfect cap-ended C₈₀ SWCNT, defect cap-ended C₈₀ SWCNT, perfect open-ended C₈₀H₂₀ SWCNT, defect open-ended C₈₀H₂₀ SWCNT, perfect cap-ended C₁₂₀ SWCNT, defect cap-ended C₁₂₀ SWCNT, perfect open-ended C₁₂₀H₂₀ SWCNT and defect open-ended C₁₂₀H₂₀ SWCNT are shown in Figure 4.7, 4.8, 4.9, 4.10, 4.11, 4.12, 4.13 and 4.14, respectively. All adsorption and strain energies of the involved adsorbing species for the reaction systems are listed in Table 4.7. The geometrical parameters of the involved adsorbing species in the systems perfect cap-ended C₈₀ SWCNT, defect cap-ended C₈₀ SWCNT, perfect open-ended C₈₀H₂₀ SWCNT, defect open-ended C₈₀H₂₀ SWCNT, perfect cap-ended C₁₂₀ SWCNT, defect cap-ended C₁₂₀ SWCNT, perfect open-ended C₁₂₀H₂₀ SWCNT and defect open-ended C₁₂₀H₂₀ SWCNT are shown in Figure A-9, A-10, A-11, A-12, A-13, A-14, A-16, respectively (the part of appendix A).

The adsorbing species; hydroxide ion, methoxide ion, ethoxide ion and n-propoxide ion are bound to carbon atom opposite to another carbon atom which bound to proton on SWCNT. The addition of adsorbing species to the protonated SWCNTs lead to the cleavage of the C-C bond. The computed adsorption energies of reaction systems were found to be exothermic processes.

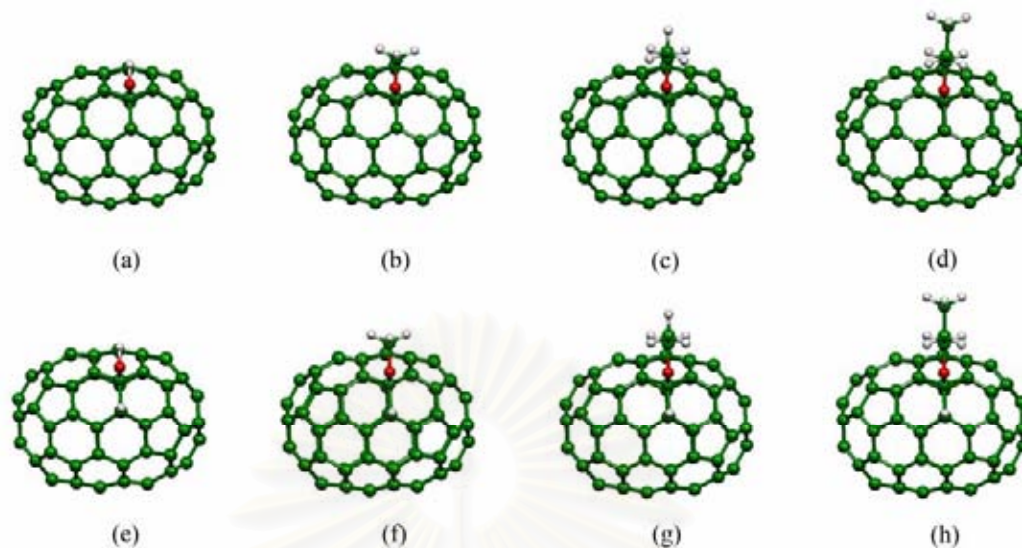


Figure 4.7 Optimized structures of various adsorbing species on the perfect cap-ended C_{80} SWCTs computed at ONIOM(B3LYP/6-31G(d):AM1) level of theory (a) SWCNT-OH⁻ (b) SWCNT-OMe⁻ (c) SWCNT-OEt⁻ (d) SWCNT-OPr⁻ (e) SWCNT-H⁺-OH⁻ (f) SWCNT-H⁺-OMe⁻ (g) SWCNT-H⁺-OEt⁻ (h) SWCNT-H⁺-OPr⁻.

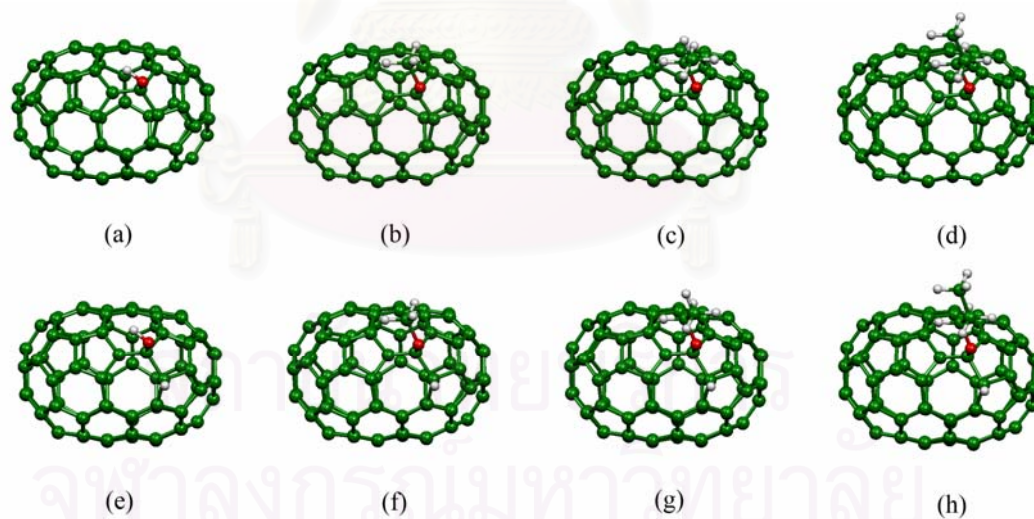


Figure 4.8 Optimized structures of various adsorbed species on the defect cap-ended C_{80} SWCT computed at ONIOM(B3LYP/6-31G(d):AM1) level of theory (a) SWCNT-OH⁻ (b) SWCNT-OMe⁻ (c) SWCNT-OEt⁻ (d) SWCNT-OPr⁻ (e) SWCNT-H⁺-OH⁻ (f) SWCNT-H⁺-OMe⁻ (g) SWCNT-H⁺-OEt⁻ (h) SWCNT-H⁺-OPr⁻.

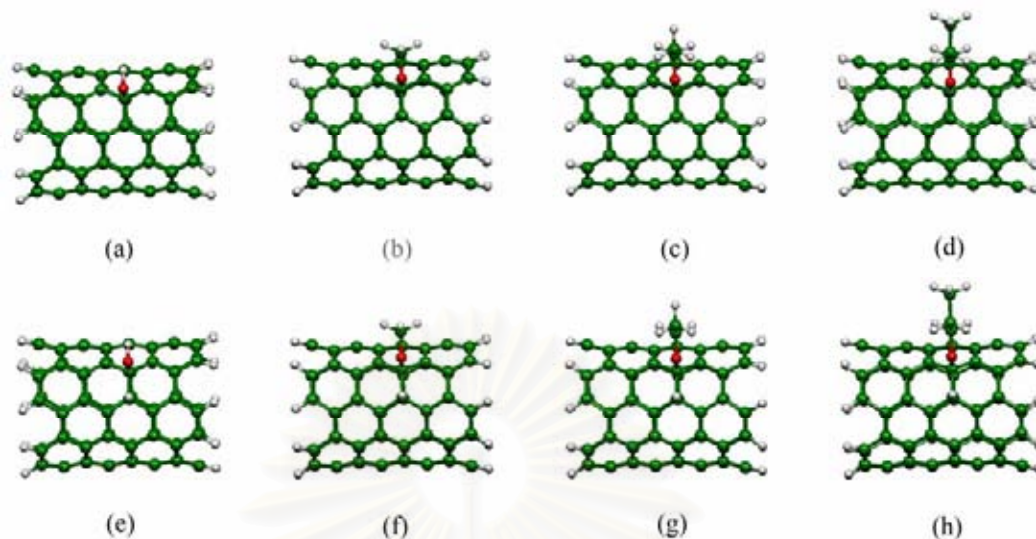


Figure 4.9 Optimized structures of various adsorbed species on the perfect cap-ended $C_{80}H_{20}$ SWCNT computed at ONIOM(B3LYP/6-31G(d):AM1) level of theory (a) SWCNT-OH⁻ (b) SWCNT-OMe⁻ (c) SWCNT-OEt⁻ (d) SWCNT-OPr⁻ (e) SWCNT-H⁺-OH⁻ (f) SWCNT-H⁺-OMe⁻ (g) SWCNT-H⁺-OEt⁻ (h) SWCNT-H⁺-OPr⁻.

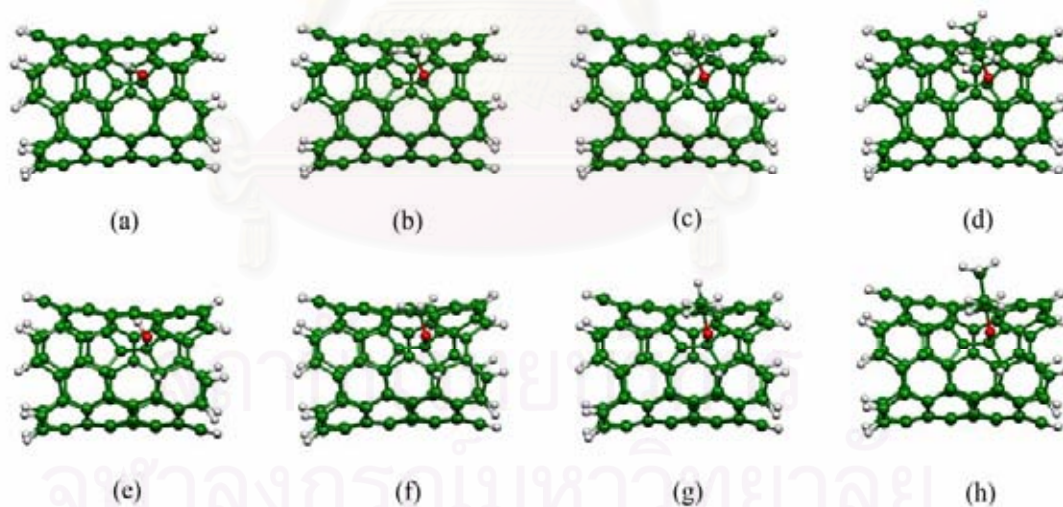


Figure 4.10 Optimized structures of various adsorbing species on the perfect cap-ended $C_{80}H_{20}$ SWCNT computed at ONIOM(B3LYP/6-31G(d):AM1) level of theory (a) SWCNT-OH⁻ (b) SWCNT-OMe⁻ (c) SWCNT-OEt⁻ (d) SWCNT-OPr⁻ (e) SWCNT-H⁺-OH⁻ (f) SWCNT-H⁺-OMe⁻ (g) SWCNT-H⁺-OEt⁻ (h) SWCNT-H⁺-OPr⁻.

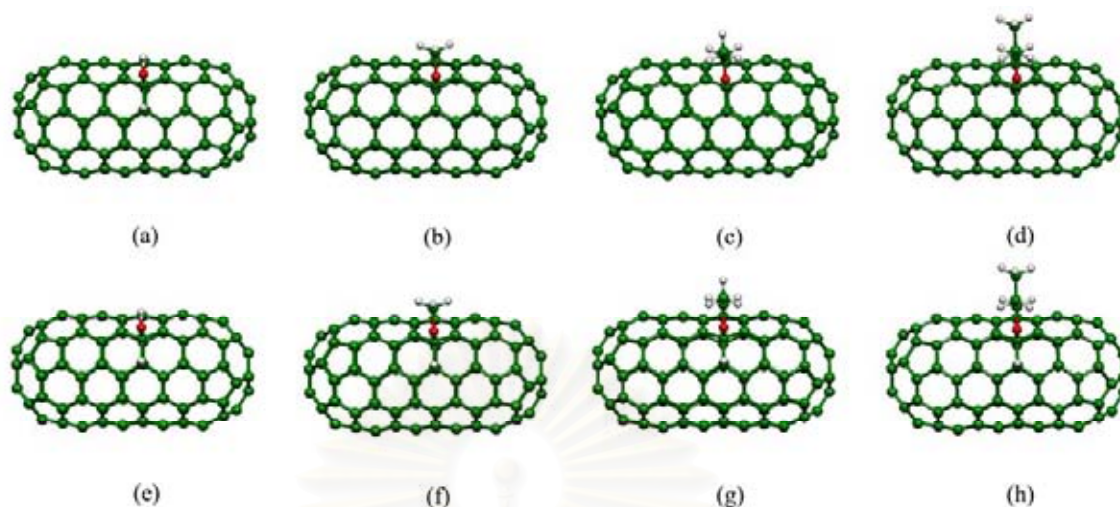


Figure 4.11 Optimized structures of various adsorbed species on the perfect cap-ended C_{120} SWCNT computed at ONIOM(B3LYP/6-31G(d):AM1) level of theory (a) SWCNT- OH^- (b) SWCNT- OMe^- (c) SWCNT- OEt^- (d) SWCNT- OPr^- (e) SWCNT- H^+ - OH (f) SWCNT- H^+ - OMe^- (g) SWCNT- H^+ - OEt^- (h) SWCNT- H^+ - OPr^- .

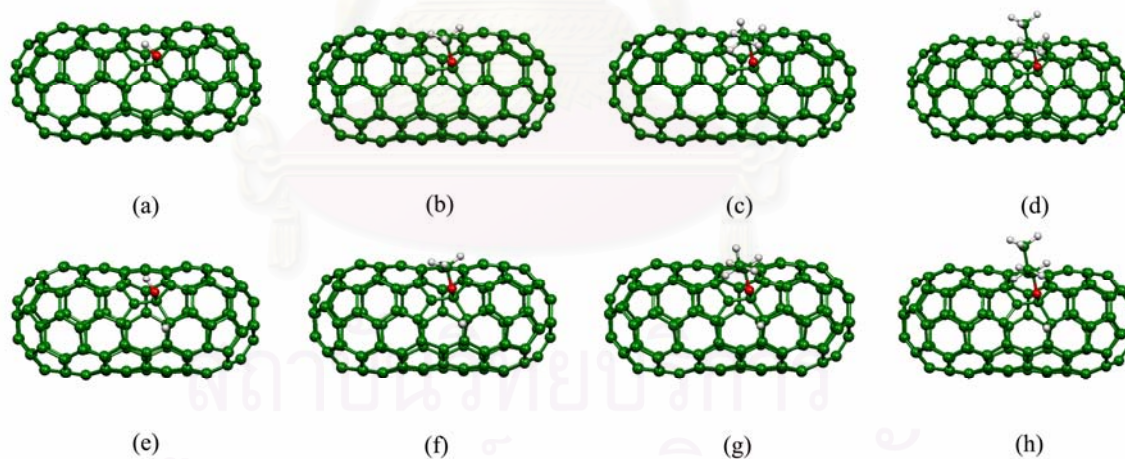


Figure 4.12 Optimized structures of various adsorbed species on the perfect cap-ended C_{120} SWCNT computed at ONIOM(B3LYP/6-31G(d):AM1) level of theory (a) SWCNT- OH^- (b) SWCNT- OMe^- (c) SWCNT- OEt^- (d) SWCNT- OPr^- (e) SWCNT- H^+ - OH (f) SWCNT- H^+ - OMe^- (g) SWCNT- H^+ - OEt^- (h) SWCNT- H^+ - OPr^- .

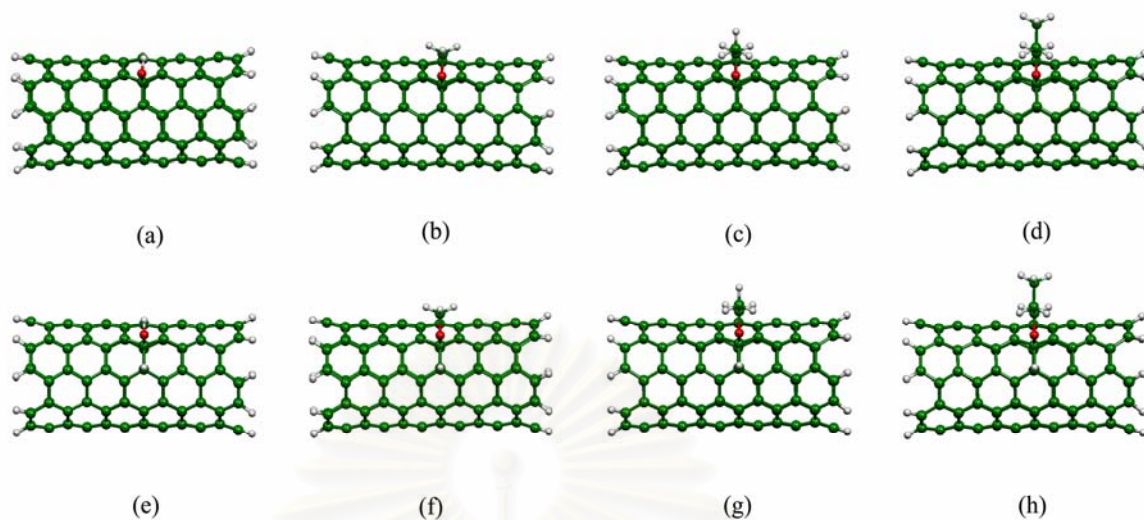


Figure 4.13 Optimized structures of various adsorbed species on the perfect cap-ended $C_{120}H_{20}$ SWCNT computed at ONIOM(B3LYP/6-31G(d):AM1) level of theory (a) SWCNT- OH^- (b) SWCNT- OMe^- (c) SWCNT- OEt^- (d) SWCNT- OPr^- (e) SWCNT- H^+-OH^- (f) SWCNT- H^+-OMe^- (g) SWCNT- H^+-OEt^- (h) SWCNT- H^+-OPr^- .

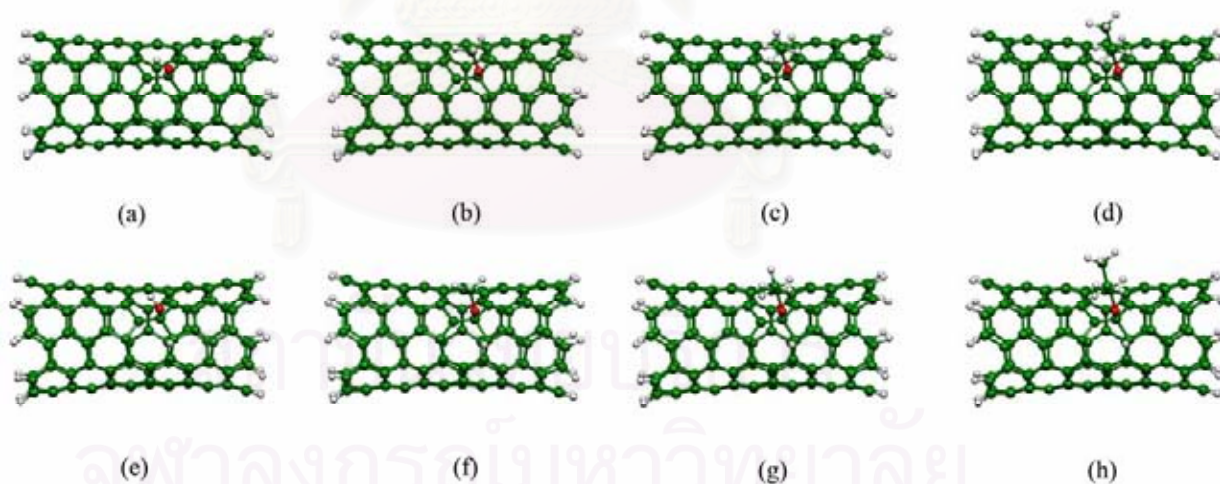


Figure 4.14 Optimized structures of various adsorbed species on the perfect cap-ended $C_{120}H_{20}$ SWCNT computed at ONIOM(B3LYP/6-31G(d):AM1) level of theory (a) SWCNT- OH^- (b) SWCNT- OMe^- (c) SWCNT- OEt^- (d) SWCNT- OPr^- (e) SWCNT- H^+-OH^- (f) SWCNT- H^+-OMe^- (g) SWCNT- H^+-OEt^- (h) SWCNT- H^+-OPr^- .

Table 4.7 Binding energies (ΔE_{bind}) in kcal/mol for SWCNTs of the various complexes computed at two-layered ONIOM(B3LYP/6-31G(d):AM1) level of theory

Tubes based on the complexes with	Perfect cap-ended C ₈₀	Defect cap-ended C ₈₀	Perfect open-ended C ₈₀ H ₂₀	Defect open-ended C ₈₀ H ₂₀	Perfect cap-ended C ₁₂₀	Defect cap-ended C ₁₂₀	Perfect open-ended C ₁₂₀ H ₂₀	Defect open-ended C ₁₂₀ H ₂₀
	$\Delta E_{\text{bind}}^{\text{a}}$	$\Delta E_{\text{bind}}^{\text{b}}$	$\Delta E_{\text{bind}}^{\text{a}}$	$\Delta E_{\text{bind}}^{\text{b}}$	$\Delta E_{\text{bind}}^{\text{a}}$	$\Delta E_{\text{bind}}^{\text{b}}$	$\Delta E_{\text{bind}}^{\text{a}}$	$\Delta E_{\text{bind}}^{\text{b}}$
H ⁺ ^c	-194.45	-228.87	-225.53	-229.36	-203.43	-213.90	-232.83	-248.52
OH ⁻ ^c	-112.65	-114.28	-83.57	-76.15	-111.39	-110.04	-98.29	-86.98
H ⁺ /OH ⁻ ^c	-222.96	-180.77	-198.14	-145.24	-206.42	-180.96	-187.92	-141.22
OMe ⁻	-84.18	-85.57	-55.38	-46.78	-83.03	-81.32	-69.91	-57.91
H ⁺ /OMe ⁻	-194.90	-152.18	-169.45	-116.13	-178.05	-152.43	-159.33	-112.17
OEt ⁻	-80.09	-81.45	-51.33	-42.69	-78.97	-77.33	-65.83	-53.85
H ⁺ /OEt ⁻	-191.01	-148.08	-165.34	-111.90	-174.07	-148.32	-155.27	-107.97
OPr ⁻	-78.74	-80.15	-50.07	-41.43	-77.64	-76.01	-64.50	-52.56
H ⁺ /OPr ⁻	-189.64	-146.87	-164.05	-110.63	-172.75	-147.04	-153.96	-106.69

^a Computed at the B3LYP/6-31G(d)//ONIOM(B3LYP/6-31G(d):AM1) of model 1.

^b Computed at the B3LYP/6-31G(d)//ONIOM(B3LYP/6-31G(d):AM1) of model 3.

The chemisorption of cap-end SWCNTs is stronger than those of open-ended SWCNTs as shown in Table 4.7. This result exhibits a good agreement with the previous theoretical study [51]. The formation of chemical bonds between adsorbing species and SWCNTs lead to the change of surface dipoles. For open-ended SWCNTs, the dangling bonds were filled with hydrogen atoms.

The adsorption energy of hydroxide ion for perfect and defect cap-ended C₈₀ SWCNTs, perfect and defect open-ended C₈₀H₂₀ SWCNTs, perfect and defect cap-ended C₁₂₀ SWCNTs, perfect and defect open-ended C₁₂₀H₂₀ SWCNTs are -112, -114.28, -83.57, -76.15, -111.39, -110.04, -98.29 and -86.98 kcal/mol, respectively. The chemisorption of perfect armchair (5,5) SWCNTs is higher than that of the Stone-Wales defect SWCNTs. This result is in agreement with previous theoretical study [27]. The pyramidalization angle with respect to C-C adsorbing atoms on perfect tube is much larger than Stone-Wales defect tube, indicating that structural feature should decrease the reactivity of Stone-Wales defect [52]. The much lower chemical reactivity at the defect site can be ascribed to the constraints of its planar local structure. The diameters of perfect and defect cap-ended C₈₀ SWCNTs are 6.9 and 6.8 Å, respectively, since the

sidewall reactivity of perfect armchair (5,5) SWCNTs decrease with an increasing of tube's diameter.

Table 4.8 Energies and thermodynamic quantities (in kcal/mol) of adsorption reaction on various types of perfect and defect SWCNTs at different computation models.

Reaction	ΔE_{ZPE}	ΔH_{298}°	ΔG_{298}°	ΔE_{ZPE}	ΔH_{298}°	ΔG_{298}°
Perfect SWCNTs						
	Cap-ended C ₈₀ , model 1 ^b			Open-ended C ₈₀ H ₂₀ , model 1 ^b		
SWCNT + OH ⁻ → SWCNT-OH ^{-d}	-109.59	-110.57	-100.15	-80.71	-81.71	-71.27
SWCNT-H ⁺ + OH ⁻ → SWCNT-H ⁺ -OH ^{-d}	-214.74	-233.25	-205.22	-188.34	-189.45	-178.84
SWCNT + OMe ⁻ → SWCNT-OMe ⁻	-80.27	-80.69	-68.20	-51.70	-52.10	-39.66
SWCNT-H ⁺ + OMe ⁻ → SWCNT-H ⁺ -OMe ⁻	-185.87	-186.34	-173.77	-158.75	-159.27	-146.61
SWCNT + OEt ⁻ → SWCNT-OEt ⁻	-76.81	-76.89	-64.51	-48.26	-48.35	-35.98
SWCNT-H ⁺ + OEt ⁻ → SWCNT-H ⁺ -OEt ⁻	-182.67	-182.78	-170.39	-155.38	-155.54	-143.12
SWCNT + OPr ⁻ → SWCNT-OPr ⁻	-75.44	-75.46	-63.09	-47.01	-47.03	-34.56
SWCNT-H ⁺ + OPr ⁻ → SWCNT-H ⁺ -OPr ⁻	-181.16	-181.23	-168.66	-153.87	-153.98	-141.38
Perfect SWCNTs						
	Cap-ended C ₁₂₀ , model 1 ^b			Open-ended C ₁₂₀ H ₂₀ , model 1 ^b		
SWCNT + OH ⁻ → SWCNT-OH ^{-d}	-108.77	-109.69	-99.39	-95.58	-96.68	-86.00
SWCNT-H ⁺ + OH ⁻ → SWCNT-H ⁺ -OH ^{-d}	-200.25	-201.36	-190.71	-179.83	-180.85	-170.44
SWCNT + OMe ⁻ → SWCNT-OMe ⁻	-79.66	-79.96	-67.73	-66.47	-66.94	-54.38
SWCNT-H ⁺ + OMe ⁻ → SWCNT-H ⁺ -OMe ⁻	-171.02	-171.45	-159.03	-150.42	-150.78	-138.55
SWCNT + OEt ⁻ → SWCNT-OEt ⁻	-76.20	-76.18	-64.10	-63.00	-63.16	-50.71
SWCNT-H ⁺ + OEt ⁻ → SWCNT-H ⁺ -OEt ⁻	-167.67	-167.78	-155.56	-146.82	-146.86	-134.78
SWCNT + OPr ⁻ → SWCNT-OPr ⁻	-74.77	-74.72	-62.41	-61.64	-61.75	-49.06
SWCNT-H ⁺ + OPr ⁻ → SWCNT-H ⁺ -OPr ⁻	-166.27	-166.34	-153.92	-145.41	-145.41	-133.12
Defect SWCNTs						
	Cap-ended C ₈₀ , model 3 ^c			Open-ended C ₈₀ H ₂₀ , model 3 ^c		
SWCNT + OH ⁻ → SWCNT-OH ^{-d}	-110.69	-111.88	-101.65	-72.10	-72.50	-63.48
SWCNT-H ⁺ + OH ⁻ → SWCNT-H ⁺ -OH ^{-d}	-178.41	-179.30	-196.09	-141.40	-142.44	-131.98
SWCNT + OMe ⁻ → SWCNT-OMe ⁻	-81.39	-81.76	-69.48	-42.01	-41.87	-30.79
SWCNT-H ⁺ + OMe ⁻ → SWCNT-H ⁺ -OMe ⁻	-148.92	-149.21	-137.03	-111.50	-111.90	-99.57
SWCNT + OEt ⁻ → SWCNT-OEt ⁻	-77.89	-77.93	-65.64	-38.59	-38.11	-27.17
SWCNT-H ⁺ + OEt ⁻ → SWCNT-H ⁺ -OEt ⁻	-145.52	-145.47	-133.50	-107.86	-107.96	-95.62
SWCNT + OPr ⁻ → SWCNT-OPr ⁻	-76.50	-76.50	-64.04	-37.28	-36.73	-25.87
SWCNT-H ⁺ + OPr ⁻ → SWCNT-H ⁺ -OPr ⁻	-144.15	-144.09	-131.73	-106.47	-106.54	-93.90
Defect SWCNTs						
	Cap-ended C ₁₂₀ , model 3 ^c			Cap-ended C ₁₂₀ H ₂₀ , model 3 ^c		
SWCNT + OH ⁻ → SWCNT-OH ^{-d}	-108.18	-109.14	-98.77	-85.55	-86.43	-76.34
SWCNT-H ⁺ + OH ⁻ → SWCNT-H ⁺ -OH ^{-d}	-177.51	-178.57	-168.02	-138.09	-138.96	-128.83
SWCNT + OMe ⁻ → SWCNT-OMe ⁻	-78.69	-79.07	-66.68	-55.62	-55.94	-43.79
SWCNT-H ⁺ + OMe ⁻ → SWCNT-H ⁺ -OMe ⁻	-148.16	-148.62	-136.00	-108.15	-52.19	-40.21
SWCNT + OEt ⁻ → SWCNT-OEt ⁻	-75.30	-75.37	-62.96	-52.19	-52.19	-40.21
SWCNT-H ⁺ + OEt ⁻ → SWCNT-H ⁺ -OEt ⁻	-144.64	-144.78	-132.18	-104.52	104.46	-92.38
SWCNT + OPr ⁻ → SWCNT-OPr ⁻	-73.93	-73.94	-61.45	-50.87	-50.81	-38.70
SWCNT-H ⁺ + OPr ⁻ → SWCNT-H ⁺ -OPr ⁻	-143.29	-143.38	-130.58	-103.17	-103.06	-90.81

^b ONIOM(B3LYP/6-31G(d):AM1) with a pyrene as a high layer model.

^c ONIOM(B3LYP/6-31G(d):AM1) with a 5-7-7-5 cluster as a high layer model.

Table 4.9 Charge on oxygen atom of adsorbing species and binding energies (in kcal/mol) in reaction systems on various types of SWCNTs at different computation models.

Tubes based on the complexes with	Perfect cap-ended C ₈₀		Defect cap-ended C ₈₀		Perfect open-ended C ₈₀ H ₂₀		Defect open-ended C ₈₀ H ₂₀	
	Charge on oxygen atom of	ΔE_{bind}^a	Charge on oxygen atom of	ΔE_{bind}^b	Charge on oxygen atom of	ΔE_{bind}^a	Charge on oxygen atom of	ΔE_{bind}^b
OH ^{-c}	-0.359	-112.65	-0.359	-114.28	-0.390	-83.57	-0.398	-76.15
H ⁺ /OH ^{-c}	-0.364	-222.96	-0.364	-180.77	-0.370	-198.14	-0.369	-145.24
OMe ⁻	-0.310	-84.18	-0.310	-85.57	-0.320	-55.38	-0.327	-46.78
H ⁺ /OMe ⁻	-0.304	-194.90	-0.301	-152.18	-0.310	-169.45	-0.312	-116.13
OEt ⁻	-0.313	-80.09	-0.313	-81.45	-0.323	-51.33	-0.330	-42.69
H ⁺ /OEt ⁻	-0.310	-191.01	-0.306	-148.08	-0.316	-165.34	0.317	-111.90
OPr ⁻	-0.314	-78.74	-0.314	-80.15	-0.324	-50.07	0.332	-41.43
H ⁺ /OPr ⁻	-0.311	-189.64	-0.307	-146.87	-0.317	-164.05	-0.318	-110.63

Tubes based on the complexes with	Perfect cap-ended C ₁₂₀		Defect cap-ended C ₁₂₀		Perfect open-ended C ₁₂₀ H ₂₀		Defect open-ended C ₁₂₀ H ₂₀	
	Charge on oxygen atom of	ΔE_{bind}^a	Charge on oxygen atom of	ΔE_{bind}^b	Charge on oxygen atom of	ΔE_{bind}^a	Charge on oxygen atom of	ΔE_{bind}^b
OH ^{-c}	-0.390	-111.39	-0.391	-110.04	-0.388	-98.29	-0.391	-86.98
H ⁺ /OH ^{-c}	-0.372	-206.42	-0.370	-180.96	-0.370	-187.92	-0.368	-141.22
OMe ⁻	-0.320	-83.03	-0.321	-81.32	-0.318	-69.91	-0.320	-57.91
H ⁺ /OMe ⁻	-0.312	-178.05	-0.313	-152.43	-0.311	-159.33	-0.310	-112.17
OEt ⁻	-0.323	-78.97	-0.325	-77.33	-0.321	-65.83	-0.323	-53.85
H ⁺ /OEt ⁻	-0.318	-174.07	-0.319	-148.32	-0.316	-155.27	-0.316	-107.97
OPr ⁻	-0.324	-77.64	-0.326	-76.01	-0.322	-64.50	-0.325	-52.56
H ⁺ /OPr ⁻	-0.319	-172.75	-0.320	-147.04	-0.317	-153.96	-0.317	-106.69

^b ONIOM(B3LYP/6-31G(d):AM1) with a pyrene as a high layer model.

^c ONIOM(B3LYP/6-31G(d):AM1) with a 5-7-7-5 cluster as a high layer model.

4.2.2 Energies and Thermodynamic Quantities

Energies and thermodynamic quantities of involved absorbing species for perfect and defect cap-ended C_{80} SWCNTs, perfect and defect open-ended $C_{80}H_{20}$ SWCNTs, perfect and defect cap-ended C_{120} SWCNTs, perfect and defect cap-ended C_{80} SWCNTs are presented in Table 4.8. Our calculation results indicate that the reaction systems are exothermic processes.

An increasing number of carbon atoms (C1 to C3) of alkoxide ions, decreasing in adsorption energy of protonated SWCNT. This is because, the more number of carbon atom of alkoxide, the more electron transfer from the tube to alkoxide. This also reflects by their larger adsorption energy (Table 4.9). The adsorption energy of involved reaction systems are in decreasing order: $SWCNT-H^+-OH^- > SWCNT-H^+-OMe^- > SWCNT-H^+-OEt^- > SWCNT-H^+-OPr^- > SWCNT-OH^- > SWCNT-OMe^- > SWCNT-OEt^- > SWCNT-H^+-OPr^-$.

Based on thermodynamic quantities, we have found that all reaction energies of the non-protonated capped model are equal to those of the defect model. For the protonated system, the perfect model is more preferred than those of defect model. Adsorption on perfect tube is preferred than those of defect tube, because of pyramidalization angle between C-C of armchair (5,5) SWCNT.

Reaction energies of any reaction systems of the capped model are higher than those of the opened model for both perfect and defect models. Difference in dipole moment between the end of the cap caused the opened cap tube is quite reacted with adsorbing species. The protonated system, hydroxide and alkoxide are adsorbed better than that of non-protonated system. The increasing carbon atom in alkoxide ion, decreasing in adsorption. It might be taken from the increasing of steric effect.

CHAPTER V

CONCLUSIONS AND SUGGESTIONS

5.1 The Adsorptions of Proton and Hydroxide on Various Types of SWCNTs

At 298.15 K, all the adsorptions of proton and hydroxide on the perfect and defect armchair (5,5) single-walled carbon nanotube (SWCNT) of cap-ended C_{80} , C_{120} and open-ended $C_{80}H_{20}$ and on their protonated structures are exothermic reactions. The protonation was found to be the most favorite process and followed by the hydroxylation reaction. All the mono hydration reaction energies on the protonated, hydroxylated and protonated- hydroxylated hydrated SWCNTs are less than 11 kcal/mol. Strain energies of all types of the SWCNTs after adsorption processes are within wide range of 6.3 to 74.8 kcal/mol. We found that the protonations of all defect types of SWCNTs are more preferable than those of their corresponding perfect tubes. On the other hand, the hydroxylations of protonated perfect SWCNTs are more preferable than those of their corresponding defect tubes.

5.2 The Chemisorptions of Hydroxide and C1 to C3 Alkoxides

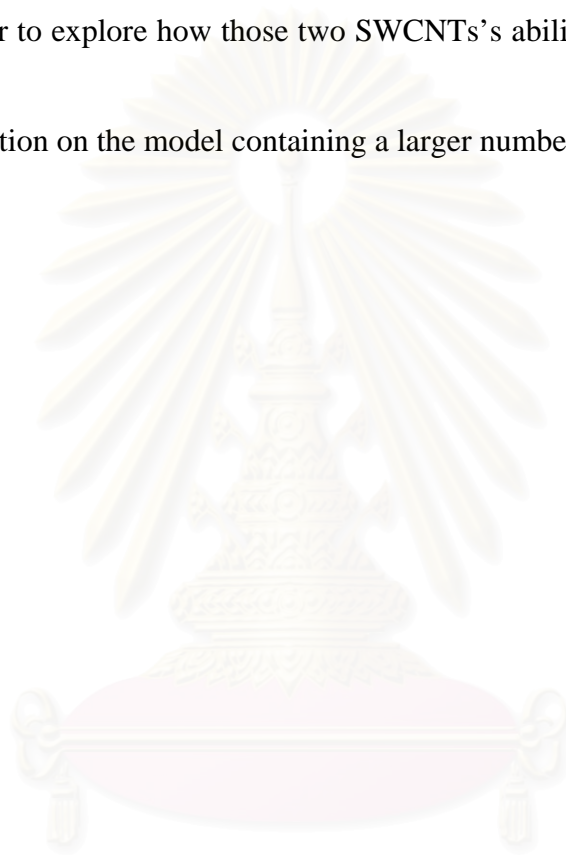
Geometry optimizations of involved adsorbing species hydroxide ion and C1 to C3 alkoxide ions on various types of SWCNTs were carried out by using ONIOM(B3LYP/6-31G(d):AM1) approach. All adsorptions on the cap-ended SWCNTs are energetically and thermodynamically more favorable than their corresponding open-ended SWCNTs. In all cases, the binding energy of adsorptions of hydroxide and alkoxide ions on the protonated either perfect or defect SWCNTs are higher than those of adsorptions on the bare SWCNTs. The binding energies of all adsorptions on various types of SWCNTs decrease while the size of alkyl group of alkoxides increase. The alkoxide-oxygen charge increases simultaneously.

5.3 Suggestions for Future Work

1. Basis set super position error (BSSE) calculation on all reaction systems to get more corrected and reliable.

2. Change the C-C bonds' position of both perfect tubed and defect tubed SWCNTs in order to explore how those two SWCNTs's ability to adsorb desired species changes.

3. Calculation on the model containing a larger number of carbon atoms.



สถาบันวิทยบริการ
จุฬาลงกรณ์มหาวิทยาลัย

REFERENCES

1. Qui, J.; Li, Y.; Wang, Y.; Li, W. Production of Carbon Nanotubes from Coal. *Fuel Processing Technology* 85 (2004): 1663-1670.
2. Flahaut, E.; Laurent, C.; Peigney, A. Catalytic CVD Synthesis of Double and Triple-Walled Carbon Nanotubes by the Control of the Catalyst Preparation. *Carbon* 43 (2005): 375-383.
3. Dupuis, C. A. The Catalyst in the CCVD of Carbon Nanotubes –a Review. *Progress in Materials Science* 50 (2005): 929-961.
4. Mokashi, V. V.; Qian, D.; Liu, Y. A Study on the Tensile Response and Fracture in Carbon Nanotube-Based Composites Using Molecular Mechanics. *Composites Science and Technology* 67 (2007): 530-540.
5. Xiao, R. J.; Gama, A. B.; Gillespie, W. J.; An Analytical Molecular Structural Mechanics Model for the Mechanical Properties of Carbon Nanotubes. *International Journal of Solids and Structures* 42 (2005): 3075-3092.
6. Margulis, A. V.; Gaiduk, A. E.; Zhidkin, N. E. Quadratic Electro-Optic Effect in Semiconductor Carbon Nanotubes. *Physics Letters A* 258 (1999): 394-400.
7. Robertson, J. Growth of Nanotubes for Electronics. *Material Today* 10 (2007): 36-43.
8. Avouris, P.; Chen, J. Nanotubes Electronics and Optoelectronics. *Material Today* 9 (2006): 46-54.
9. Novak, P. J.; Lay, D. M.; Perkins, K. F.; Snow, S. E. Macroelectronics Applications of Carbon Nanotube networks. *Solid-State Electronics* 48 (2004): 1753-1756.
10. Munoz, E.; Maser, K. W.; Benito, A. M.; de la Fuente, F. G.; Matínez, T. M. Single-Walled Carbon Nanotubes Produced by Laser Ablation Under Different Inert Atmospheres. *Synthetic Metals* 103 (1999): 2490-2491.
11. Galvan, H. D.; Aguilar-Elguézabal, A.; Alonso, G. High Resolution TEM Studies of Carbon Nanotubes Produced by Spray Pyrolysis. *Optical Materials* 29 (2006): 140-143.

12. Hubler, U.; Jess, P.; Lang, P. H.; Güntherodt, J. H.; Salvétat, P. J.; Forró, L. Scanning Probe Microscopy of Carbon Nanotubes. *Carbon* 36 (1998): 697-700.
13. Lin, T.; Zhang, W. D.; Huang, J.; He, C. A DFT Study of the Amination of Fullerenes and Carbon Nanotubes: Reactivity and Curvature. *Journal of Physical Chemistry B* 109 (2005): 13755-13760.
14. Baughman, R. H.; Zakhidov, A. A.; Heer, W. A. Carbon Nanotubes-the Route Toward Applications. *Science's Compass* 297 (2002): 787-792.
15. Tasis, D.; Tagmatarchis, N.; Bianco, A.; Prato, M. Chemistry of Carbon Nanotubes. *Chemical Reviews* 106 (2006): 1105-1136.
16. Bianco, A.; Kostarelos, K.; Prato, M. Application of Carbon Nanotubes in Drug Delivery. *Current Opinion in Chemical Biology* 9 (2005): 674-679.
17. Li, W.; Bai, Y.; Zhang, Y.; Sun, M.; Cheng, R.; Xu, X.; Chen, Y.; Mo, Y. Effect of Hydroxyl Radical on the Structure of Multi-Walled Carbon Nanotubes. *Synthetic Metals* 155 (2005): 509-515.
18. Tsai, M-H.; Lin, H-M.; Tsai, W-L.; Hwu, Y. Examine the Gas Absorption Properties of Single-Walled Carbon Nanotubes by X-ray Absorption Techniques. *Reviews Advance Material Science* 5 (2003): 302-305.
19. Jia, G.; Li, J.; Zhang, Y. Electronic Structures and Hydrogenation of a Chiral Single-Walled (6,4) Carbon Nanotube: A Density Functional Theory Study. *Chemical Physics Letters* 418 (2006): 40-45.
20. Heroux, L.; Krungleviciute, V.; Calbi, M.M.; Migone, A. D. CF₄ on Carbon Nanotubes: Physisorption on Grooves and External Surfaces. *Journal of Physical Chemistry B* 110 (2006): 12597-12602.
21. Byl, O.; Liu, J.; Yates, J. T. Characterization of Single Wall Carbon Nanotubes by Nonane Preadsorption. *Carbon* 44 (2006): 2039-2044.
22. Xu, Y-J.; Li, J-Q. The Interaction of N₂ with Active Sites of Single-Walled Carbon Nanotube. *Chemical Physics Letters* 412 (2005): 439-443.
23. Chen, R. J.; Choi, H. C.; Bangsaruntip, S.; Yenilmez, E.; Tang, X.; Wang, Q.; Chang, Y-L.; Dai, H. An Investigation of the Mechanism of Electronic Sensing of Protein Adsorption on Carbon Nanotubes Devices. *Journal of American Chemical Society* 126 (2004): 1563-1568.

24. Luo, J.; Zhang, Z. X.; Xue, Z. Q.; Wul, J. L.; Calculations of Adsorption of O₂ and H₂O on a Carbon Nanotubes tip in field-emission conditions. *Journal of Physics D: Applied Physics* 36 (2003): 3034-3038.
25. Muris, M.; Dufau, N.; Bienfait, M.; Pavlovsk y, D. P.; Grillet, Y.; Palmari, J. P. Methane and Krypton Adsorption on Single-Walled Carbon Nanotubes. *Langmuir* 16 (200): 7019-7022.
26. Nischa, J. A.; Yudasaka, M.; Bandow, S.; Kokai, F.; Takahashi, K. Adsorption and Catalytic Properties of Single-Walled Carbon Nanohorns. *Chemical Physics Letters* 328 (2000): 381-386.
27. Lu, X.; Chen, Z.; Schleyer, R. P. Are Stone-Wales Defect Sites Always More Reactive Than Perfect Sites in the Sidewalls of Single-Wall Carbon Nanotubes? *Journal of American Chemical Society* 127 (2005): 20-21.
28. Yang, H-T.; Yang, L.; Chen, J.; Dong, J. Antiresonance Effect due to Stone-Wales Defect in Carbon Nanotubes. *Physics Letters A* 325 (2004): 287-293.
29. Udomvech, A.; Kerdcharoen, T.; Osotchan, T. First Principles of Li and Li⁺ Adsorbed on Carbon Nanotube: Variation of Tubule of Diameter and Length. *Chemical Physics Letters* 406 (2005): 161-166.
30. Chang, H.; Lee, D. J.; Lee, M. S.; Lee, H. Y. Adsorption of NH₃ and NO₂ Molecules on Carbon Nanotube. *Applied Physics Letters* 79 (2001): 3863-3865.
31. Ellison, D. M.; Crotty, J. M.; Koh, D.; Spray, L. R.; Tate, E. K. Adsorption of NH₃ and NO₂ on Single-Walled Carbon Nanotube. *Journal of Physical Chemistry B* 108 (2004): 7938-7943.
32. Ricca, A.; Drocco, A. J. Interaction of O₂ with a (9,0) Carbon Nanotube. *Chemical Physics Letters* 362 (2002): 217-223.
33. Sourescu, C. D.; Jordan, D. K. Theoretical Study of Oxygen Adsorption on Graphite and the (8,0) Single-Walled Carbon Nanotube. *Journal of Physical Chemistry B* 109 (2005): 8967-8972.
34. Chakrapani, N.; Zang, M. Y.; Nayak, K. S.; Moore, A. J.; Carroll, L. D.; Choi, Y. Y.; Ajayan, M. P. Chemisorption of Acetone on Carbon nanotubes *Journal of Physical Chemistry B* 107 (2003): 9308-9311.
35. Luo, J.; Zhang, X. Z.; Peng, L. M.; Xue, Q. Z.; Wu, L. J. Calculations of Adsorption of O₂ and H₂O on a Carbon Nanotube Tip in Field-

- Emission Conditions. *Journal of Physics D: Applied Physics* 36 (2003): 3034-3038.
36. Ellison, D. M.; Good, P. A.; Kinnaman, S. C.; Padgett, E. N. Interaction of Water with Single-Walled Carbon Nanotubes: Reaction and Adsorption. *Journal of Physical Chemistry B* 109 (2005): 10640-10646.
 37. Han, S. S.; Lee, M. H. Adsorption Properties of Hydrogen on (10,0) Single-Walled Carbon Nanotube through Density Functional Theory. *Carbon* 42 (2004): 2169-2177.
 38. Bettinger, F. H. "The Reactivity of Defects at the Sidewalls of Single-Walled Carbon Nanotubes: The Stone-Wales Defect" *Journal of Physical Chemistry B Letters* 109 (2005): 6922-6924.
 39. Xu, Y-J.; Li, J-Q. The Interaction of N₂ with Active Sites of a Single-Wall Carbon Nanotube. *Chemical Physics Letters* 412 (2005): 439-443.
 40. Gómez and, B.; Martínez-Magadán, M. J. A Theoretical Study of Dibenzothiophene Absorbed on Open-Ended Carbon Nanotubes. *Journal of Physical Chemistry B* 110 (2005): 14868-14875.
 41. Mavrandonakis, A.; Farantos, C. S.; Froudakis, E. G. Glycine Interaction with Carbon Nanotubes: An Ab Initio Study. *Journal of Physical Chemistry B* 110 (2006): 6048-6050.
 42. Crespo, D.; Yang, T. R. Adsorption of Vapors on Single-Walled Carbon Nanotubes. *Industrial & Engineering Chemistry Research* 45 (2006): 5524-2230.
 43. Levine, N. I. Quantum Chemistry. 5th ed. University of New York: Prentice Hall, 2000.
 44. Lewar, E. Computational Chemistry. United States of America: Kluwer Academic Publishers, 2003.
 45. Jensen, F. Introduction to Computational Chemistry. Odense University: John Wiley & Sons, 1999.
 46. Dapprich, S.; Komáromi, I.; Byun, S. K.; Morokuma, K. A New ONIOM Implementation in Gaussian98. Part I. The Calculation of Energies, Gradients, Vibrational Frequencies and Electric Field Derivatives. *Journal of Molecular Structure (Theochem)* 461-462 (1999): 1-21.
 47. Yumura, T.; Bandow, S.; Yoshizawa, K.; Iijima, S. The role of Fullerene Hemispheres in Determining Structural Features of Finite-Length

- Carbon Nanotubes. *Journal of Physical Chemistry B* 108 (2004): 11426-11434.
48. Park, A. K.; Seo, K.; Lee, H. L. Adsorption of Atomic Hydrogen on Single-Walled Carbon Nanotubes. *Journal of Physical Chemistry B* 109 (2005): 8967-8972.
49. Collignon, B.; Hoang, M. N. P.; Picaud, S.; Rayez, C.J. Ab Initio Study of the Water Adsorption on Hydroxylated Graphite Surfaces. *Chemical Physics Letters* 406 (2005): 430-435.
50. Wannan, B.; Du, A. J.; Ruangpornvisuti, V. Addition of Diazomethane to Armchair Single-Walled Carbon Nanotubes and their Reaction Sequences: A Computational Study. *Chemical Physics Letters* 436 (2007): 218-223.
51. Basiuk, A. V. ONIOM Studies of Chemical Reactions on Carbon Nanotube Tips: Effects of the Lower Theoretical Level and Mutual Orientation of the Reactants. *Journal of Physical Chemistry B* 107 (2003): 8890-8897.
52. Kar, T.; A, B.; D, X.; P, R. A Theoretical Study of Functionalized Single-Walled Carbon Nanotubes: ONIOM Calculations. *Chemical Physics Letters* 392 (2004): 176-180.



APPENDICES

สถาบันวิทยบริการ
จุฬาลงกรณ์มหาวิทยาลัย

APPENDIX A

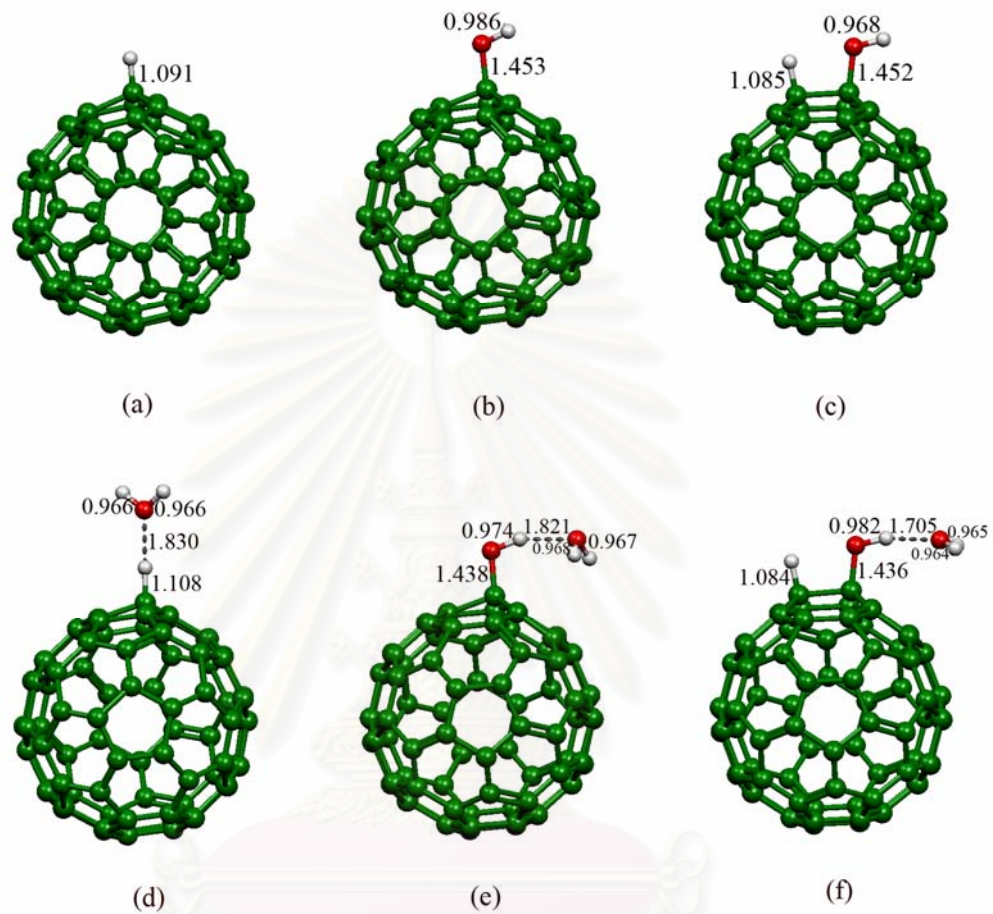


Figure A-1 The bond lengths (Å) of the adsorptions of proton, hydroxide ion and water molecule with perfect cap-ended C₈₀ SWCNTs computed at the HF/3-21G level of theory.

สถาบันวิทยบริการ
จุฬาลงกรณ์มหาวิทยาลัย

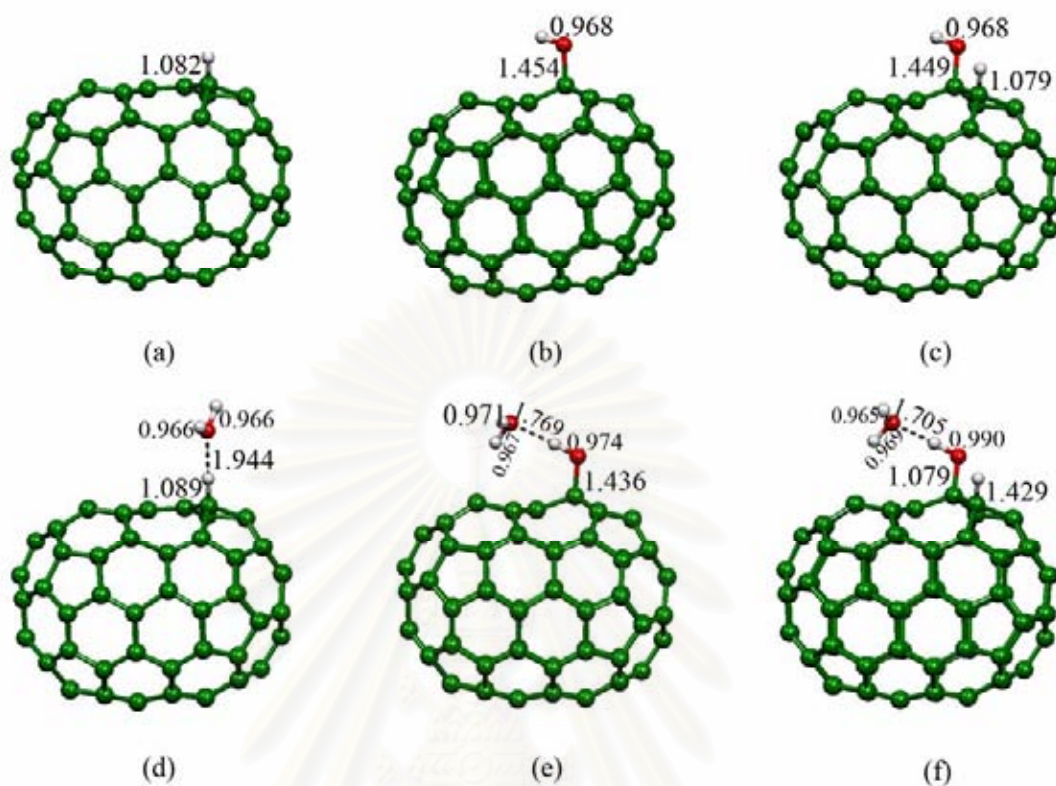


Figure A-2 The bond lengths (Å) of the adsorptions of proton, hydroxide ion and mono-hydration with perfect cap-ended C_{80} SWCNTs computed at the HF/3-21G level of theory.

สถาบันวิทยบริการ
จุฬาลงกรณ์มหาวิทยาลัย

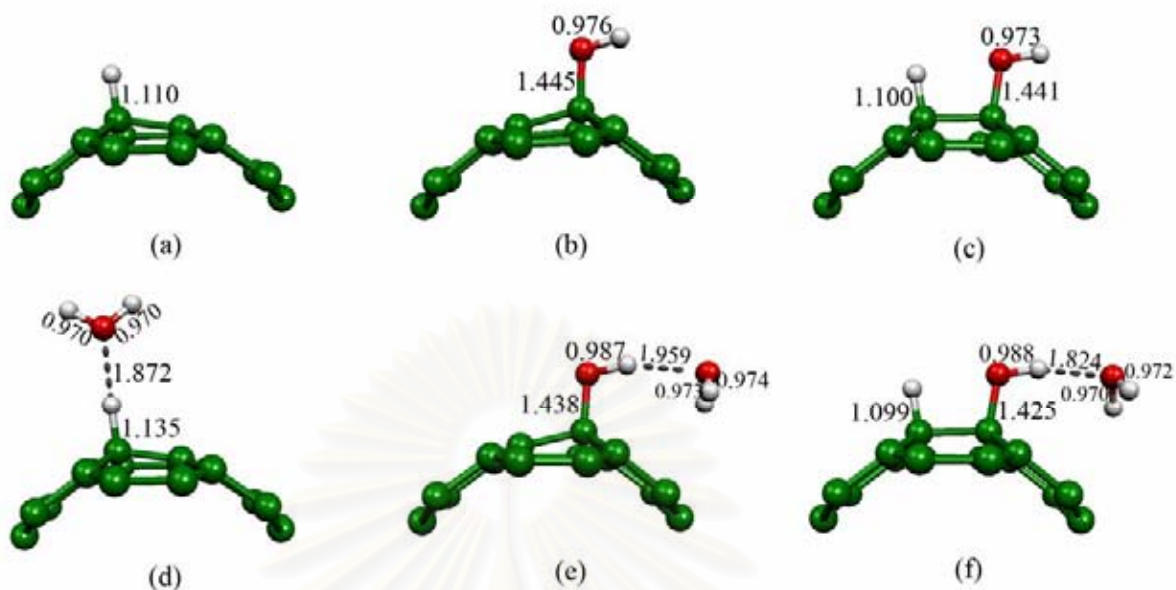


Figure A-3 The bond lengths (Å) of adsorptions of proton, hydroxide ion and mono-hydration with perfect cap-ended C_{80} SWCNTs model 1 (high layer) computed at ONIOM(B3LYP/6-31G(d):AM1) level of theory.

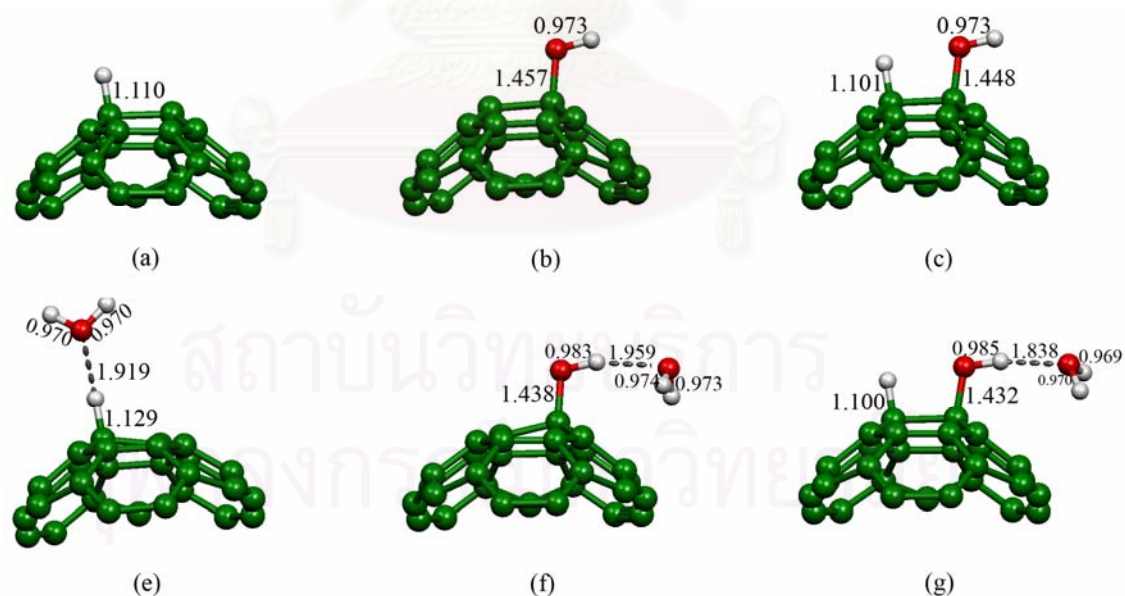


Figure A-4 The bond lengths (Å) of the adsorptions of proton, hydroxide ion and mono-hydration with perfect cap-ended C_{80} SWCNTs model 2 (high layer) computed at the ONIOM(B3LYP/6-31G(d):AM1) level of theory.

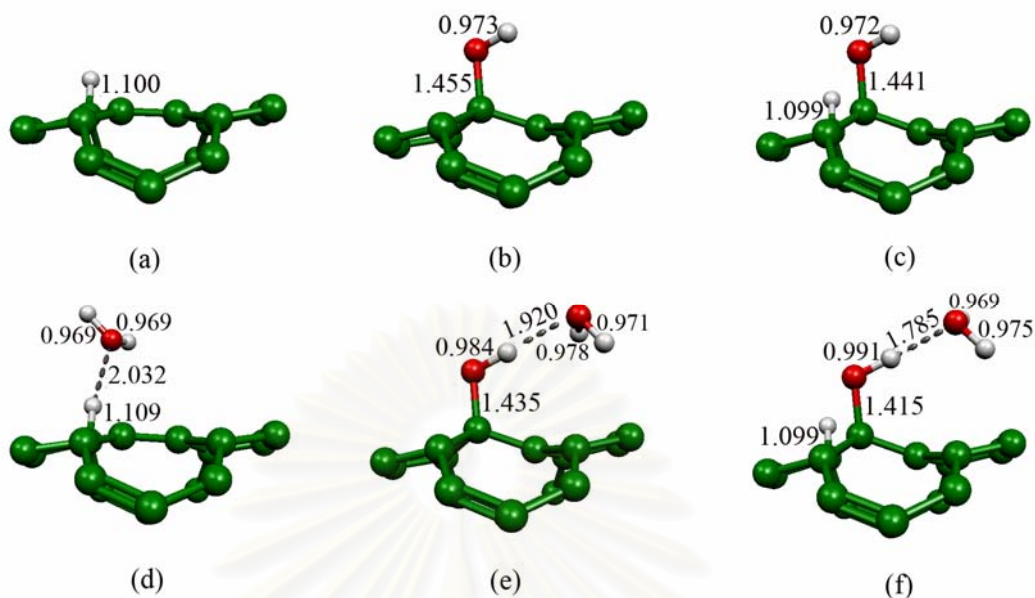


Figure A-5 The bond lengths (Å) of the adsorptions of proton, hydroxide ion and mono-hydration with defect cap-ended C_{80} SWCNTs model 3 (high layer) computed at the ONIOM(B3LYP/6-31G(d):AM1) level of theory

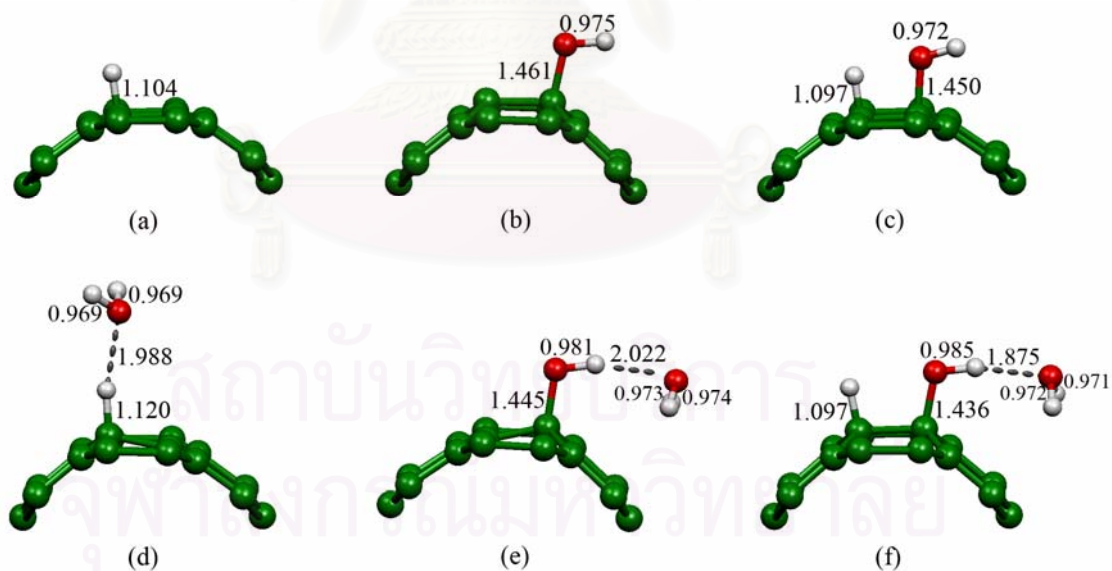


Figure A-6 The bond lengths (Å) at a high-layered ONIOM method of the adsorptions of proton, hydroxide ion and mono-hydration with perfect cap-ended $C_{80}H_{20}$ SWCNTs model 1 (high layer) computed at the ONIOM(B3LYP/6-31G(d):AM1) level of theory

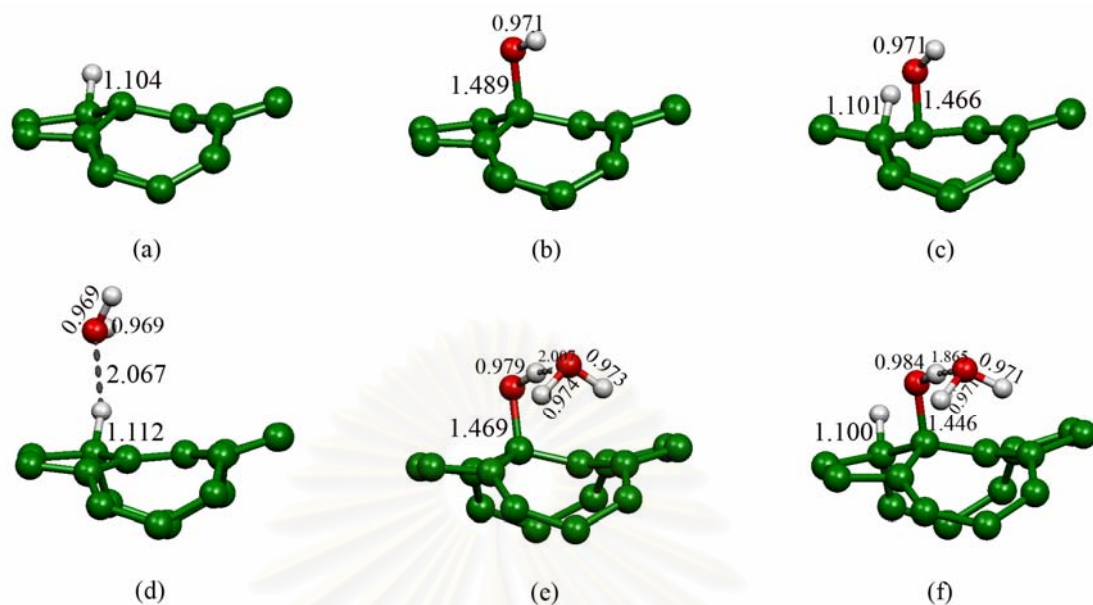


Figure A-7 The bond lengths (Å) of adsorptions of proton, hydroxide ion and monohydration with defect cap-ended $C_{80}H_{20}$ SWCNTs model 3 (high layer) computed at the ONIOM(B3LYP/6-31G(d):AM1) level of theory

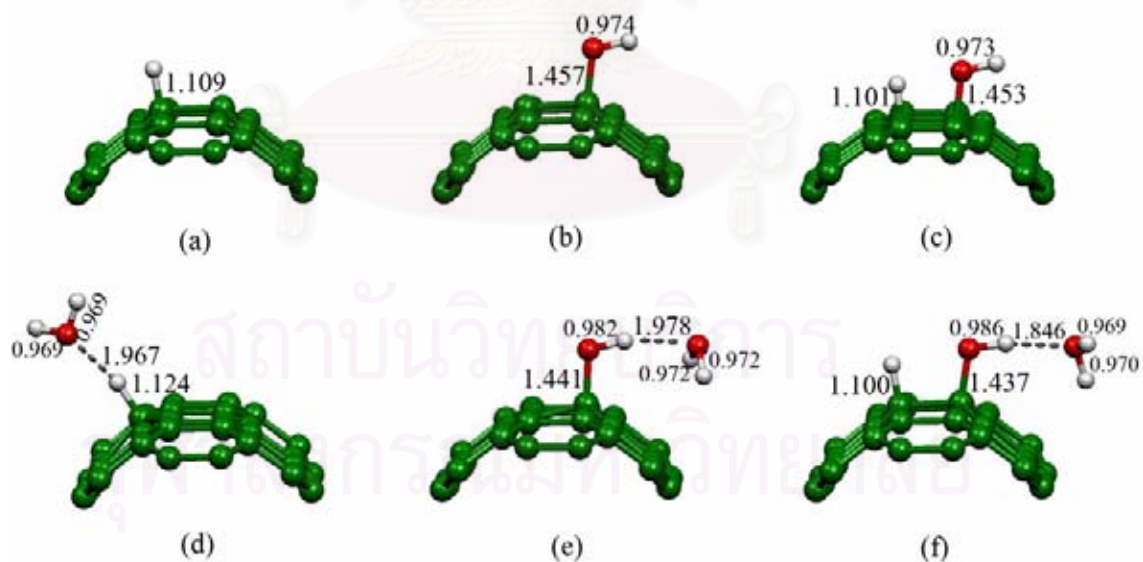


Figure A-8 The bond lengths (Å) of adsorptions of proton, hydroxide ion and monohydration with perfect cap-ended C_{120} SWCNTs model 4 (high layer) computed at the ONIOM(B3LYP/6-31G(d):AM1) level of theory

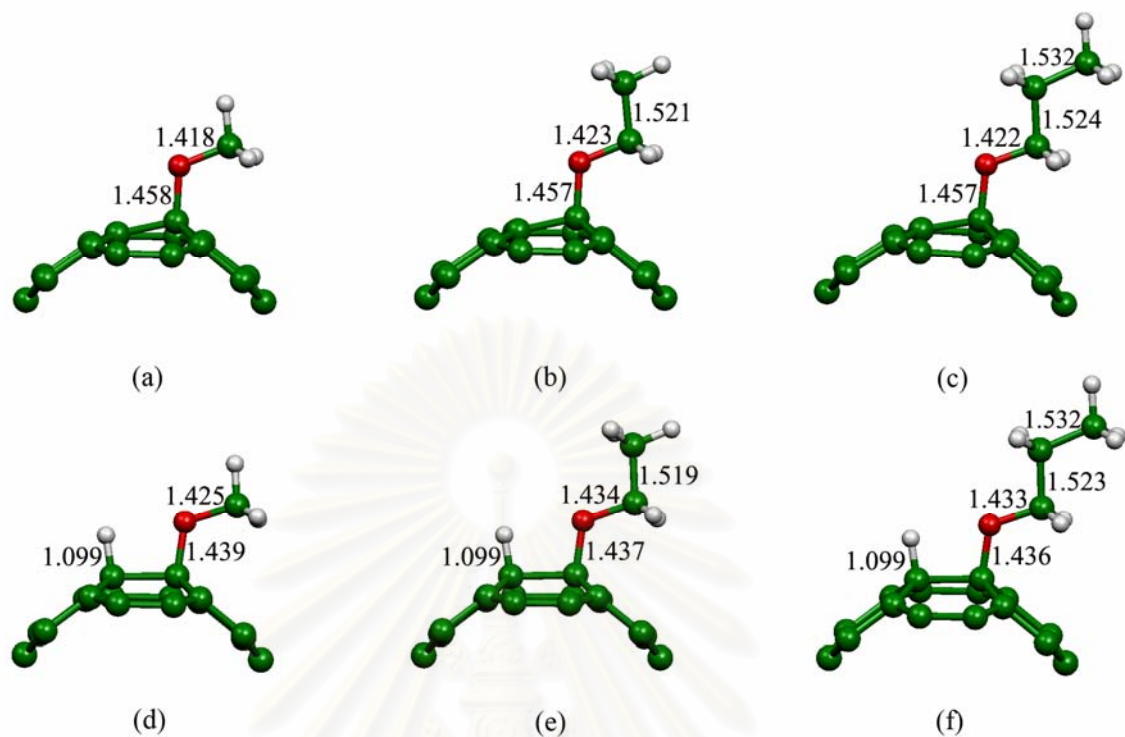


Figure A-9 The bond lengths (\AA) of adsorptions of proton and C1 to C3 alkoxide ions with perfect cap-ended C_{80} SWCNTs model 1 (high layer) computed at the ONIOM(B3LYP/6-31G(d):AM1) level of theory

สถาบันวิทยบริการ
จุฬาลงกรณ์มหาวิทยาลัย

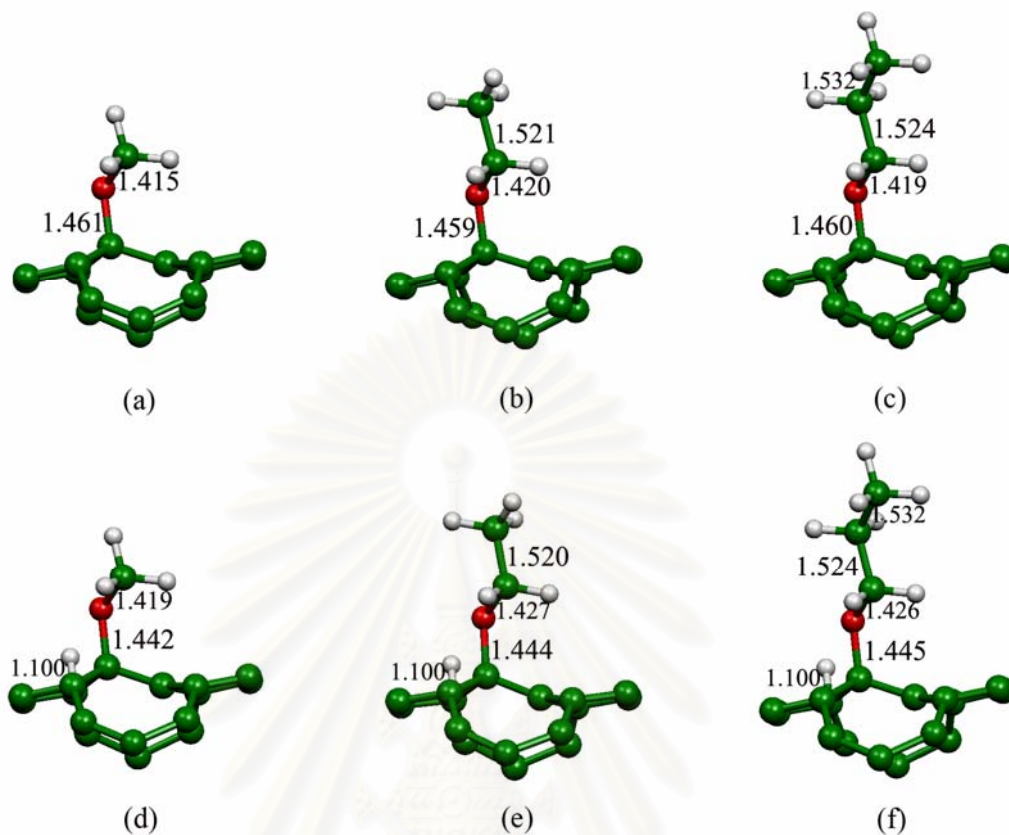


Figure A-10 The bond lengths (\AA) of adsorptions of proton and C1 to C3 alkoxide ions with perfect cap-ended C_{80} SWCNTs model 3 (high layer) computed at the ONIOM(B3LYP/6-31G(d):AM1) level of theory

สถาบันวิทยบริการ
จุฬาลงกรณ์มหาวิทยาลัย

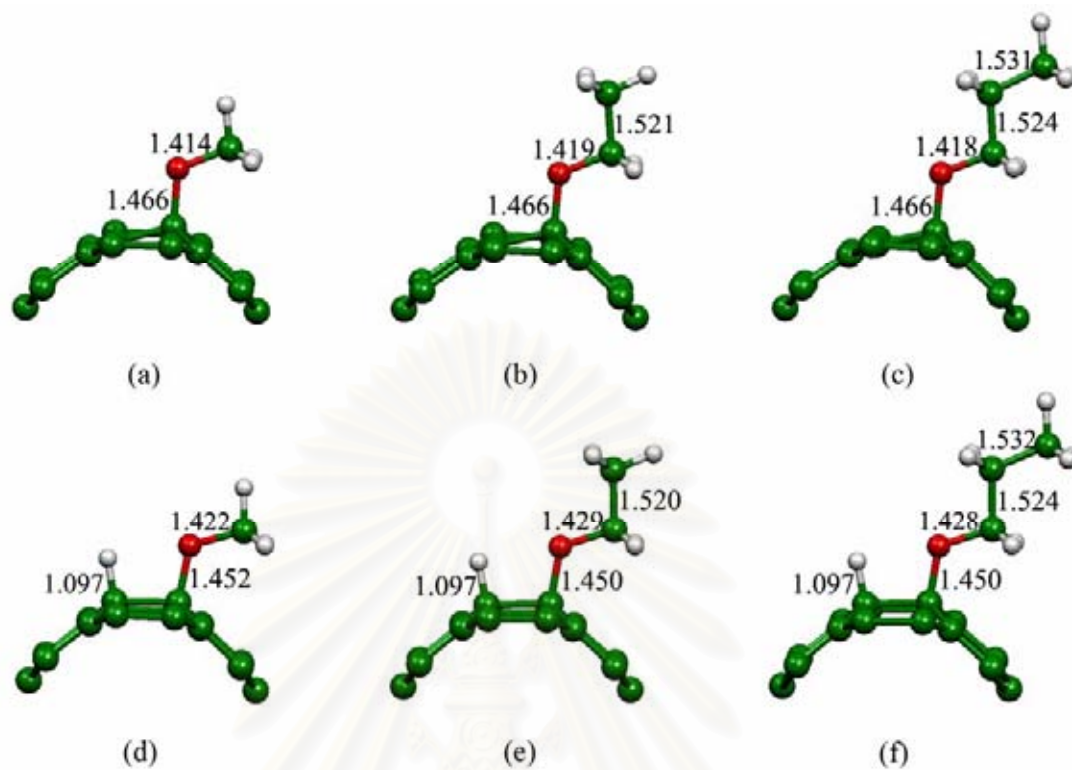


Figure A-11 The bond lengths (Å) of adsorptions of proton and C1 to C3 alkoxide ions with perfect cap-ended C₈₀H₂₀ SWCNTs model 1 (high layer) computed at the ONIOM(B3LYP/6-31G(d):AM1) level of theory.

สถาบันวิทยบริการ
จุฬาลงกรณ์มหาวิทยาลัย

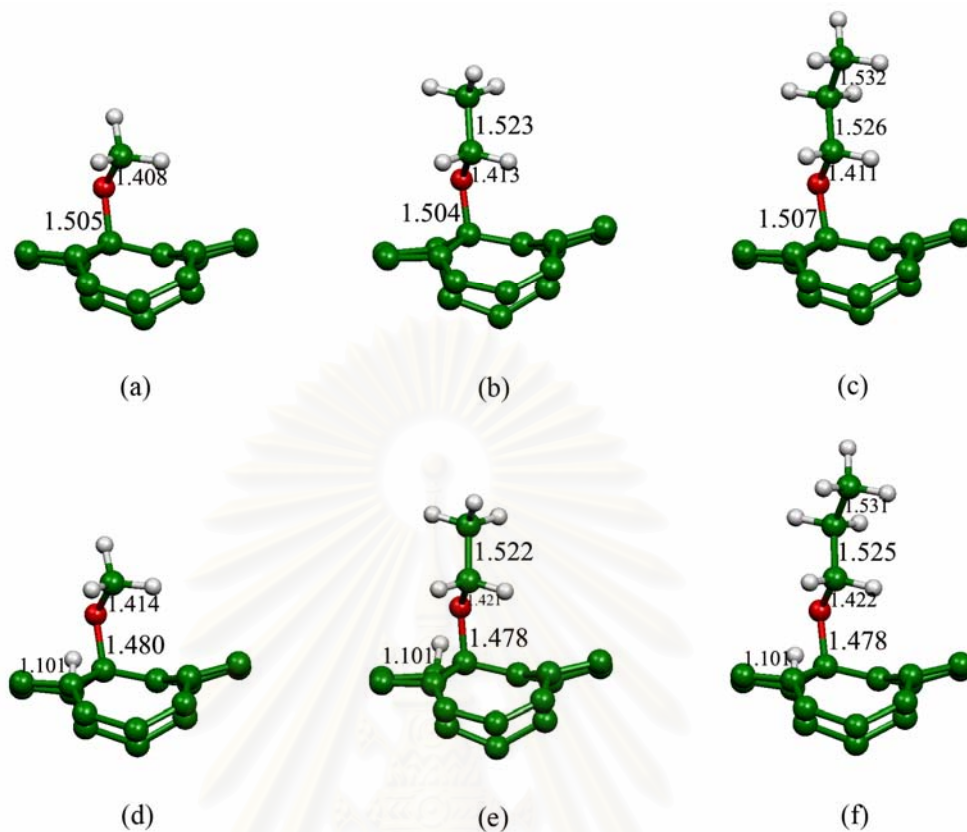


Figure A-12 The bond lengths (Å) of adsorptions of proton and C1 to C3 alkoxide ions with perfect cap-ended C₈₀H₂₀ SWCNTs model 3 (high layer) computed at the ONIOM(B3LYP/6-31G(d):AM1) level of theory.

สถาบันวิทยบริการ
จุฬาลงกรณ์มหาวิทยาลัย

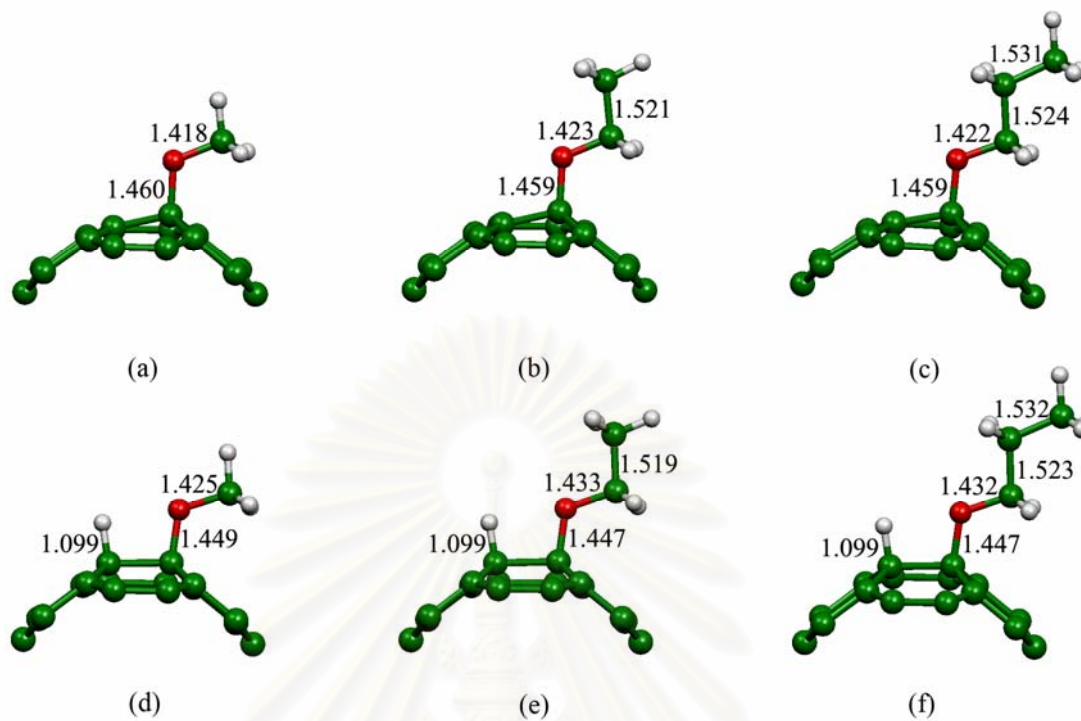


Figure A-13 The bond lengths (Å) of adsorptions of proton and C1 to C3 alkoxide ions with perfect cap-ended C₁₂₀ SWCNTs model 1 (high layer) computed at the ONIOM(B3LYP/6-31G(d):AM1) level of theory

สถาบันวิทยบริการ
จุฬาลงกรณ์มหาวิทยาลัย

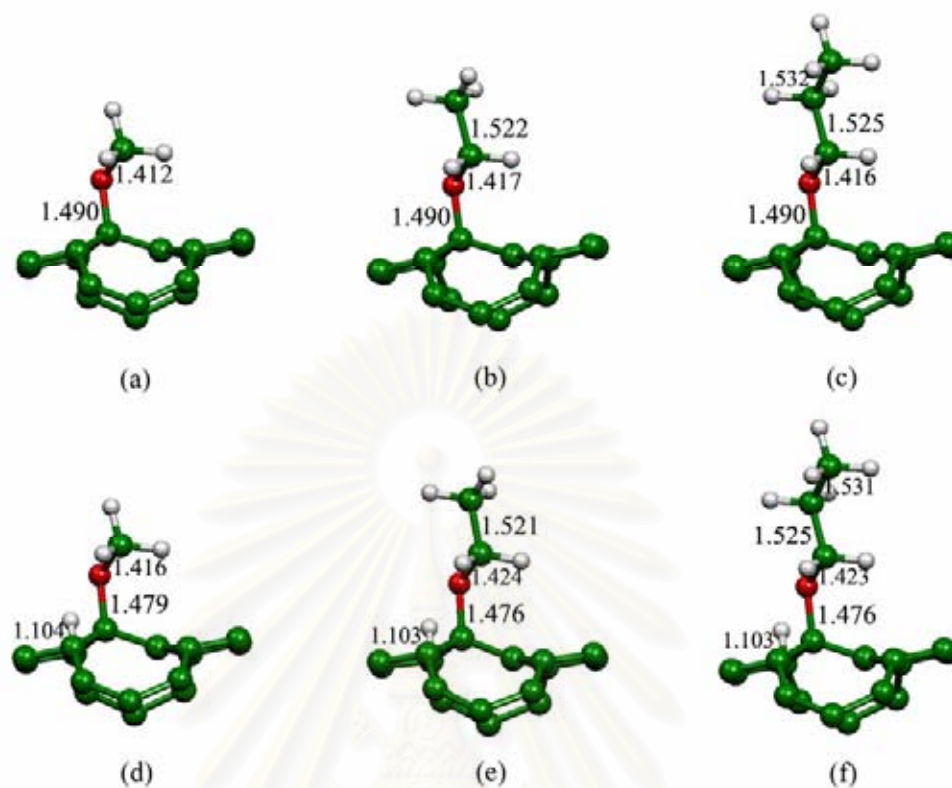


Figure A-14 The bond lengths (Å) of adsorptions of proton and C1 to C3 alkoxide ions with defect cap-ended C₁₂₀ SWCNTs model 3 (high layer) computed at at the ONIOM(B3LYP/6-31G(d):AM1) level of theory

สถาบันวิทยบริการ
จุฬาลงกรณ์มหาวิทยาลัย

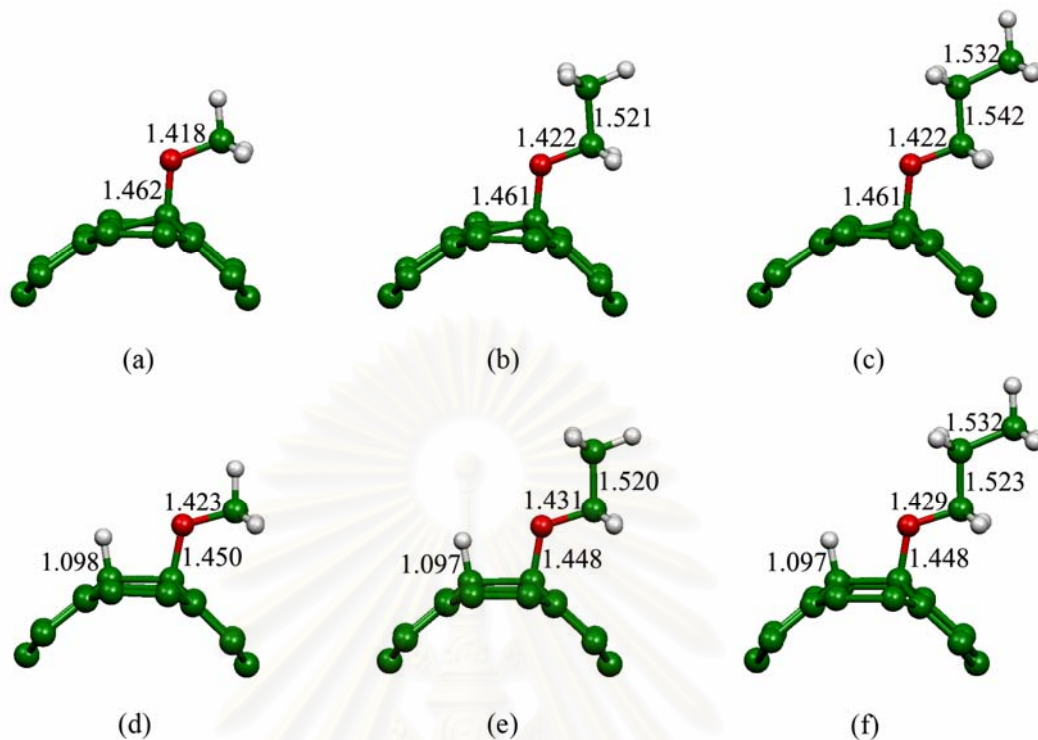


Figure A-15 The bond lengths (Å) of adsorptions of proton and C1 to C3 alkoxide ions with perfect open-ended C₁₂₀H₂₀ SWCNTs model 1 (high layer) computed at the ONIOM(B3LYP/6-31G(d):AM1) level of theory

สถาบันวิทยบริการ
จุฬาลงกรณ์มหาวิทยาลัย

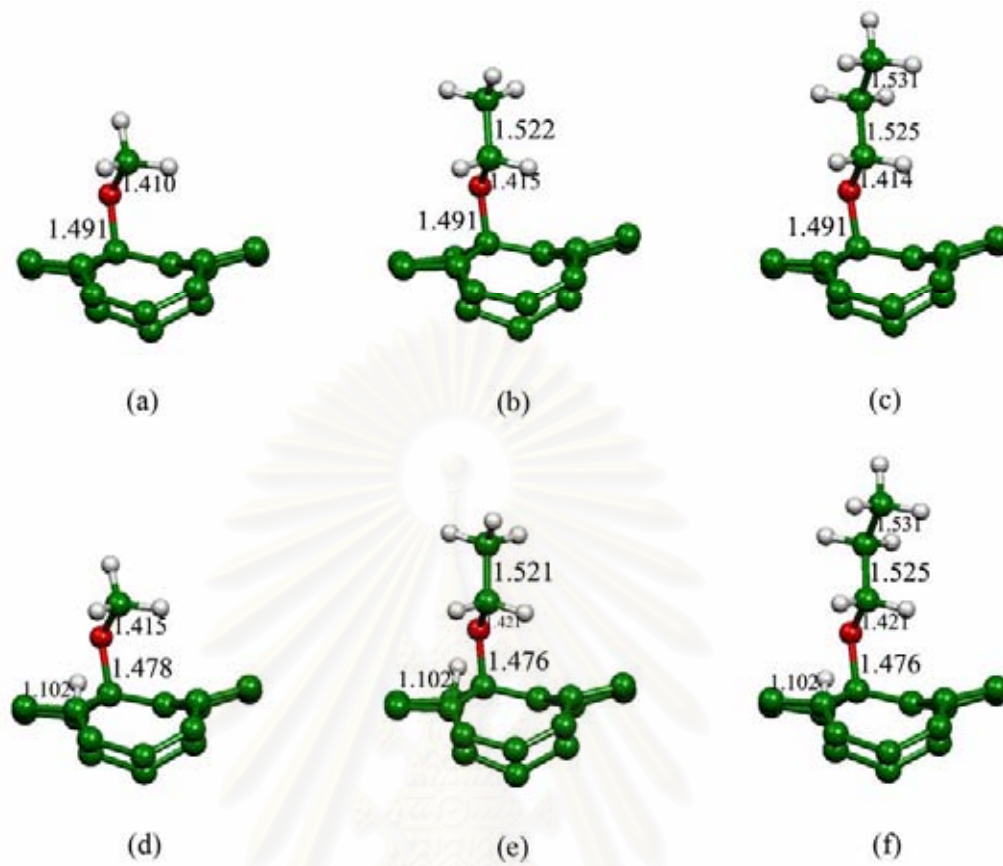


Figure A-16 The bond lengths (\AA) of adsorptions of proton and C1 to C3 alkoxide ions with defect open-ended $\text{C}_{120}\text{H}_{20}$ SWCNTs model 3 (high layer) computed at at the ONIOM(B3LYP/6-31G(d):AM1) level of theory

สถาบันวิทยบริการ
จุฬาลงกรณ์มหาวิทยาลัย

APPENDIX B

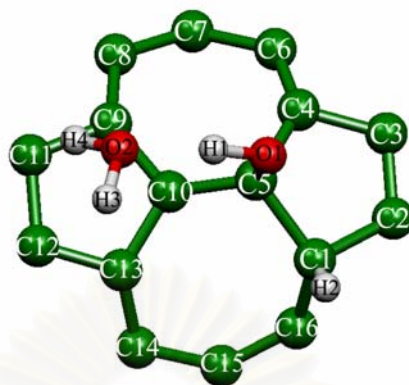


Table B-1 The bond lengths (Å) for the geometries of defect cap-ended C_{80} and defect open-ended SWCNTs (model 3) complexes with proton, hydroxide and water molecule computed at HF/3-21G and ONIOM(B3LYP/6-31G(d) levels of theory

Parameters	Cap-ended C_{80}		Open-ended $C_{80}H_{20}$	Cap-ended C_{120}
	HF/3-21G	ONIOM (B3LYP/6-31G(d):AM1)	ONIOM (B3LYP/6-31G(d):AM1)	
SWCNT				
C1-C2	1.525	1.534	1.529	1.515
C2-C3	1.349	1.400	1.362	1.480
C3-C4	1.452	1.427	1.460	1.407
C4-C5	1.524	1.556	1.514	1.525
C1-C5	1.581	1.624	1.568	1.581
C4-C6	1.389	1.500	1.406	1.447
C6-C7	1.444	1.415	1.479	1.489
C7-C8	1.441	1.512	1.437	1.461
C8-C9	1.476	1.454	1.437	1.457
C9-C10	1.423	1.478	1.401	1.395
C9-C11	1.415	1.422	1.459	1.446
C11-C12	1.435	1.487	1.449	1.418
C12-C13	1.393	1.393	1.411	1.429
C10-C13	1.452	1.455	1.464	1.456
C5-C10	1.456	1.452	1.460	1.439
C13-C14	1.460	1.511	1.420	1.405
C14-C15	1.492	1.486	1.482	1.497
C15-C16	1.390	1.433	1.455	1.419
C1-C16	1.556	1.571	1.548	1.571
Absorbent				
C1-H2	1.079	1.099	1.100	1.103
C5-O1	1.429	1.415	1.446	1.446
O1-H1	0.990	0.991	0.984	0.986
H1...O2	1.675	1.785	1.865	1.843
angle				
O1-H1-O2	174.0	171.5	168.5	168.7
C5-O1-H1	112.4	110.0	107.6	107.3

Table B-2 Energy gap (in eV) of various types of SWCNTs with adsorbing species computed at ONIOM(B3LYP6-31G(d):AM1)

Tubes based on the complexes with	Energy gap							
	Perfect cap- ended	Defect cap- ended	Perfect open- ended	Defect open- ended	Perfect cap- ended	Defect cap- ended	Perfect open- ended	Defect open- ended
	C ₈₀	C ₈₀	C ₈₀ H ₂₀	C ₈₀ H ₂₀	C ₁₂₀	C ₁₂₀	C ₁₂₀ H ₂₀	C ₁₂₀ H ₂₀
Bare tube	5.76	5.46	6.20	6.06	6.50	6.01	6.58	6.12
OH ⁻	5.27	4.87	5.60	5.41	5.66	5.68	5.66	5.87
H ⁺ /OH ⁻	5.17	5.46	6.09	6.47	6.17	6.42	6.12	6.36
OMe ⁻	5.33	4.89	5.63	5.46	5.68	5.71	5.66	5.87
H ⁺ /OMe ⁻	5.19	5.55	6.06	6.50	6.01	6.34	6.09	6.42
OEt ⁻	5.33	4.89	5.60	5.46	5.68	5.71	5.68	5.90
H ⁺ /OEt ⁻	5.19	5.55	6.09	6.04	6.04	6.39	5.66	6.44
OPr ⁻	5.33	4.92	5.63	5.46	5.68	5.71	6.09	5.87
H ⁺ /OPr ⁻	5.17	5.55	6.09	6.50	6.04	6.34	6.06	6.44

สถาบันวิทยบริการ
จุฬาลงกรณ์มหาวิทยาลัย

APPENDIX C

Part I : Publication (Chemical Physics Letters (2007)); In Press
Adsorptions of proton, hydroxide on various cap-ended and open-ended
armchair (5,5) single-walled carbon nanotubes

Raina Wanbayor, Vithaya Ruangpornvisuti *

*Supramolecular Chemistry Research Unit, Department of Chemistry, Faculty of Science,
Chulalongkorn University 10330, Bangkok, Thailand*

* Corresponding author. Tel.: +66-2218-7644; Fax: +66-2254-1309.

E-mail address: vithaya.r@chula.ac.th (V. Ruangpornvisuti).

Abstract

The adsorptions of proton and hydroxide on the perfect and defect armchair (5,5) single-walled carbon nanotubes (SWCNTs) of cap-ended C_{80} , C_{120} and open-ended $C_{80}H_{20}$ and on their protonated structures in the systems with and without water were studied using the Hartree-Fock and two-layered ONIOM(MO:MO) methods. The binding energies of all the adsorptions on various types of armchair (5,5) SWCNTs were obtained at the ONIOM(B3LYP/6-31G(d):AM1) level of theory. The strain energies for all the adsorbed-state structures of SWCNTs and thermodynamic properties for all the adsorptions computed at various levels of theory were obtained.

Keywords: Carbon nanotube; SWCNT; adsorption; proton; hydroxide; pyrene; ovalene; Hartree-Fock; ONIOM;

1. Introduction

The adsorptions of NH_3 and NO_2 molecules on semiconducting single-walled carbon nanotubes (SWCNTs) were investigated using density functional theory (DFT). Both NH_3 and NO_2 molecules were found to bind to carbon nanotubes via physisorption. [1] Various gas molecules such as NO_2 , O_2 , NH_3 , N_2 , CO_2 , CH_4 , H_2O , H_2 and Ar on SWCNTs and bundles were studied and found that most molecules were weakly adsorbed on SWCNTs. [2] Adsorptions of O_2 and H_2O on a SWCNT tip, cap-ended and open-ended SWCNTs were studied by DFT calculations. [3] The interaction of simple aliphatic amines with carboxylated zigzag and armchair SWCNT models was theoretically studied. [4] The ionization potentials of both (4,4) and (6,0) SWCNTs were found to be increased by their negative intrinsic dipole moments, and localized electronic states existed at both of their open ends. [5] The transmission coefficient and the local density of states for different carbon nanotubes with a 5–7–7–5 defect, called Stone–Wales defect, were calculated. [6]

The adsorption of N_2 at the edge of a SWCNT was investigated employing an ONIOM approach and found that N_2 can be chemisorbed at the edge site of zigzag SWCNT surface and the N–N bond is activated and found that the adsorption at the edge site of armchair SWCNT surface is rather weak. [7] The addition reactions of methylamine to fullerenes C_{50} and C_{60} or SWCNTs (5,5) and (10,0) were studied using DFT approach and found that the reaction energy of the addition of methylamine onto C_{60} or the closed caps of (5,5) and (10,0) is rather low. [8]

The adsorption of molecular hydrogen on the external surface of (5, 5), (6, 4), (8, 1) and (16, 2) carbon nanotubes and binding energies of single molecules were studied using DFT calculations. [9]. Several model sizes of purified SWCNT as the open-ended carboxylated C(10, 0) and C(5, 5) were studied by ONIOM approach. [10] Previous work, the addition of diazomethane to armchair SWCNTs of various sizes were carried out using the ONIOM(B3LYP/6-31G(d):PM3) approach. [11]

In this letter, we examine several models within ONIOM approach compared to B3LYP/6-31G(d) method on the adsorptions of proton and hydroxide on the perfect cap-ended C_{80} SWCNT. The adsorptions of proton and hydroxide in systems with and without water on perfect and defect cap-ended C_{80} , C_{120} , open-ended $\text{C}_{80}\text{H}_{20}$ and their

protonated structures have been studied. The objective of this research is to describe stabilities of protonated, hydroxylated forms of perfect and defect SWCNTs and their complexes with water.

2. Computational details

Geometry optimizations of the perfect and defect armchair (5,5) SWCNTs and their complexes with adsorbing species were performed using the ab initio Hartree–Fock (HF) [12] with 3-21G basis set [13] and the two-layered ONIOM(MO:MO) approach with two different models. [14,15] For the two-layered ONIOM approach, the DFT calculations [16] of the hybrid density functional B3LYP [17] level with 6-31G(d) basis set and the semi-empirical PM3 and AM1 methods [18, 19] were employed as the high and low layers respectively. Reliability of various ONIOM(MO:MO) models in terms of energy were compared to full DFT-B3LYP/6-31G(d) energies. Reaction energies of protonation and hydroxylation of the perfect cap-ended C_{80} SWCNT computed at the ONIOM(B3LYP/6-31G(d):AM1) were found to be closer to their corresponding B3LYP/6-31G(d) energies than other ONIOM(MO:MO) energies as shown in Table S1, supplementary data.

Six different characteristics of (5,5) SWCNTs structures categorized into 3 types, namely (1) the cap-ended perfect and defect C_{80} , (2) the cap-ended perfect and defect C_{120} and (3) the open-ended perfect and defect $C_{80}H_{20}$ were investigated. Four models defined using the clusters of (1) a pyrene (C_{16}) as model 1, (2) a 5-6-6-pyrene-5-5-6 (C_{29}) as model 2, (3) a 5-7-7-5 (C_{16}) defect structure as model 3 and (4) an ovalene (C_{32}) as model 4 were employed as the high layer of the two-layered ONIOM(B3LYP/6-31G(d):AM1) approach. Definitions of the low and high layers for the two-layered ONIOM approach are given in Fig. S1. Strain energies of the adsorption-state structures of SWCNTs based on various reactions were evaluated at the HF/3-21G and B3LYP/6-31G(d)//HF/3-21G levels of theory. Thermodynamic properties for all reactions were obtained from the frequencies calculations at the two-layered ONIOM(B3LYP/6-31G(d):AM1) level. All calculations were performed with the GAUSSIAN 03 program [20]. The MOLDEN 4.2 program [21] was used to display the molecular structure and

observe the molecular geometry convergence via the gaussian output files. The molecular graphics of all related species were generated with the MOLEKEL 4.3 program [22].

Binding energy ($\Delta E_{binding}$) of adsorbates on the SWCNTs and strain energy (ΔE_{st}) of adsorption-state structures of the SWCNTs are defined as Eqs. (1) and (2) and those obtained from the ONIOM calculations are evaluated using Eqs. (3) and (4), respectively.

$$\Delta E_{binding} = E_{SWCNT-adsorbate} - E_{adsorbate} - E_{SWCNT}$$

(1)

$$\Delta E_{st} = E_{SWCNT(\text{complex form})} - E_{SWCNT(\text{isolated form})}$$

(2)

$$\begin{aligned} \Delta E_{binding} &= E[ONIOM(B3LYP/6-31G(d):AM1)]_{SWCNT-adsorbate} \\ &\quad - E[ONIOM(B3LYP/6-31G(d):AM1)]_{adsorbate} \\ &\quad - E[ONIOM(B3LYP/6-31G(d):AM1)]_{SWCNT} \end{aligned}$$

(3)

$$\begin{aligned} \Delta E_{st} &= E[ONIOM(B3LYP/6-31G(d):AM1)]_{SWCNT(\text{complex form})} \\ &\quad - E[ONIOM(B3LYP/6-31G(d):AM1)]_{SWCNT(\text{isolated form})} \end{aligned}$$

(4)

The standard enthalpy ΔH_{298}^0 and Gibbs free ΔG_{298}^0 energy changes of adsorption reactions have been derived from the frequency calculations at the ONIOM approach.

3. Results and discussion

3.1 Adsorption models, strain energies and structures

The two-layered ONIOM calculations at the ONIOM(HF/3-21G:PM3), ONIOM(HF/3-21G:AM1) and ONIOM(B3LYP/6-31G(d):AM1) levels of theory were examined and compared to the HF/3-21G and B3LYP/6-31G(d) energies for the proton and hydroxide ions adsorptions on the perfect cap-ended (5,5) C₈₀ SWCNT as shown in Table S1, supplementary data. Binding energies of proton and hydroxide ions on the perfect cap-ended C₈₀ SWCNT and its protonated structure in the systems with and without a water molecule were obtained as shown in Table 1. It shows that all the HF/3-

21G results for the protonation and hydroxylation on the perfect cap-ended C₈₀ SWCNT are under estimated as compared to their corresponding ONIOM results.

For the hydroxylation reactions on the protonated cap-ended SWCNT, all the ONIOM results related to the HF/3-21G computation are over estimated, except the computed at the ONIOM(B3LYP/6-31G(d):AM1) level (-213.69 kcal/mol) of which the energy is close to the HF/3-21G result (-221.13 kcal/mol). The mono-hydration for protonated and hydroxylated perfect cap-ended C₈₀ SWCNT are somewhat weak as shown at the last three lines in Table 1. For the hydration reaction, the HF/3-21G and all the ONIOM(HF/3-21G:MO) calculations seem to be over-estimated as compared to the ONIOM(B3LYP/6-31G(d):AM1) energies. The ONIOM(B3LYP/6-31G(d):AM1) level was therefore selected as more reliable method to be employed for all the calculations of adsorptions on either cap-ended and open-ended (5,5) SWCNTs. Geometrical data for the structures of cap-ended C₈₀ SWCNT complexes with proton and hydroxide in the systems with and without water computed at various methods are listed in Table S2.

Strain energies for perfect and defect cap-ended C₈₀, C₁₂₀ and open-ended C₈₀H₂₀ SWCNTs of the various complexes computed at the HF/3-21G and ONIOM(B3LYP/6-31G(d):AM1) levels of theory are listed in Table 2. Table 2 shows that all the zwitterionic water (H⁺/OH⁻) anchored SWCNTs highly affect to the SWCNTs structures of which strain energies in the systems without and with a water molecule are within the ranges of 33.02-61.60 and 33.87-47.67 kcal/mol, respectively. In the systems without and with a water molecule, strain of the SWCNTs caused by the hydroxylation being larger than that caused by the protonation were found. The ONIOM(B3LYP/6-31G(d):AM1)-optimized structures for the perfect and defect cap-ended C₈₀, C₁₂₀, open-ended C₈₀H₂₀ SWCNTs and their complexes are shown in Figs.1, 2 and 3, respectively.

3.2 Energies and thermodynamic quantities

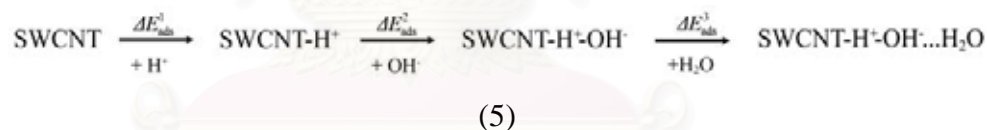
Energetics of adsorption reactions on various perfect and defect SWCNTs computed at various levels of theory and the enthalpy (ΔH_{298}°) and Gibbs free (ΔG_{298}°) energies at 298.15 K of adsorptions on perfect and defect cap-ended C₈₀ SWCNT computed at the HF/3-21G level are given in Table 3. The ZPVE corrected energies and thermodynamic

properties for all adsorptions on the perfect and defect cap-ended C₈₀, C₁₂₀, open-ended C₈₀H₂₀, their protonated and hydration reactions of complex species computed at various ONIOM models are shown in Table S3.

All the adsorptions at 298.15 K are exothermic reactions. In the systems without water, the protonation and hydroxylation of all types of SWCNTs and hydroxylation of their protonated structures are spontaneous reactions. Relative stabilities of adsorptions on the perfect SWCNTs are in decreasing order: open-ended C₈₀H₂₀ > cap-ended C₁₂₀ ~ cap-ended C₈₀ for protonation and cap-ended C₈₀ > cap-ended C₁₂₀ > open-ended C₈₀H₂₀ for their protonated forms, and on the defect SWCNTs are cap-ended C₈₀ ~ open-ended C₈₀H₂₀ > cap-ended C₁₂₀ for protonation and cap-ended C₈₀ ~ cap-ended C₁₂₀ > open-ended C₈₀H₂₀ for their protonated forms.

3.3 Reaction sequence on the cap-ended C₁₂₀ SWCNT

On the cap-ended C₁₂₀ SWCNT, the most preferable adsorption mechanism can be proposed as a reaction sequence: protonation, hydroxylation and hydration, as shown in Eq. (5).



For the perfect cap-ended C₁₂₀ SWCNT, the reaction energies (kcal/mole) obtained at the ONIOM(B3LYP/6-31G(d):AM1) and B3LYP/6-31G(d)//ONIOM(B3LYP/6-31G(d):AM1) (in parenthesis) levels are $\Delta E_{ads}^1 = -202.3$ (-226.8), $\Delta E_{ads}^2 = -204.9$ (-171.6) and $\Delta E_{ads}^3 = -9.8$ (-8.2), as given in Table S4. For the defect cap-ended C₁₂₀ SWCNT, the preferable reaction energies obtained at the ONIOM(B3LYP/6-31G(d):AM1) level are $\Delta E_{ads}^1 = -213.9$, $\Delta E_{ads}^2 = -180.9$ and $\Delta E_{ads}^3 = -8.0$ kcal/mole, as given in Table 3. The hydroxylation of protonated perfect cap-ended C₁₂₀ SWCNT is more preferable than that of its corresponding defect tube by 9.3 kcal/mole.

4. Conclusions

At 298.15 K, all the adsorptions of proton and hydroxide on the perfect and defect armchair (5,5) single-walled carbon nanotube (SWCNT) of cap-ended C_{80} , C_{120} and open-ended $C_{80}H_{20}$ and on their protonated structures are exothermic reactions. The protonation was found to be the most favorite process and followed by the hydroxylation reaction. All the mono hydration reaction energies on the protonated, hydroxylated and zwitterionic hydrated SWCNTs are less than 11 kcal/mol. Strain energies of all types of the SWCNTs after adsorption processes are within wide range of 6.3 to 74.8 kcal/mol. We found that the protonations of all defect types of SWCNTs are more preferable than those of their corresponding perfect tubes. On the other hand, the hydroxylations of protonated perfect SWCNTs are more preferable than those of their corresponding defect tubes.

Acknowledgements

This research was financially supported by the National Nanotechnology Center (NANOTEC), grant number NN-B-22-m10-10-49-18, National Science and Technology Development Agency, Thailand. IBM (Thailand) is acknowledged for providing on an efficient server with the special low price.

Appendix A Supplementary data

Supplementary data associated with this letter can be found, in the online version, at [doi:10.1016/j.cplett.200x.xx.xxx](https://doi.org/10.1016/j.cplett.200x.xx.xxx).

References

- [1] H. Chang, J. D. Lee, *Appl. Phys. Lett.* 79 (2001) 3863.
- [2] J. Zhao¹, A. Buldum¹, J. Han, J. P. Lu, *Nanotechnology* 13 (2002) 195.
- [3] V. A. Basiuk, *J. Phys. Chem. B* 107 (2003) 8890.
- [4] J. Luo, Z. X. Zhang, L.-M. Peng, Z. Q. Xue, J. L. Wu, *J. Phys. D: Appl. Phys.* 36 (2003) 3034.
- [5] S. Hou, Z. Shen, X. Zhao, Z. Xue, *Chem. Phys. Lett.* 373 (2003) 308.
- [6] H.-T. Yang, L. Yang, J. Chen, J. Dong, *Phys. Lett. A* 325 (2004) 287.
- [7] Y.-J. Xu, J.-Q. Li, *Chem. Phys. Lett.* 412 (2005) 439.
- [8] T. Lin, W.-D. Zhang, J. Huang, C. He, *J. Phys. Chem. B* 109 (2005) 13755.
- [9] S. Picaud, B. Collignon, P. N. M. Hoang, *J. Phys. Chem. B* 110 (2006) 8398.
- [10] I. Cabria, M.J. López, J.A. Alonso, *Comput. Mater. Sci.* 35 (2006) 238.
- [11] B. Wann, A.J. Du, V. Ruangpornvisuti, S.C. Smith, *Chem. Phys. Lett.* 436 (2007) 218.
- [12] R. McWeeny, G. Dierksen, *J. Chem. Phys.* 49 (1968) 4852.
- [13] K. D. Dobbs, W. J. Hehre, *J. Comput. Chem.* 8 (1987) 880.
- [14] F. Maseras, K. Morokuma, *J. Comput. Chem.* 16 (1995) 1170.
- [15] S. Humbel, S. Sieber, K. Morokuma, *J. Chem. Phys.* 105 (1996) 1959.
- [16] A. D. Becke, *J. Phys. Rev. A* 38 (1988) 3098.
- [17] C. Lee, W. Yang, R.G. Parr, *Phys. Rev. B* 37 (1988) 785.
- [18] J. J. P. Stewart, *J. Comput. Chem.* 10 (1989) 221.
- [19] M. J. S. Dewar, C. H. Reynolds, *J. Comput. Chem.* 2 (1986) 140.
- [20] M. J. Frisch et al., GAUSSIAN 03, Revision D.02, Gaussian, Inc., Wallingford, CT, 2006.
- [21] MOLDEN 4.2: G. Schaftenaar, CAOS/CAMM Center Nijmegen, Toernooiveld, Nijmegen, The Netherlands, 1991.
- [22] P. Flükiger, H.P. Lüthi, S. Portmann, J. Weber, MOLEKEL 4.3: Swiss Center for Scientific Computing, Manno, Switzerland, 2000.

Table 1

Reaction energies on the perfect cap-ended C_{80} SWCNT computed at the various methods

Reactions	$\Delta_r E^a$						
	HF/3-21G	ONIOM					
		(HF/3-21G:PM3)		(HF/3-21G:AM1)		(B3LYP/6-31G(d):AM1)	
		model 1	model 2	model 1	model 2	model 1	model 2
SWCNT + H^+ \rightarrow SWCNT- H^+	-224.71	-197.96	-190.30	-193.09	-183.94	-194.45	-188.62
SWCNT + OH^- \rightarrow SWCNT- OH^-	-144.77	-119.11	-122.49	-123.81	-128.29	-112.65	^b
SWCNT- H^+ + OH^- \rightarrow SWCNT- H^+ - OH^-	-221.13	-228.92	-235.57	-233.71	-241.73	-222.96	-213.69
SWCNT- H^+ + H_2O \rightarrow SWCNT- H^+ \cdots H_2O	-14.05	-15.52	-15.19	-15.89	-15.87	-11.27	-10.65
SWCNT- OH^- + H_2O \rightarrow SWCNT- OH^- \cdots H_2O	-13.65	-13.88	-13.79	-13.78	-13.76	-11.45	^b
SWCNT- H^+ - OH^- + H_2O \rightarrow SWCNT- H^+ - OH^- \cdots H_2O	-14.97	-14.99	-15.28	-15.18	-15.64	-11.14	-10.26

^a In kcal/mol. ^b No convergence is found.

Table 2

Strain energies (in kcal/mol) for perfect and defect cap-ended C_{80} , C_{120} and open-ended $C_{80}H_{20}$ SWCNTs of the various complexes computed at various levels of theory

Tubes based on the complexes with	ΔE_{st}							
	Perfect cap-ended C_{80} ^a	Defect cap-ended C_{80} ^a	Perfect cap-ended C_{80} ^b	Defect cap-ended C_{80} ^c	Perfect cap-ended C_{120} ^d	Defect cap-ended C_{120} ^c	Perfect open-ended $C_{80}H_{20}$ ^b	Defect open-ended $C_{80}H_{20}$ ^c
H^+	16.51	28.07	16.21	8.83	6.18	43.87	37.06	25.30
OH^-	16.17	36.89	25.25	31.88	10.60	41.94	25.72	25.64
H^+/OH^-	33.02	66.79	42.87	34.36	32.33	62.96	39.20	61.66
H^+ with H_2O	6.30	24.09	13.56	4.52	3.55	29.33	19.35	22.61
OH^- with H_2O	20.75	42.61	27.82	33.11	16.23	74.81	26.98	34.66
H^+/OH^- with H_2O	33.87	56.53	44.67	35.34	40.76	65.10	41.52	67.68

^a Computed at the HF/3-21G level.

^b Computed at the B3LYP/6-31G(d)//ONIOM(B3LYP/6-31G(d):AM1) of model 1.

^c Computed at the B3LYP/6-31G(d)//ONIOM(B3LYP/6-31G(d):AM1) of model 3.

^d Computed at the B3LYP/6-31G(d)//ONIOM(B3LYP/6-31G(d):AM1) of model 4.

Table 3

Energetics of adsorption reactions on various perfect and defect SWCNTs computed at various levels of theory and thermodynamic properties of adsorptions on perfect and defect cap-ended C₈₀ SWCNT computed at the HF/3-21G level

Reaction	ΔE^a	ΔE_{ZPE}^a	$\Delta H_{298}^o^a$	$\Delta G_{298}^o^a$	ΔE^a	ΔE^a
Perfect SWCNTs						
		Cap-ended, C ₈₀ ^b			Open-ended, C ₈₀ H ₂₀ ^c	Cap-ended, C ₁₂₀ ^d
SWCNT + H ⁺ → SWCNT-H ⁺	-224.71	-215.65	-215.63	-215.78	-225.53	-202.28
SWCNT + OH ⁻ → SWCNT-OH ⁻	-114.77	-139.31	-140.45	-129.78	-83.57	-107.62
SWCNT-H ⁺ + OH ⁻ → SWCNT-H ⁺ -OH ⁻	-221.13	-215.58	-216.63	-206.00	-198.14	-204.91
SWCNT-H ⁺ + H ₂ O → SWCNT-H ⁺ ...H ₂ O	-14.05	-12.81	-12.66	-5.60	-8.05	-9.26
SWCNT-OH ⁻ + H ₂ O → SWCNT-OH ⁻ ...H ₂ O	-13.65	-10.63	-11.23	-1.75	-10.89	-9.18
SWCNT-H ⁺ -OH ⁻ + H ₂ O → SWCNT-H ⁺ -OH ⁻ ...H ₂ O	-14.97	-12.77	-12.92	-4.67	-10.84	-9.82
Defect SWCNTs						
		Cap-ended, C ₈₀ ^b			Open-ended, C ₈₀ H ₂₀ ^e	Cap-ended, C ₁₂₀ ^e
SWCNT + H ⁺ → SWCNT-H ⁺	-259.96	-251.29	-251.59	-251.47	-229.36	-213.90
SWCNT + OH ⁻ → SWCNT-OH ⁻	-118.87	-114.74	-115.62	-105.45	-76.15	-110.04
SWCNT-H ⁺ + OH ⁻ → SWCNT-H ⁺ -OH ⁻	-192.76	-188.09	-189.10	-178.66	-145.24	-180.96
SWCNT-H ⁺ + H ₂ O → SWCNT-H ⁺ ...H ₂ O	-12.41	-11.06	-10.82	-4.22	-7.04	-8.04
SWCNT-OH ⁻ + H ₂ O → SWCNT-OH ⁻ ...H ₂ O	-15.99	-13.05	-13.73	-4.04	-10.93	-10.51
SWCNT-H ⁺ -OH ⁻ + H ₂ O → SWCNT-H ⁺ -OH ⁻ ...H ₂ O	-16.64	-13.86	-14.47	-5.14	-9.96	-9.63

^a In kcal/mol.

^b Based on the HF/3-21G.

^c Based on the ONIOM(B3LYP/6-31G(d):AM1) with model 1.

^d Based on the ONIOM(B3LYP/6-31G(d):AM1) with model 4.

^e Based on the ONIOM(B3LYP/6-31G(d):AM1) with model 3.

Part II : Presentation (Poster Session); 32th Congress on Science and Technology
of Thailand, 10-12 October 2006. Queen Sirikit National Convention Center,
Bangkok, Thailand.

การดูดซับไฮดรอกไซด์ โปรตอน และน้ำบนท่อนาโนคาร์บอนปลายปิด

**HYDROXIDE, PROTON AND WATER ADSORPTIONS ON CLOSED SINGLE-
WALLED CARBON NANOTUBES**

ไรนา หวันบะหอย, วิทยา เรืองพรวิสุทธิ

Raina Wanbayor, Vithaya Ruangpornvisuti

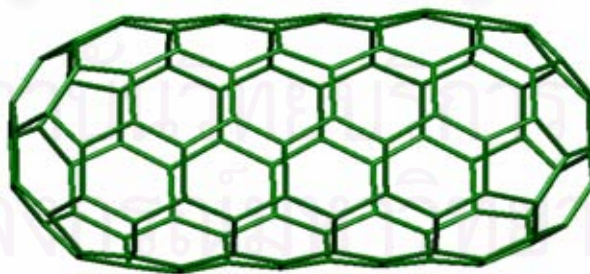
Supramolecular Chemistry Research Unit, Department of Chemistry, Faculty of Science,
Chulalongkorn University, Bangkok 10330, Thailand.

บทคัดย่อ: การศึกษาการดูดซับไฮดรอกไซด์ โปรตอน และน้ำ บนท่อนาโนคาร์บอนปลายปิดชนิดอาร์มเชอร์ (5,5) ขนาด $C_{40}+C_{20_n}$, $n = 2$ และ 3 โดยวิธี Hartree-Fock และ ONIOM(MO:MO) การคำนวณโดยทฤษฎี HF/3-21G พบว่าพลังงานการเกิดปฏิกิริยาระหว่างท่อนาโนคาร์บอนขนาด $C_{40}+C_{40}$ กับ โปรตอนและไฮดรอกไซด์มีค่าเท่ากับ -224.71 และ -144.77 kcal/mol ตามลำดับ และ พลังงานการเกิดปฏิกิริยากับไฮดรอกไซด์บนท่อนาโนคาร์บอนปลายปิดที่ถูกโปรโตรเนตมีค่าเท่ากับ -221.13 kcal/mol พลังงานอันตรปฏิกิริยาบนท่อนาโนคาร์บอนที่ถูกโปรโตรเนต ไฮดรอกซิเลต และ สวิตเตอร์ไอออนิก-วอเตอร์ กับโมเลกุลน้ำมีค่าเท่ากับ -14.05 , -13.65 และ -14.97 kcal/mol ตามลำดับ

Abstract: The adsorptions of hydroxide, proton and water on the closed armchair (5,5) single-walled carbon nanotube (SWCNT) of sizes $C_{40}+C_{20_n}$, $n = 2$ and 3 were studied using Hartree-Fock and two-layered ONIOM(MO:MO). Based on the HF/3-21G computations, the reaction energies between the SWCNT of size $C_{40}+C_{40}$ and proton, and hydroxide, computed are -224.71 and -144.77 kcal/mol, respectively and the reaction energy with hydroxide ion of the protonated SWCNT are -221.13 kcal/mol. The interaction energies of the protonated, hydroxylated and zwitterionic-water added SWCNTs with a water molecule are -14.05 , -13.65 and -14.97 kcal/mol, respectively.

Introduction: Single-walled carbon nanotubes (SWCNTs) that consist of a graphene sheet wrapped to form a cylinder, are a material that has been extensively studied both experiment and theoretical. In particular, adsorption on the surface of SWCNTs continues to be an intriguing and important subject because of its wide potential applications in many respects. These theoretical results suggest that water adsorbed on hydroxylated graphite surface and SWCNTs to form adsorbed -H and -OH groups. In this study, we carried out the adsorption of hydroxide, proton and water on sidewall of SWCNT using Hartree-Fock and two-layered ONIOM(MO:MO) methods.

Methodology: Geometry optimization of various sizes of SWCNTs, their complexes with adsorbents were performed using ab initio Hartree-Fock (HF) with 3-21G basis set and the two-layered ONIOM(MO:MO) approach using B3LYP/6-31G(d) as high model and semiempirical such as PM3 and AM1 methods were tested as low model. The two-layered ONIOM(B3LYP/6-31G(d):AM1) were mainly used in all computations. Based on the clusters for high model of the ONIOM, two different models by selecting pyrene (C16) as model 1 and C7 + pyrene + C6 (C23) as model 2 have been employed in the computations. The strain energies of studied SWCNT based on various reactions were evaluated at the HF/3-21G level. Thermodynamic properties for all the reactions were obtained by frequencies calculations at the two-layered ONIOM(B3LYP/6-31G(d):AM1).



C40+C60

Results, Discussion and Conclusion: The reaction energies of protonation, hydroxylation, and zwitterionic-water addition on the closed armchair (5,5) single-walled carbon nanotube (SWCNT) of sizes C40+C40 and C40+C60 and their binding energies with water and their thermodynamic quantities were obtained, strain energies of the adsorption-state SWNTs obtained are within the range of 6.30-33.87 kcal/mol.

References:

- (1) Collignon, B., Hoang, P.N.M., Picaud, Rayez, J.C. (2005) *Chem. Phys. Lett.* **406**, 430.

Keywords: Adsorption, SWNCT, reaction energies, binding energies, HF, O



สถาบันวิทยบริการ
จุฬาลงกรณ์มหาวิทยาลัย

CURRICULUM VITAE

NAME : Miss Raina Wanbayor

BIRTH DATE : June 17th, 1979

BIRTH PLACE : Nakorn Srithammarat Province, Thailand

EDUCATION : **YEAR** **INSTITUTION** **DEGREE/DIPLOMA**

1998 Kallayanee Srithammarat High School

2002 Rajamangala Univ. B.S. (Chemistry)

2007 Chulalongkorn Univ. M.S.(Chemistry)

ADDRESS : 421/1, Soi, Pechburee 7, Rachtaevee, Bangkok,
10400, Thailand. Tel. 089-1717929

E-MAIL : wanbayor_r@hotmail.com

PUBLICATION

Raina Wanbayor and Vithaya Ruangpornvisuti*, Adsorptions of proton, hydroxide on various cap-ended and open-ended armchair (5,5) single-walled carbon nanotubes. Chemical Physics Letters;2007 (In press).

PRESENTATION

Raina Wanbayor and Vithaya Ruangpornvisuti*, Hydroxid, proton and water adsorptions on closed single-walled carbon nanotubes. (Poster Session): 32th Congress on Science and Technology of Thailand, 10-12 October 2006. Queen Sirikit National Convention Center, Bangkok, Thailand.